Chapter 9: Isentropic potential vorticity & mid-latitude disturbances

Sources:

- Martin, 2006, Chapter 9
- other textbooks:
  - Holton, 2004: section 4.6
  - Bluestein, 1993: p. 180-218
- papers:
  - Hoskins, B.J., M.E. McIntyre and A.W. Robertson, 1985: On the use and significance of isentropic potential vorticity maps. Quart. J. Roy. Meteor. Soc., **111**, 877-946.
  - Thorpe, A.J., 1985: Diagnosis of a balanced vortex structure using potential vorticity. J. Atmos. Sci., **42**, 397-406.
  - Aebischer, U., and C. Schär, 1998: Low-Level Potential Vorticity and Cyclogenesis to the Lee of the Alps. J. Atmos. Sci., **55**, 186-207.

topics

- isentropic coordinates
  - equations of motion
  - visualizing flow on isentropic surfaces, isentropic divergence
  - isentropic analysis: meted module, by J. Moore
- Chapter 9.1: Isentropic Potential Vorticity
  - definition of PV
  - IPV conservation
  - a more in-depth derivation can be found in Holton Chapter 4.6 (p. 109-111)
- Chapter 9.2: PV anomalies: idealized structure and real examples
  - upper level
  - surface
  - diagnosis of vertical motion
  - Rossby waves
- Chapter 9.3: baroclinic instability
- Chapter 9.4: generation of low-level PV by diabatic (latent) heating
- Chapter 9.5: additional applications
  - piecewise PV inversion
  - PV perspective of occlusion & lee cyclogenesis
  - PV superposition & attenuation
  - PV generation & break-up by friction (orography)

isentropic coordinates

isobaric coordinates

isentropic coordinates

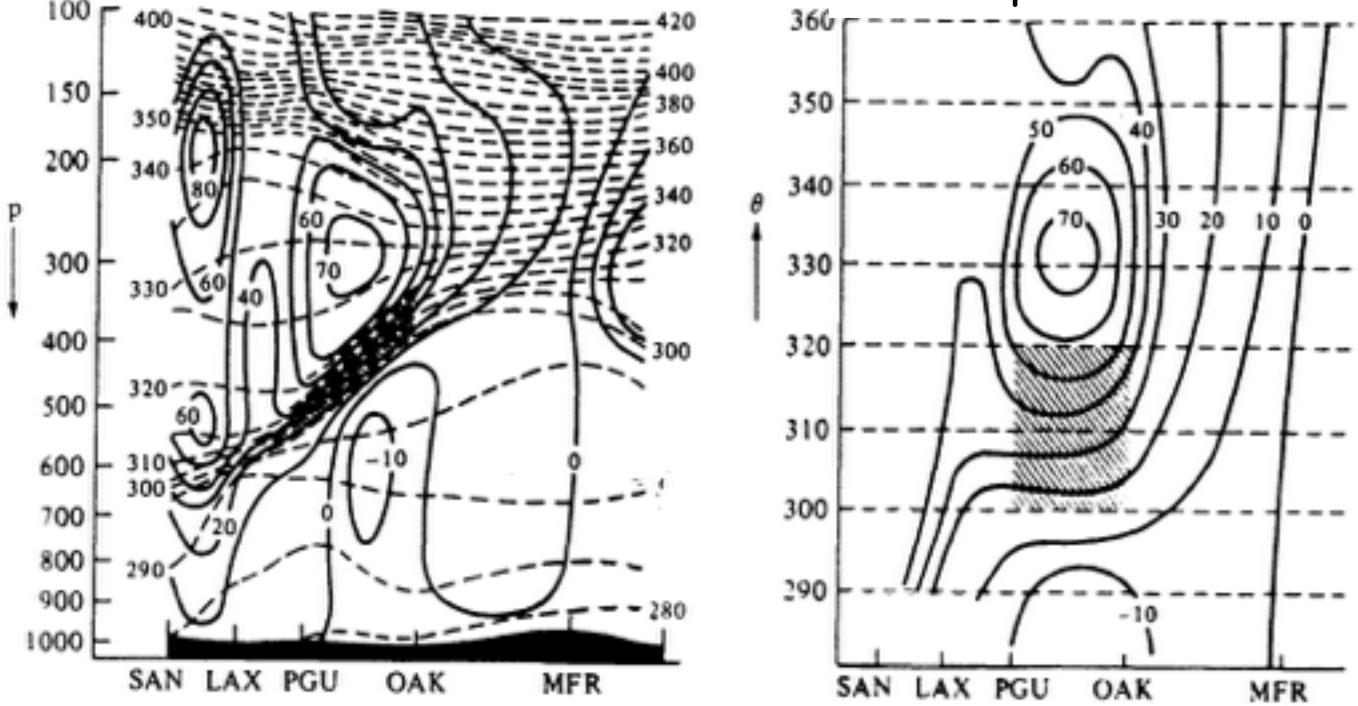

FIGURE 7.10

Comparison of resolution in isobaric and isentropic coordinates. The cross section on the left is the traditional form of presenting isotachs and isentropes with pressure as the vertical coordinate. An upper-level front or baroclinic zone is identified by the shaded area on the cross section. The figure on the right shows the same area as it would be represented in isentropic coordinates, making it clear that the dynamics of this structure could be analyzed or predicted more accurately in isentropic coordinates. *(Illustration provided by Dr. Rainer Bleck, National Center for Atmospheric Research. The figure on the left is from M. A. Shapiro and J. T. Hastings, 1973: "Objective Cross-Section Analysis by Hermite Polynomial Interpolation on Isentropic Surfaces," J. Appl. Meteorol., 12:753–762.)*

Isentropic maps: some examples
infer vertical motion

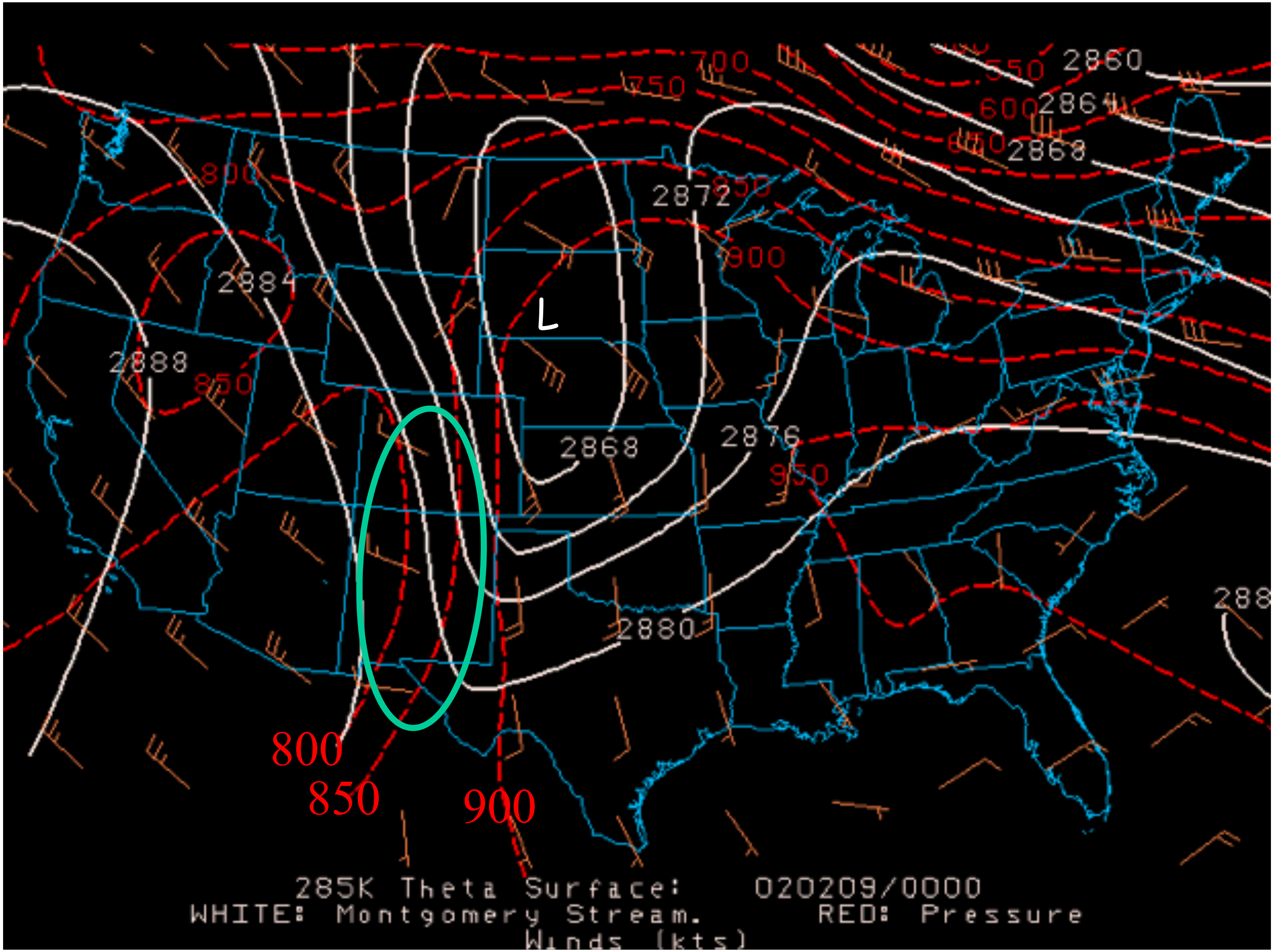

295 K

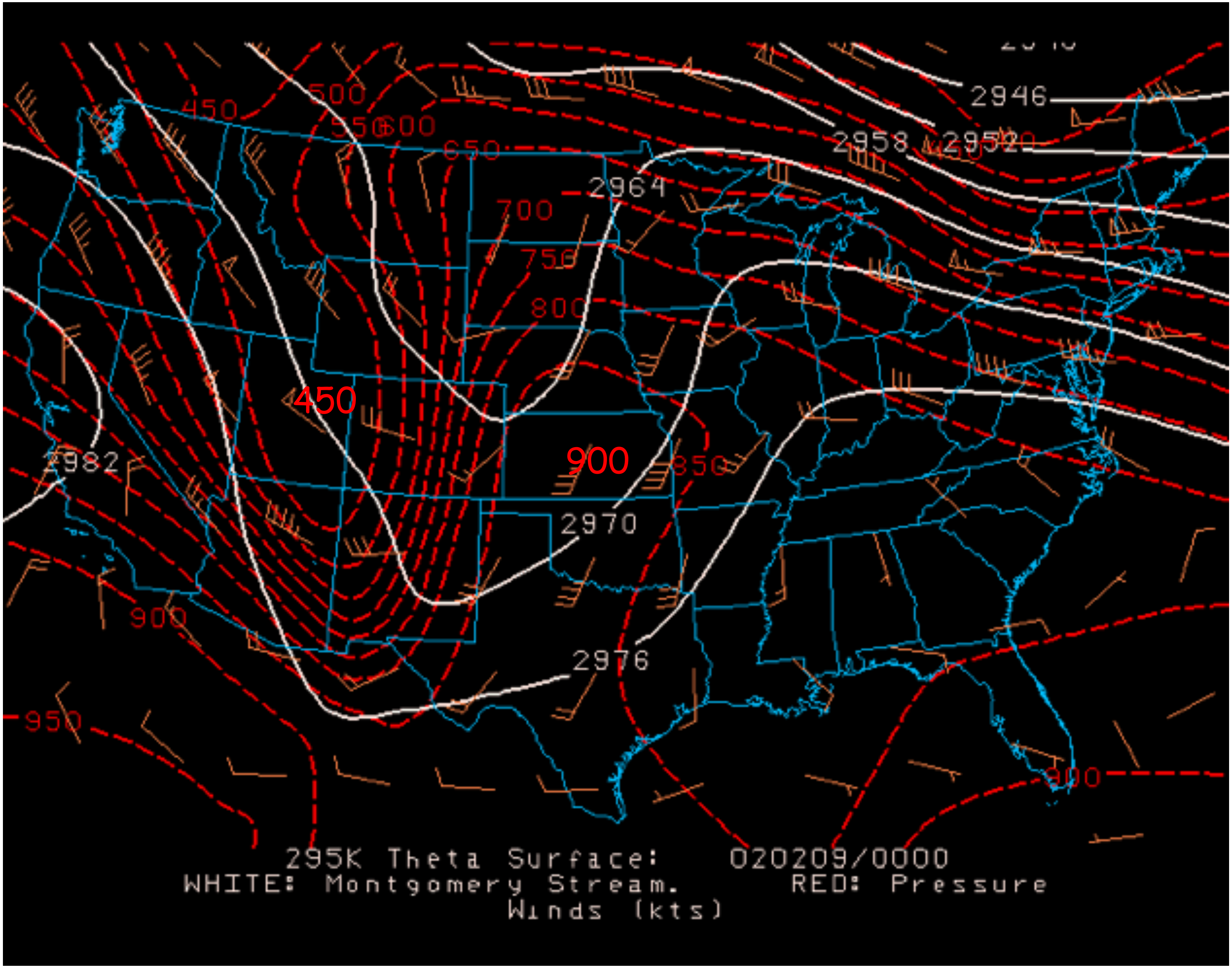

2946
2958
2952
2964
2970
2976
2982
450
500
550
600
650
700
750
800
850
900
950
295K Theta Surface: 020209/0000
WHITE: Montgomery Stream. RED: Pressure
Winds (kts)

295 K – relative humidity suggests that storm-relative motion has an easterly component in E Montana

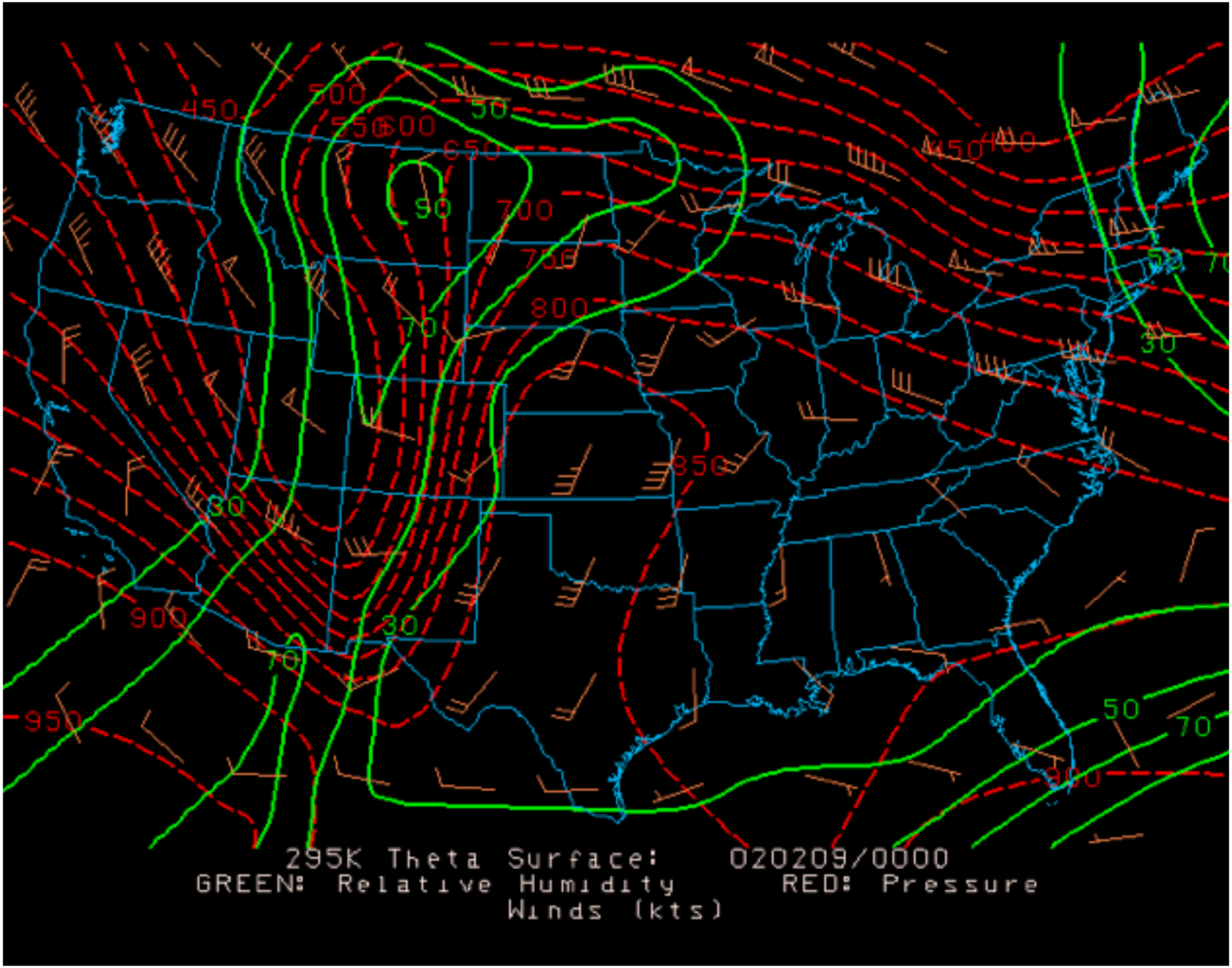

325 K

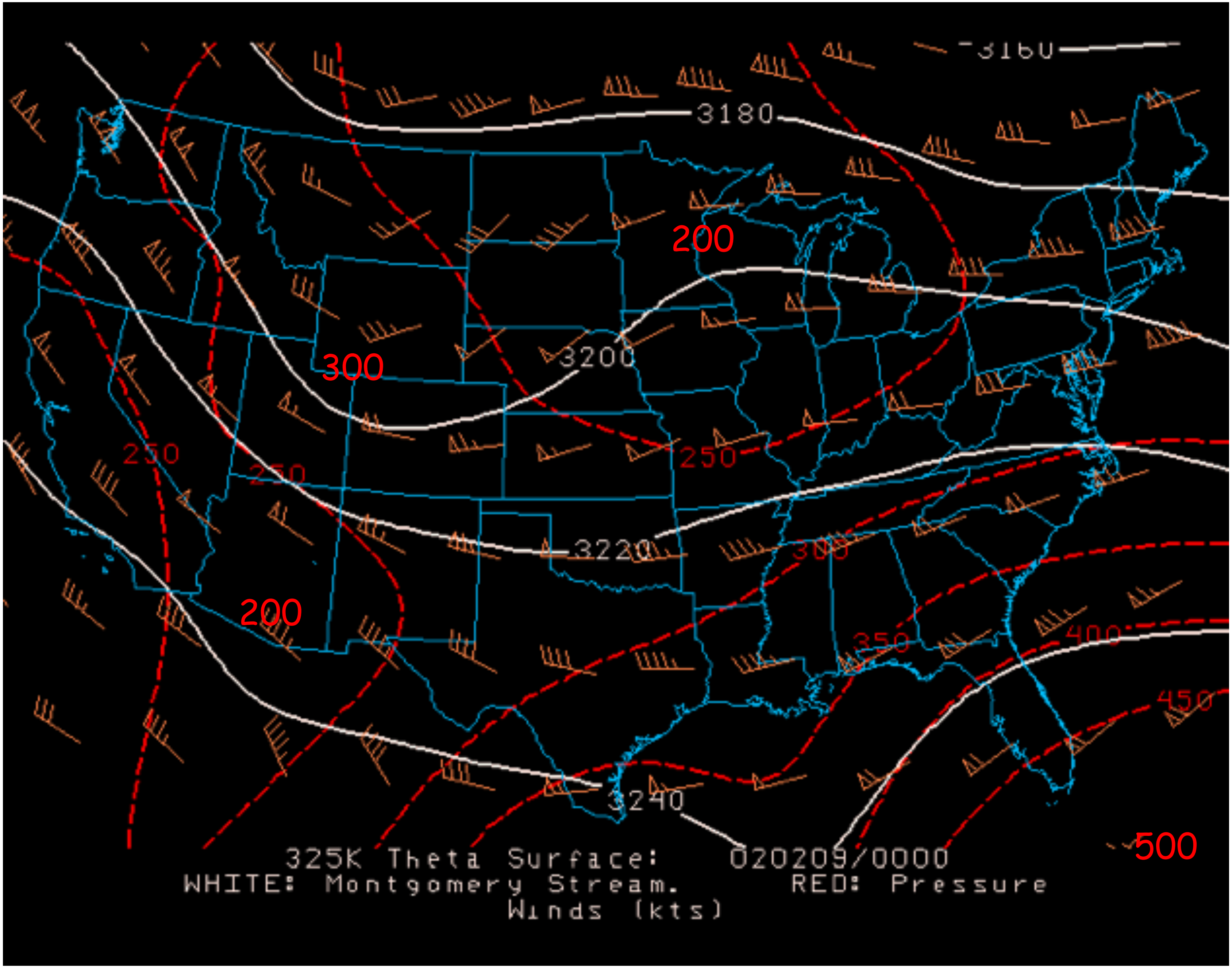
3160
3180
3200
3220
3240
200
300
250
250
250
300
200
350
400
450
500
325K Theta Surface: 020209/0000
WHITE: Montgomery Stream. RED: Pressure
Winds (kts)

current isentropic charts showing winds, pressure, and winds

- http://weather.cod.edu/analysis/analysis.isentropic.html

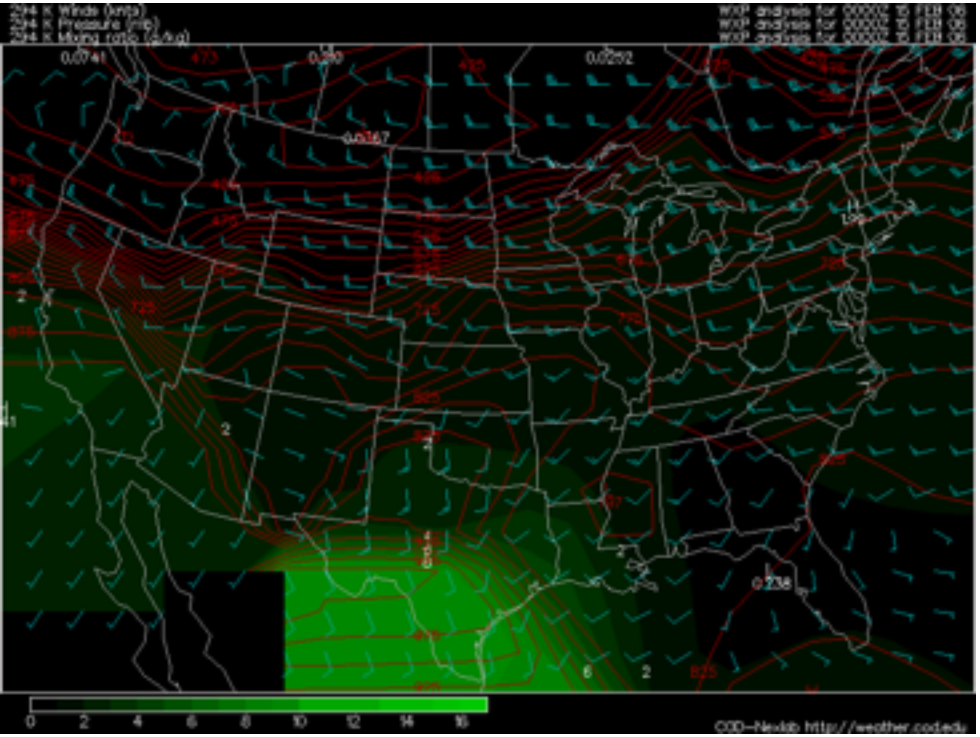

296 K

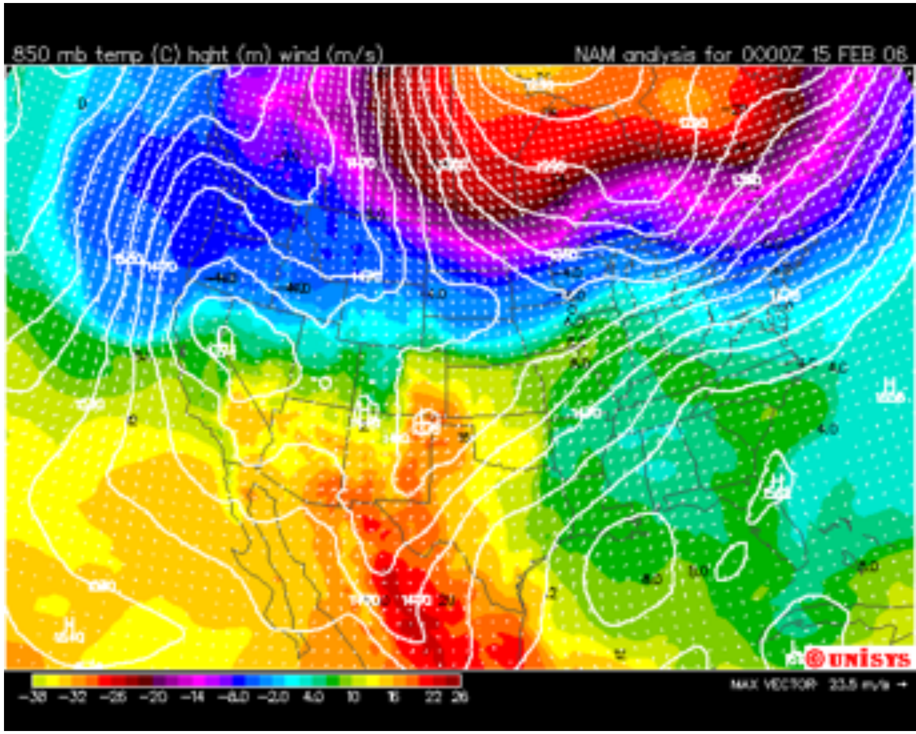

850 mb

Chapter 9.1: PV and isentropic divergence

Definition of PV

$$P = g(\zeta_\theta + f)\left(-\frac{\partial\theta}{\partial p}\right)$$

in words: the product of
isentropic abs vorticity and static stability

Conservation of PV

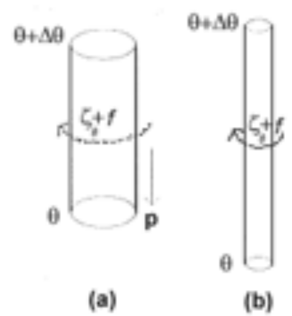

P is generally conserved (DP/Dt=0)
for adiabatic, inviscid processes.

In a saturated environment P_e is conserved:

$$P_e = g(\zeta_\theta + f)\left(-\frac{\partial\theta_e}{\partial p}\right)$$

potential vorticity on isentropic charts

try the current animations at
http://www.atmos.washington.edu/~hakim/tropo/310_pv.html
courtesy of Hakim, U Washington

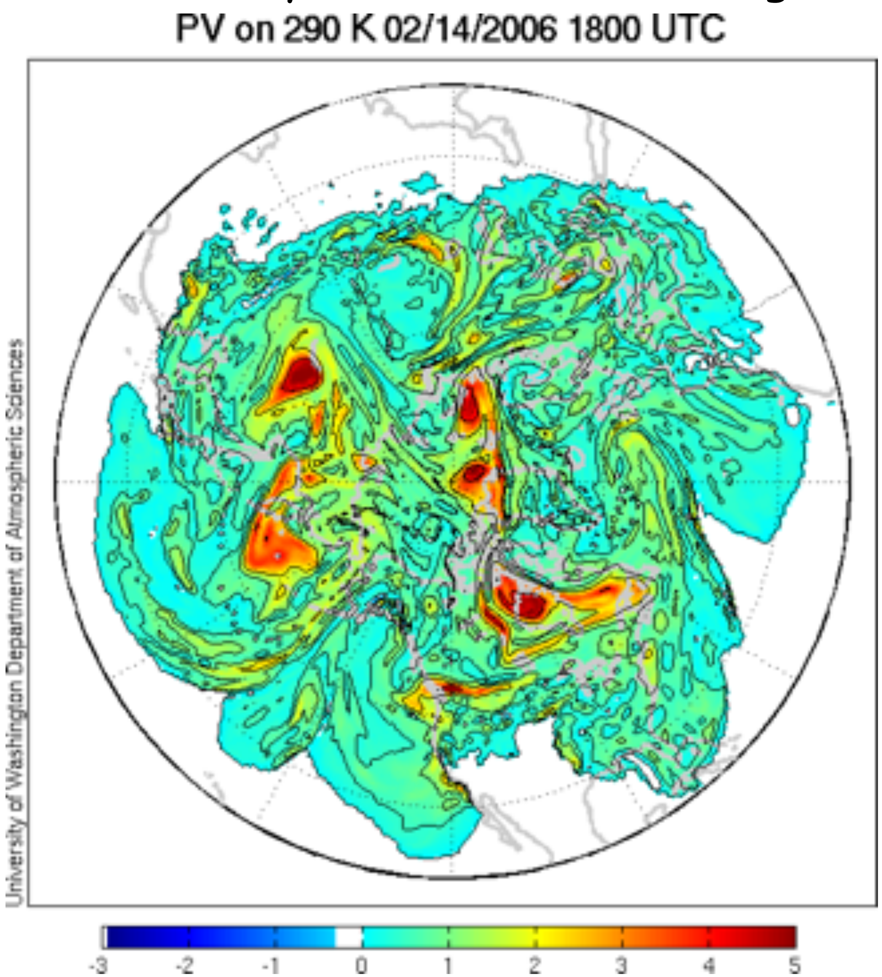

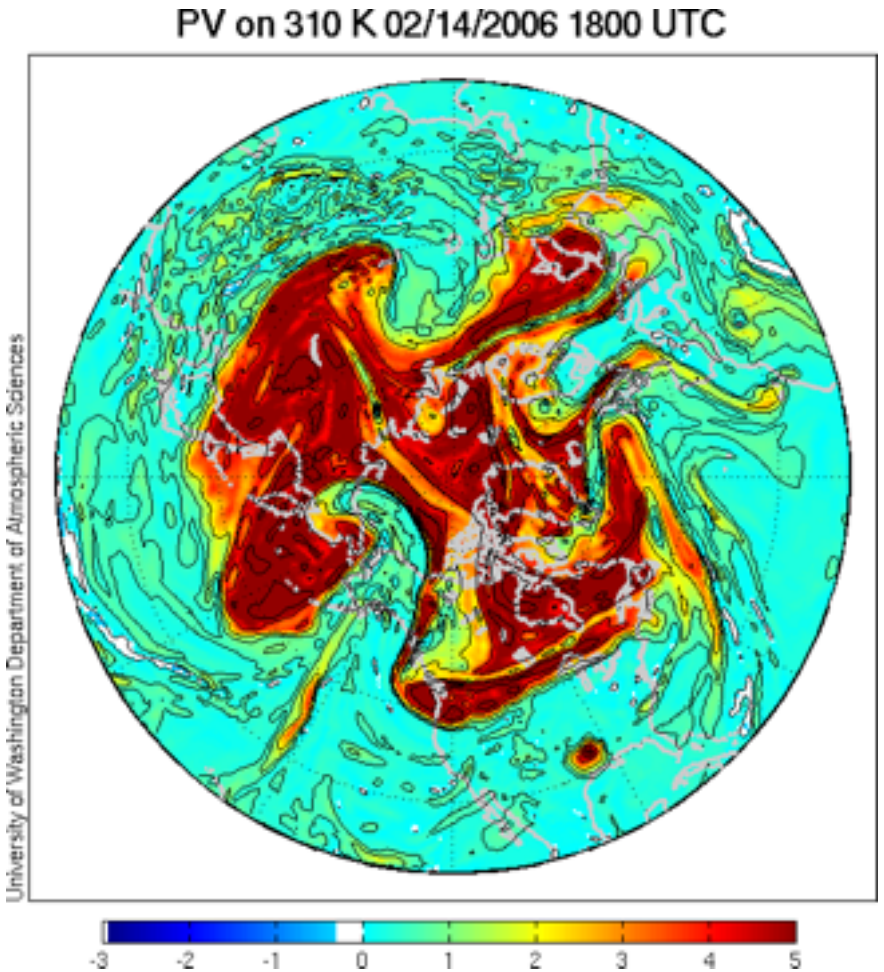

Units: PV = 10^{-6} m^2 s^{-1} K kg^{-1} = 1 PV unit or 1 PVU

PV >2 PVU: stratospheric air

An example of synoptic variations of PV

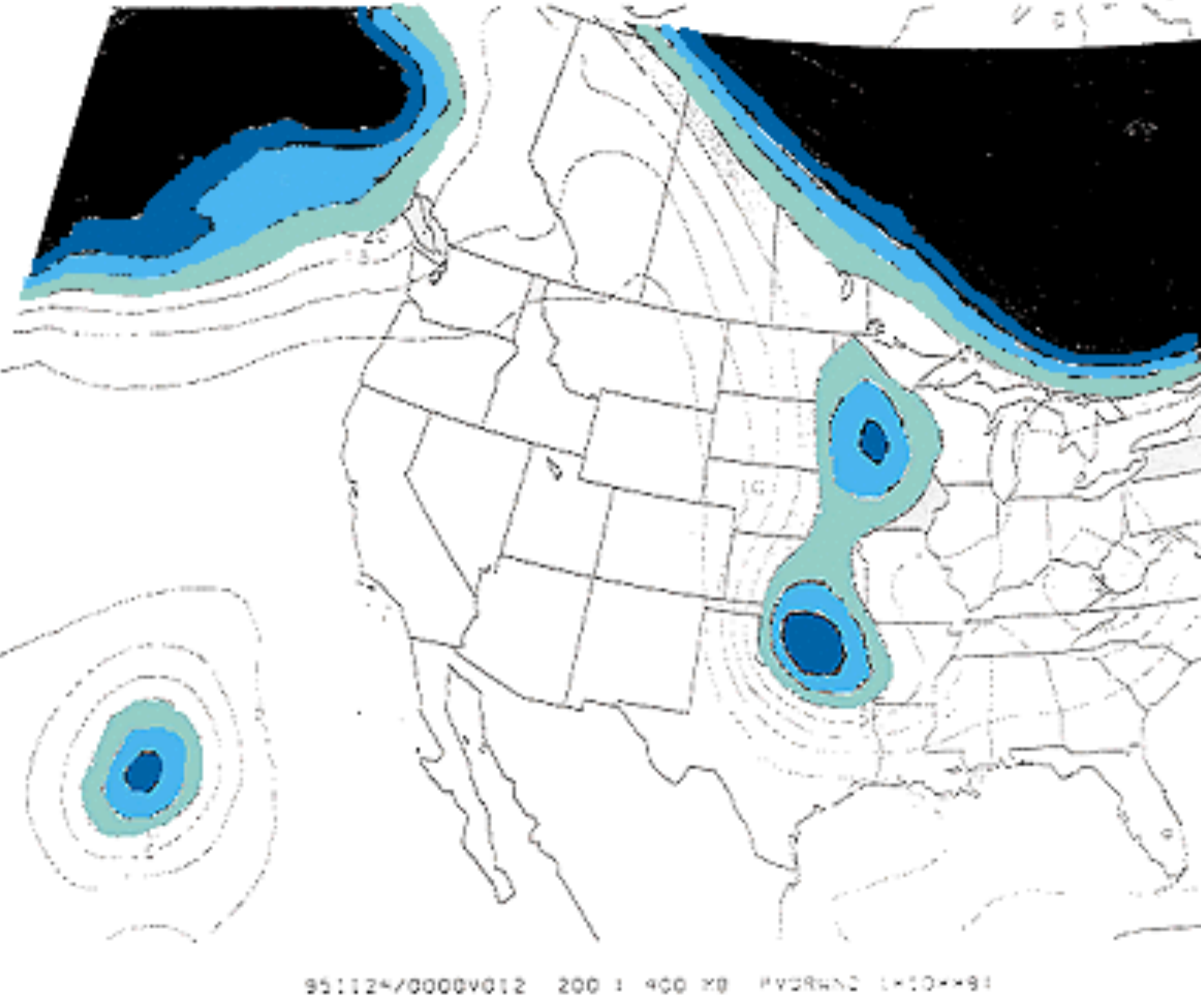

PV
200-400 mb

Colored contours at 2, 2.5, 3, and 4 PVU

300 mb height – same time

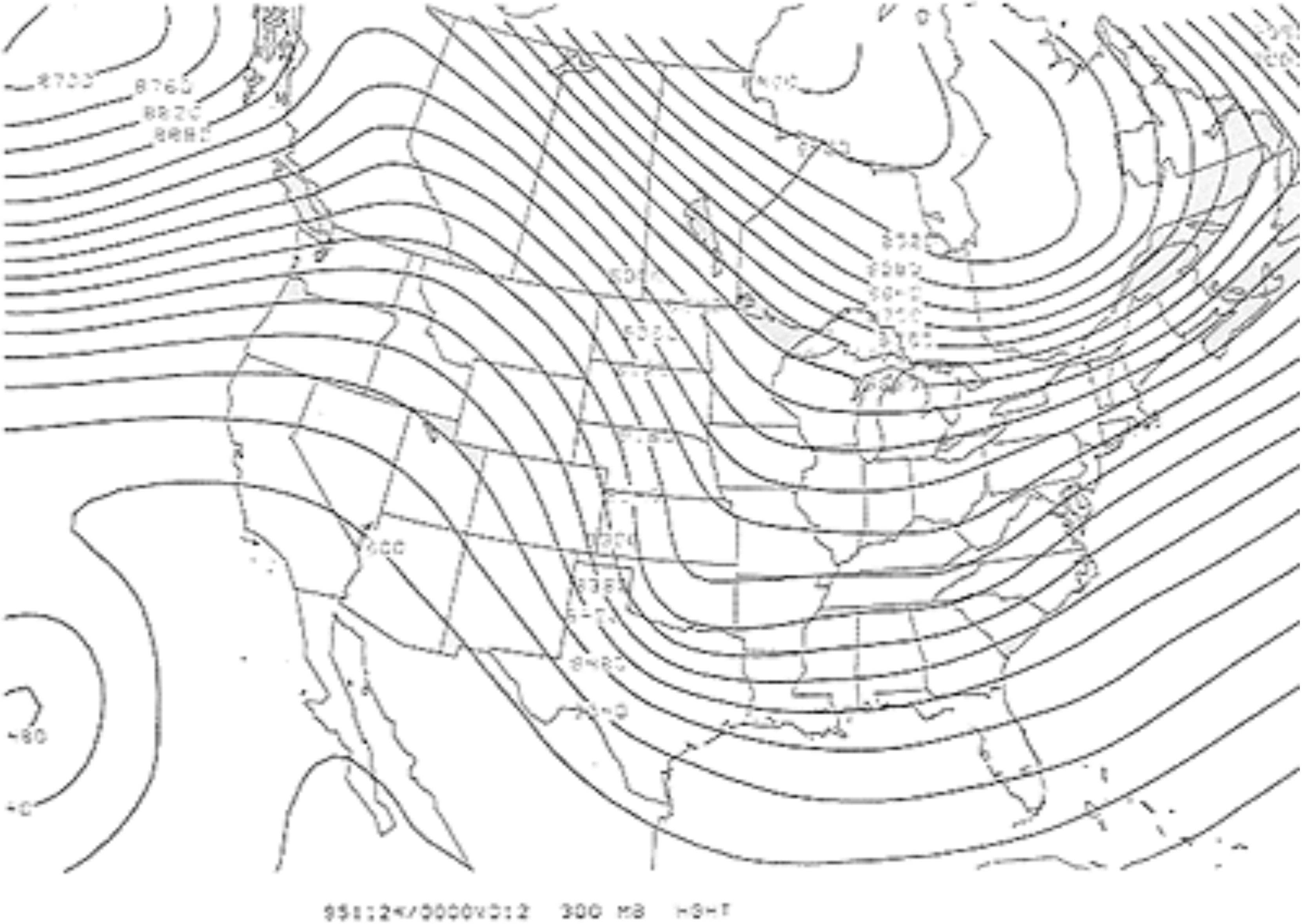

zonal-mean meridional transect: climatology of PV and θ

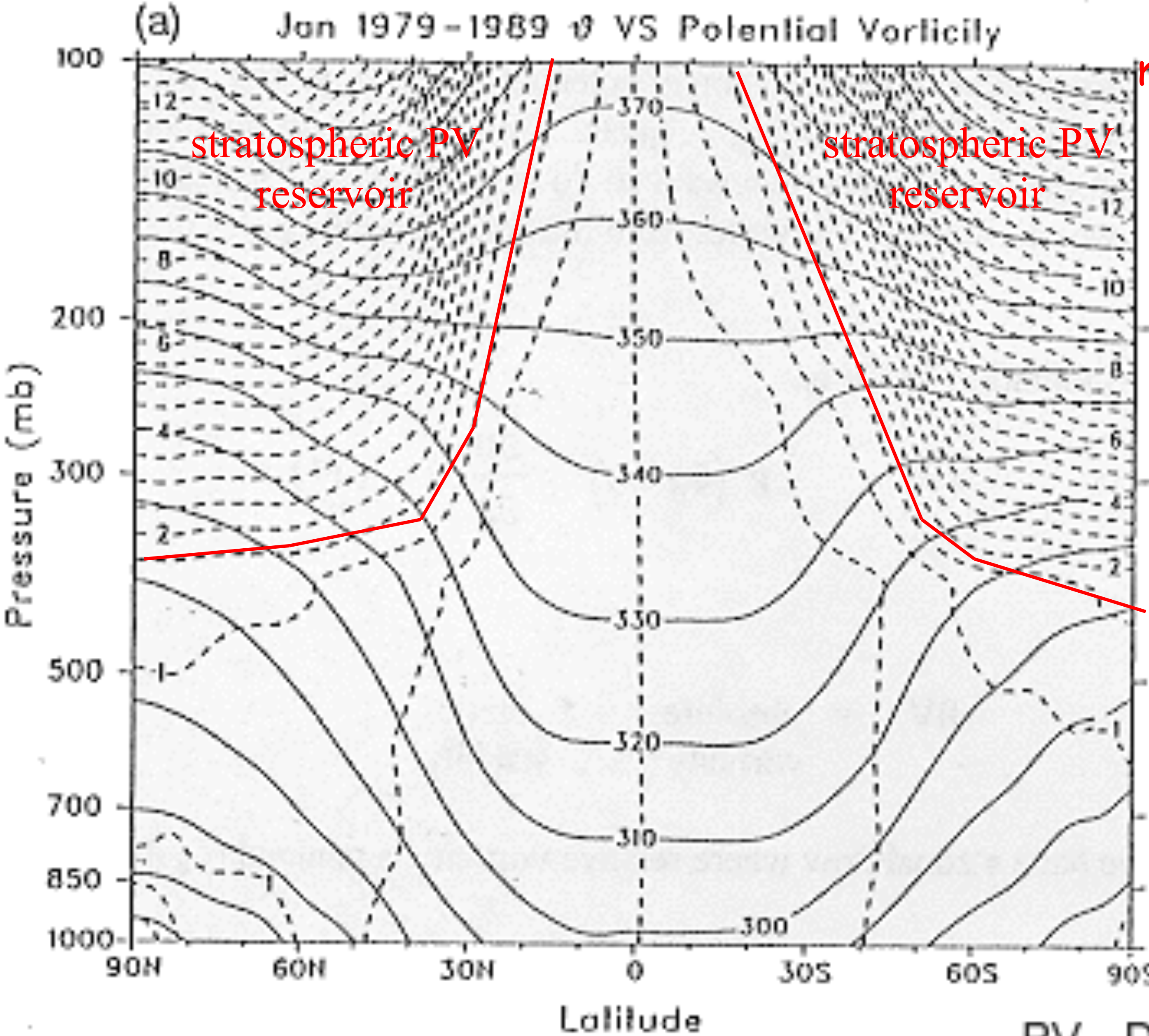

At low latitudes, the troposphere ranges from 300 to 370 K (70 K depth).

Poleward of the polar jet, the troposphere ranges from 265-300 K (35 K depth).

units of PV: $10^{-6}\ m^2\ s^{-1}\ K\ kg^{-1}$

PV - Dashed

Theta - Solid

Figure one

ECMWF T511/L60 Operational Analyses

320 K IPV

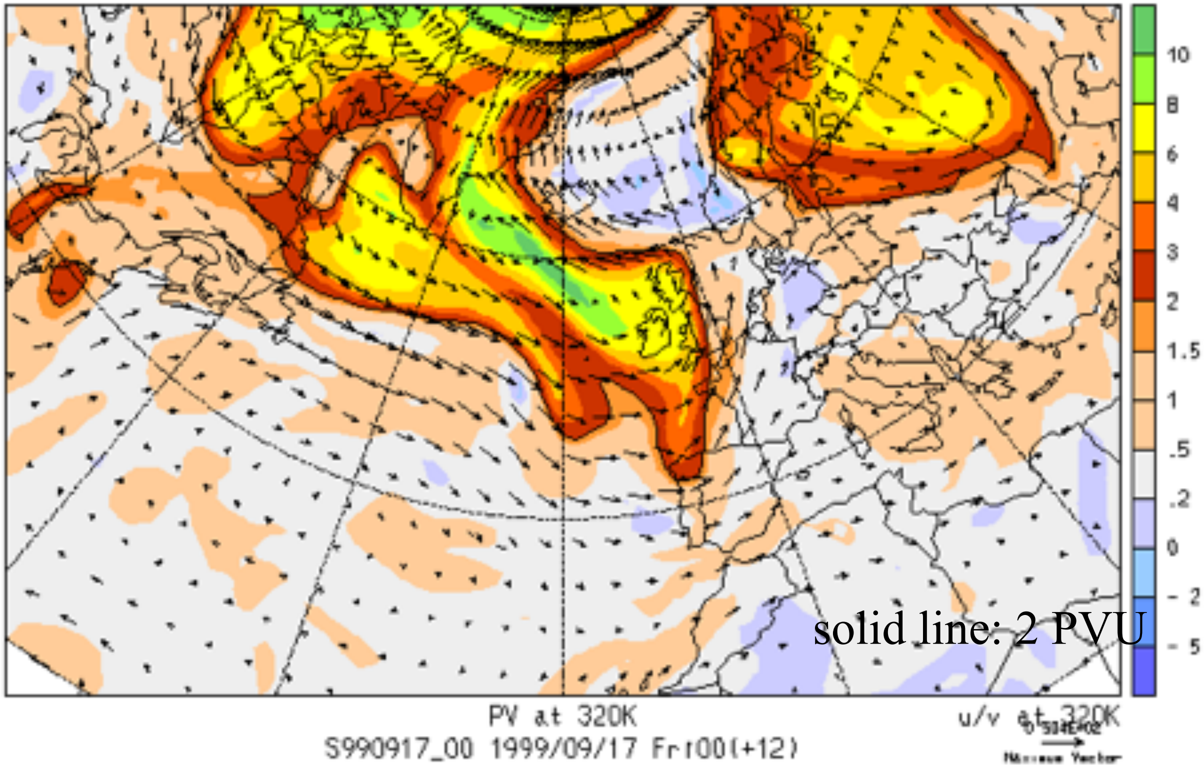

(Hoskins et al 1985)

zonal-mean meridional transect

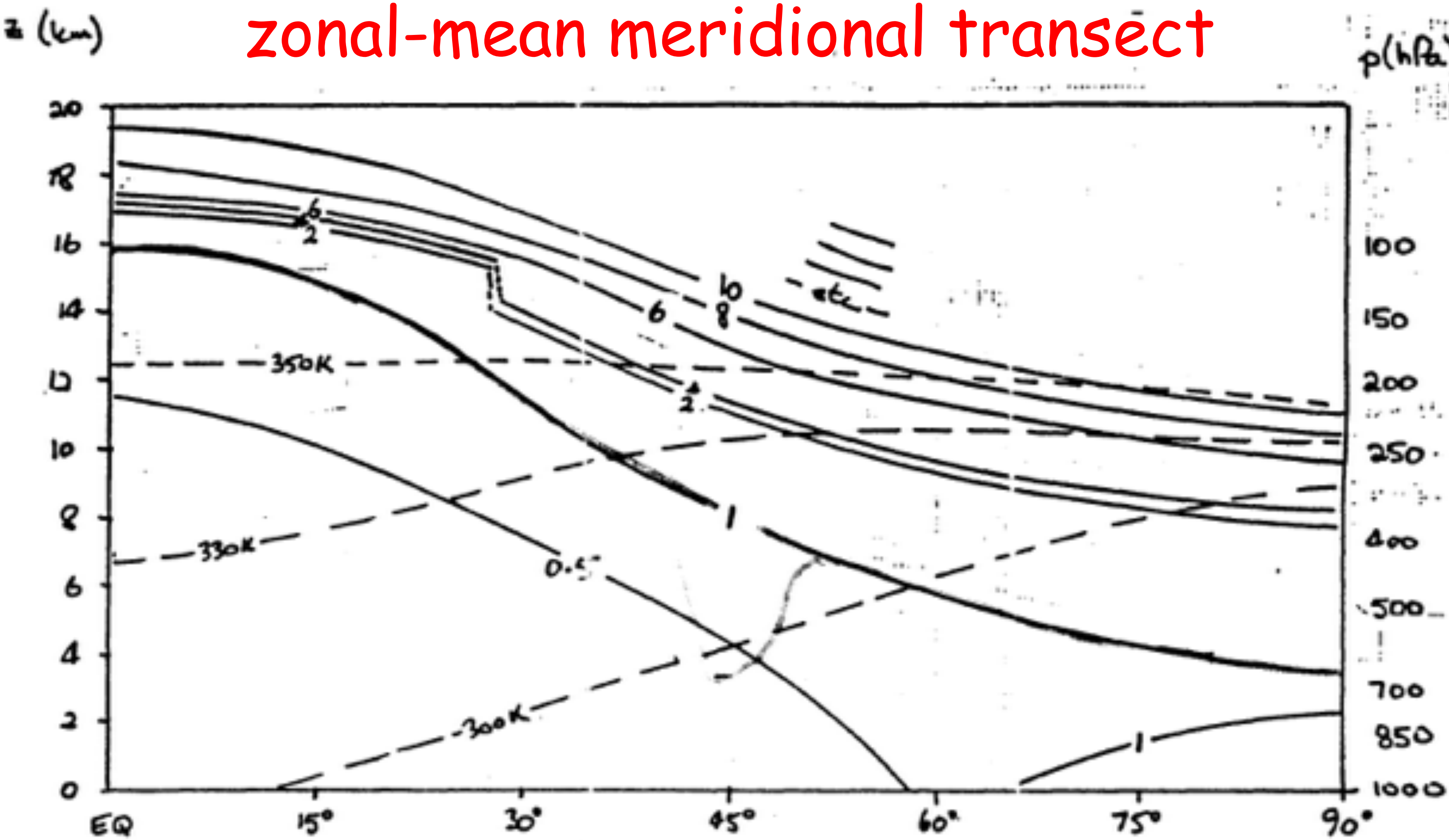

Fig 1. Schematic distribution of P and θ in the atmosphere, based on $\zeta_r = 0$ and the US standard atmosphere for various latitudes. Redrawn from data in Hoskins *et al* (1985) Fig 1. Units are $10^{-6}m^2.K.s^{-1}.kg^{-1}$.

Invertibility principle (Hoskins, McIntyre and Robinson 1985)

- Any storm system at any scale may be regarded as a superposition of IPV anomalies, positive or negative, at the top and bottom boundary of the troposphere.

- The true wind is the sum of all wind fields associated with each anomaly.

- The IPV field can be predicted (advected, deformed), and the wind and stability fields can be extracted from the IPV distribution at any time
  - if boundary conditions are available
  - if a balance condition exists

  e.g.: geostrophic balance

  barotropic vorticity equation

$$\vec{v}_g = \frac{\hat{k}}{f} \times \nabla\phi \quad or \quad \zeta_g = \frac{\nabla^2\phi}{f}$$

$$\frac{D\zeta_g}{Dt} = 0$$

$$\zeta_g \quad can\ be\ predicted: \frac{\partial\zeta_g}{\partial t} = -\vec{v}_g \bullet \nabla\zeta_g$$

$$\vec{v}_g \ and\ \phi\ can\ be\ derived,\ given\ BC$$

- IPV anomalies 'induce' a wind field that extends beyond the IPV anomaly itself.

PV anomaly vertical dimensions

- the vertical influence of PV anomaly on wind field (e-folding scale), a.k.a. the Rossby scale height, can be estimated as follows

$$\Delta\theta = f_o L \sqrt{\rho\theta_{ref}\left(-\partial\theta/\partial p\right)_{ref}} = f_o L \sqrt{\frac{\theta_{ref}}{g}\left[\frac{\partial\theta}{\partial z}\right]_{ref}} = \frac{f_o L \theta_{ref} N_{ref}}{g}$$

assume

$$N_{ref} = 10^{-2} s^{-1}$$

$$f_o = 10^{-4} s^{-1}$$

$$\theta_{ref} = 300K$$

$$then \quad |\Delta\theta| = 3\cdot 10^{-5} L$$

$$for\ L = 10^6 m \quad \boxed{|\Delta\theta| = 30K}$$

à the depth of influence is proportional to:

à L (the diameter of the P' anomaly).

→ N (the Brunt-Vaissalla freq):

$$\Delta\theta \propto \sqrt{\left(-\partial\theta/\partial p\right)_{ref}} \propto N$$

(e.g., Bluestein 1993, p. 193 – but Martin p. 282, says $\Delta\theta \propto \frac{1}{N}$

which is the entire troposphere at high latitudes, and maybe half the troposphere at low latitudes

Chapter 9.2: PV anomalies

idealized depiction of upper-level PV anomalies: positive anomaly

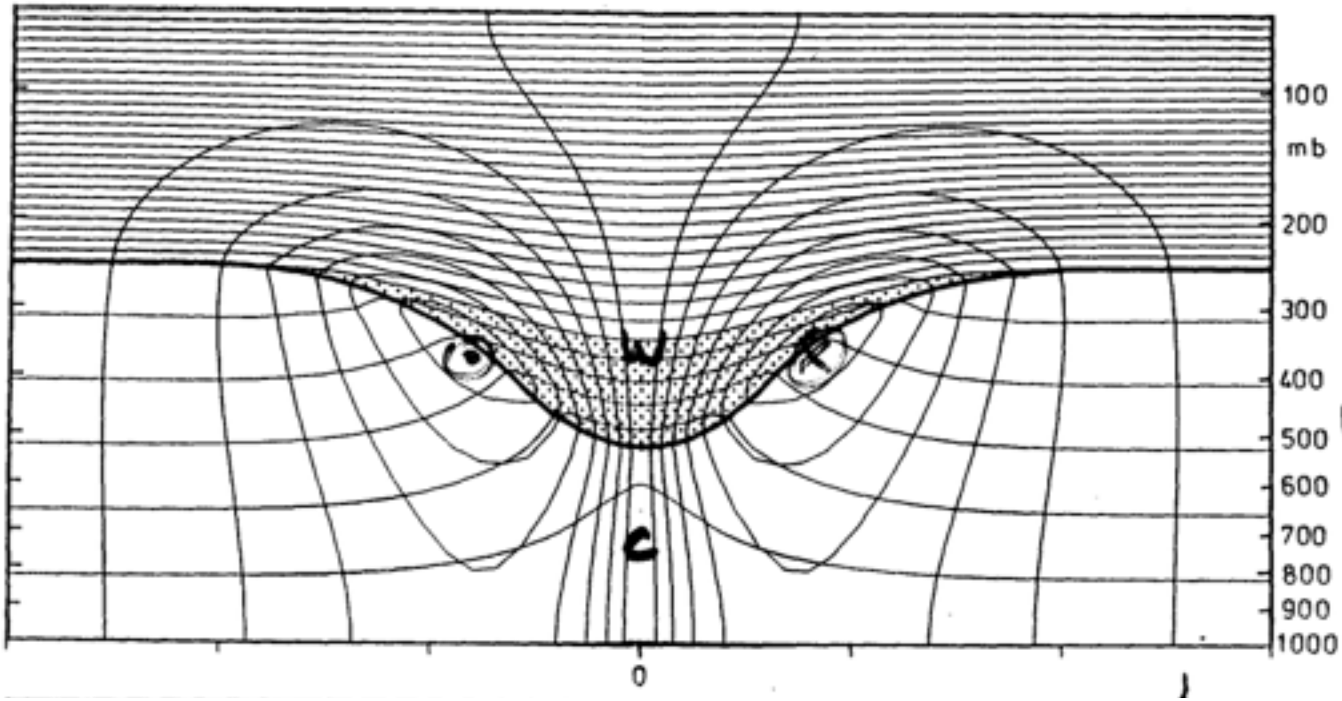

Figure 15. Circularly symmetric flows induced by simple, isolated, IPV anomalies (whose locations are shown stippled) as described in the text. The basic static stability $\tilde{N}$ and therefore $\tilde{P}$ (defined in (34)) was uniform in the tropospheric region and six times larger in the stratospheric region. The vertical coordinate z is nearly the same as physical height but is defined exactly in (35), g/θ_0 being taken to be $(1/30)\,\mathrm{m\,s^{-2}K^{-1}}$. The reference tropospheric 'height' z was 10 km and the total domain 'height' 16·67 km: f was taken to be $10^{-4}\mathrm{s}^{-1}$. The IPV anomaly was defined by taking the tropopause potential temperature to vary in the manner $\frac{1}{2}A\{\cos(\pi\tilde{r}/r_0)+1\}$ for $\tilde{r}<r_0$, where $\tilde{r}=r(f_{\mathrm{loc}}/f)^{1/2}$. Here the amplitude A was taken to be -24 K in (a) and $+24$ K in (b) which may be compared with a potential temperature increase of 30 K over the depth of the reference troposphere. The parameter r_0 was taken to be 1667 km. The undisturbed θ distribution was imposed as a boundary condition at $\tilde{r}=5000$ km, and the solutions obtained had only a weak dependence of $C_b(\theta)$ upon θ as well as a far-field stratification approximating the reference stratification (16). (In terms of our definitions, the IPV anomaly in the stippled regions must therefore strictly speaking be considered to be embedded in a suitable 'surround' of much weaker anomalies, as noted below (17b).) Only the region $r<2500$ km is shown here, and the tick marks below the axes are drawn every 833 km. The thick line represents the tropopause and the two sets of thin lines the isentropes every 5 K and the transverse velocity every $3\,\mathrm{m\,s^{-1}}$. The zero isotach on the axis of symmetry is omitted. In (a) the sense of the azimuthal wind is cyclonic and in (b) it is anticyclonic, in both cases the maximum contour value being $21\,\mathrm{m\,s^{-1}}$. The surface pressure anomaly is -41 mb in (a) and $+13$ mb in (b) and the relative vorticity extrema (located at the tropopause) are $1{\cdot}7f$ in (a) and $-0{\cdot}6f$ in (b). The maximum surface winds are $15\,\mathrm{m\,s^{-1}}$ and $6\,\mathrm{m\,s^{-1}}$ respectively. For more details of the method of computation, see Thorpe (1985).

wind in
thermal wind balance

$$\frac{\partial v_g}{\partial Z} \propto K\left(\frac{\partial T}{\partial x}\right)$$

Upper-level PV anomalies: positive anomaly

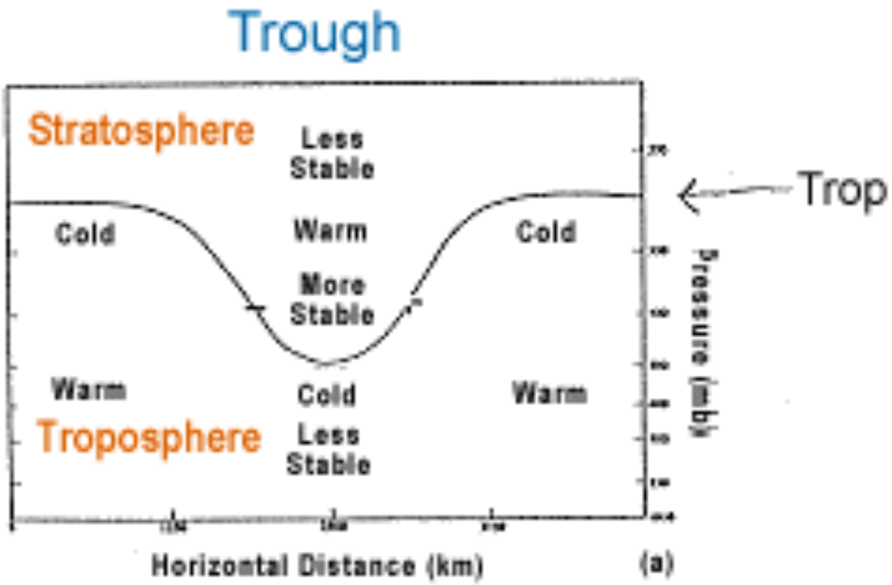

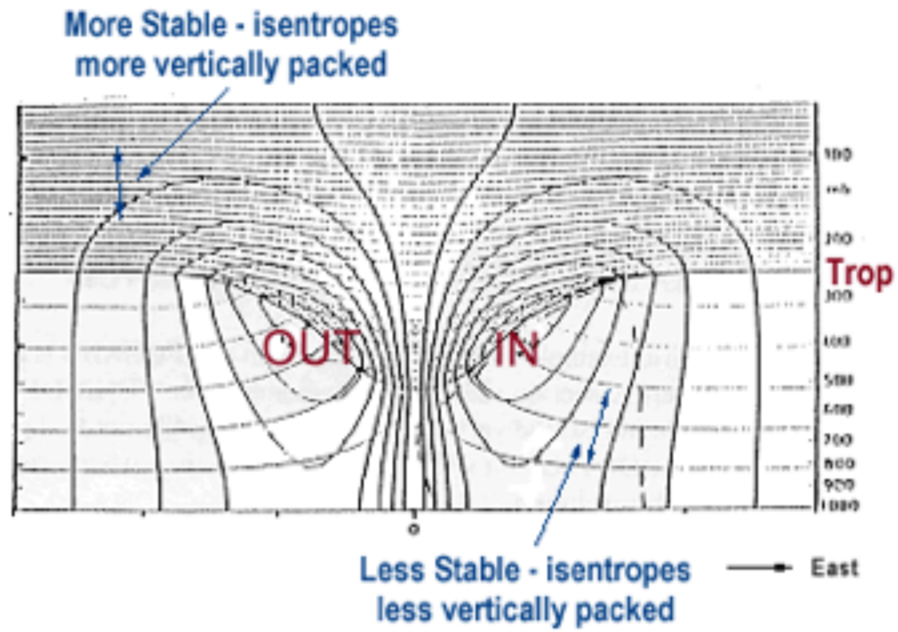

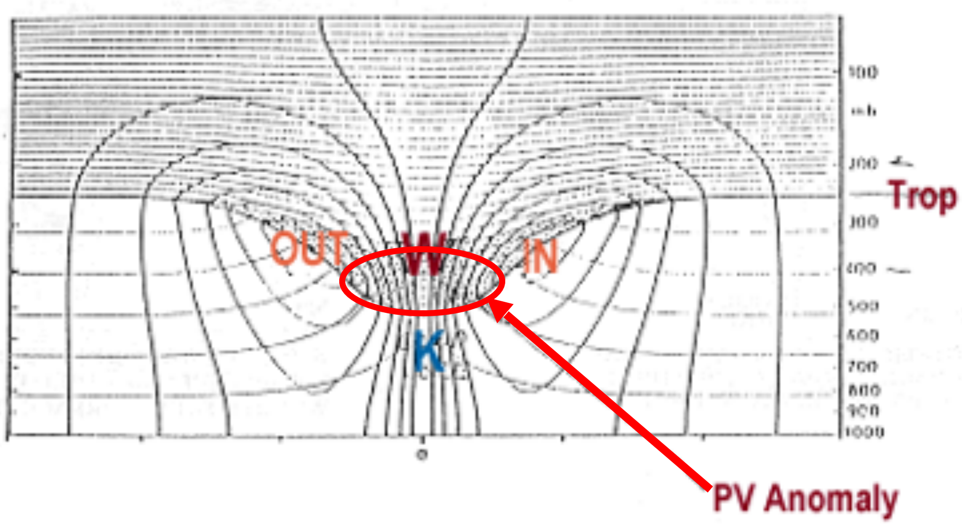

Upper-level PV anomalies: negative anomaly

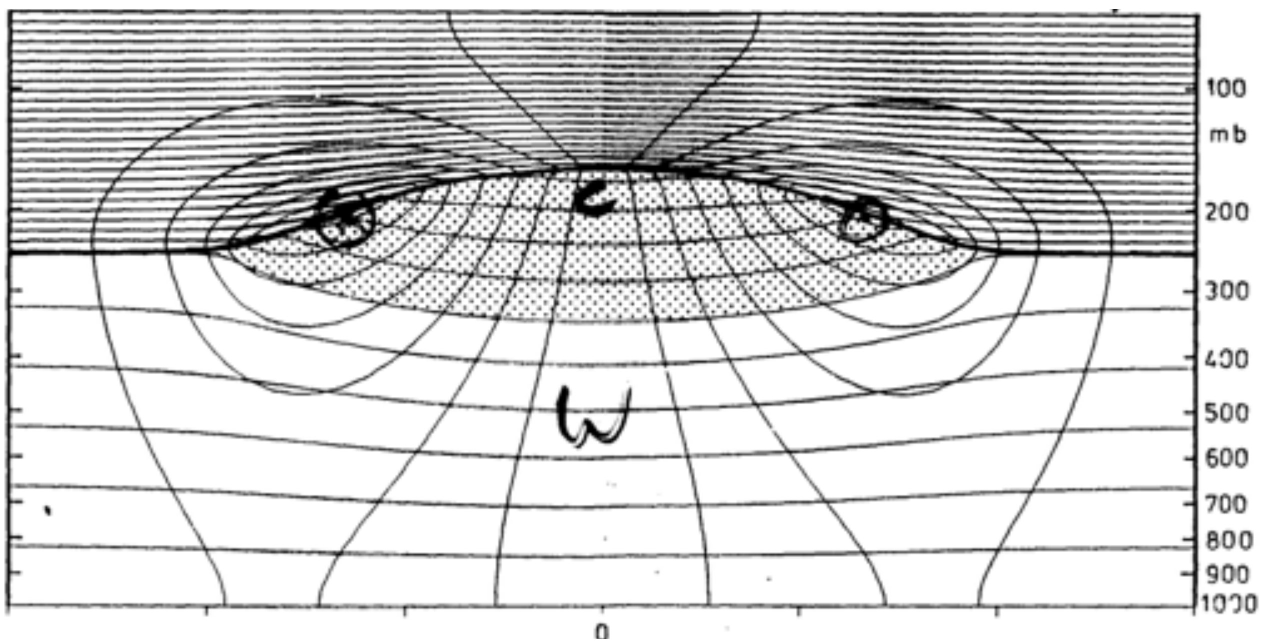

Ridge

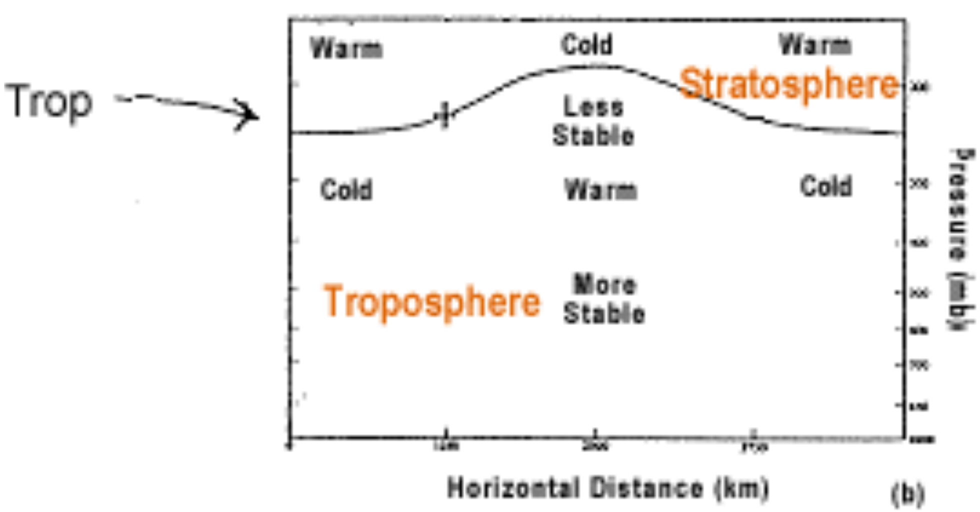

examples

UL positive PV′

UL negative PV′

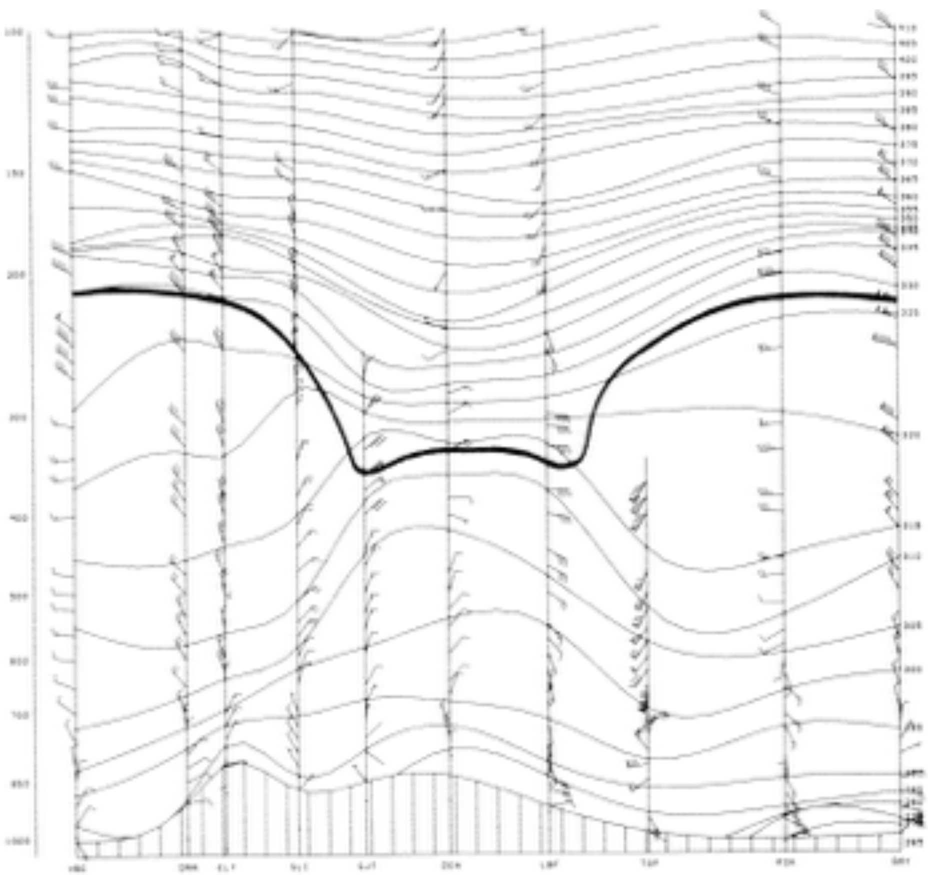

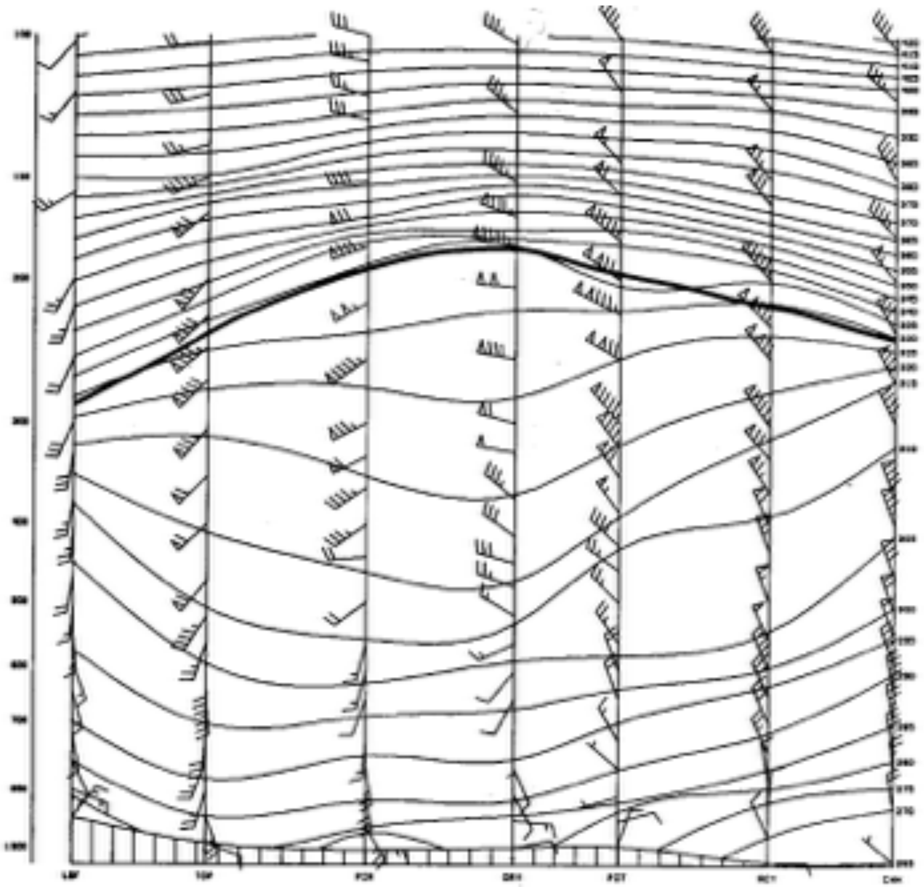

Isentropes and winds

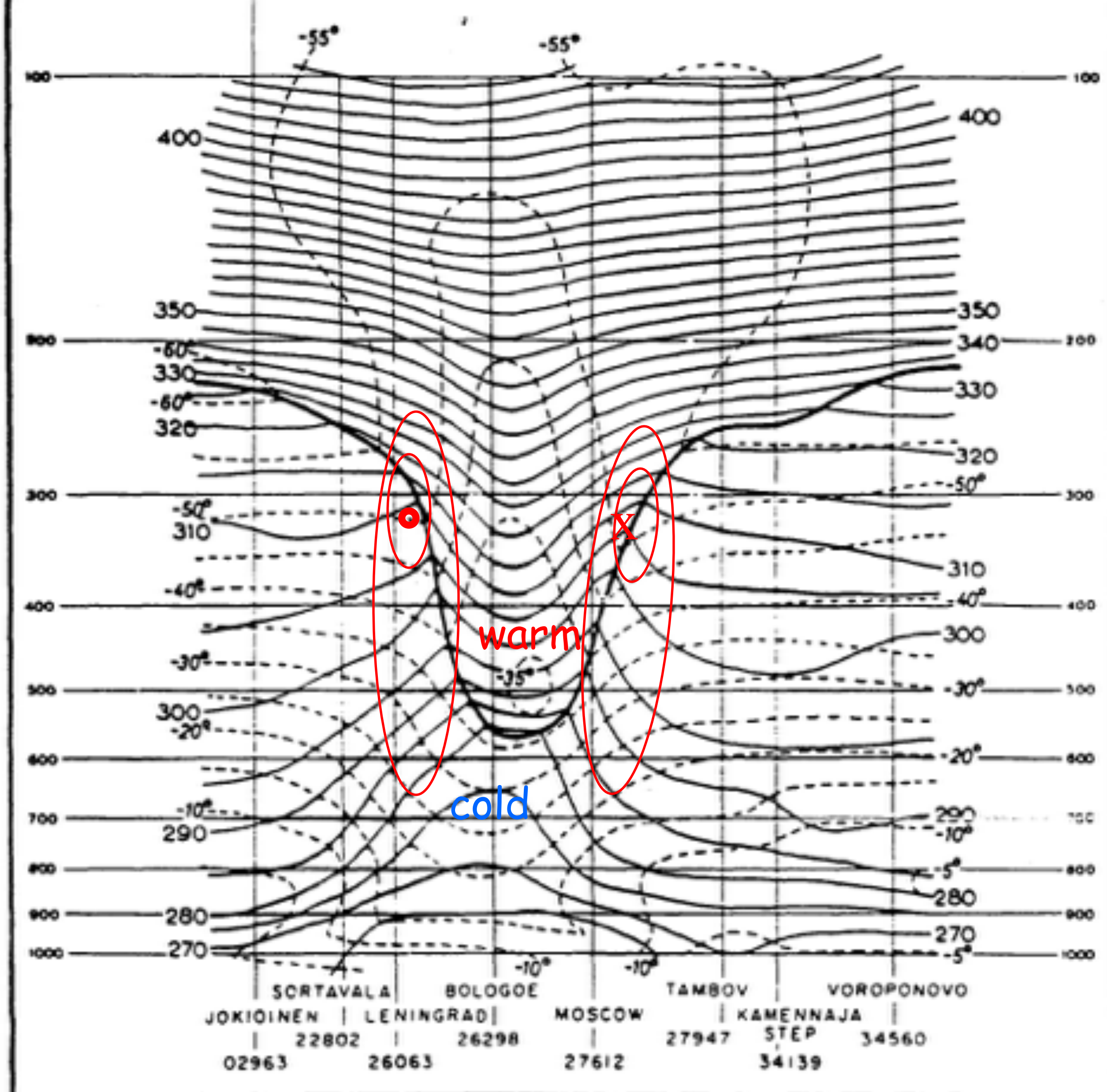

Fig 7 Vertical cross section through a cutoff low at 12Z on 16 November 1959 from Peltonnen (1963). The heavy line is the tropopause, dashed lines are isotherms every 5 C and light lines isentropes every 5 K.

P and θ contours

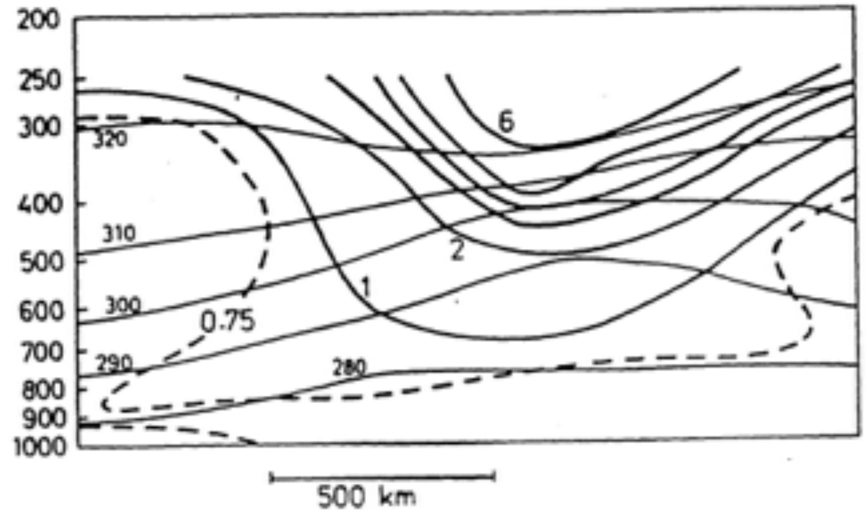

Fig 8 Vertical section of P (heavy lines) and θ (light lines) for the Icelandic low of 12 April 1983, derived from routine ECMWF analyses. Compare with Fig 2.

Positive PV’

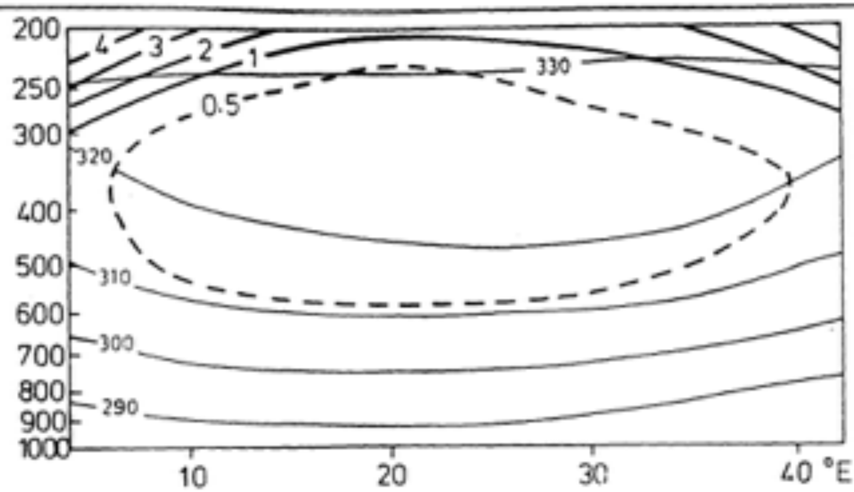

Fig 10 Cross section of P (heavy lines) and θ (light lines) through a blocking anticyclone, derived from routine ECMWF analyses. Note the warm core and the low P area below the tropopause.

Negative PV’

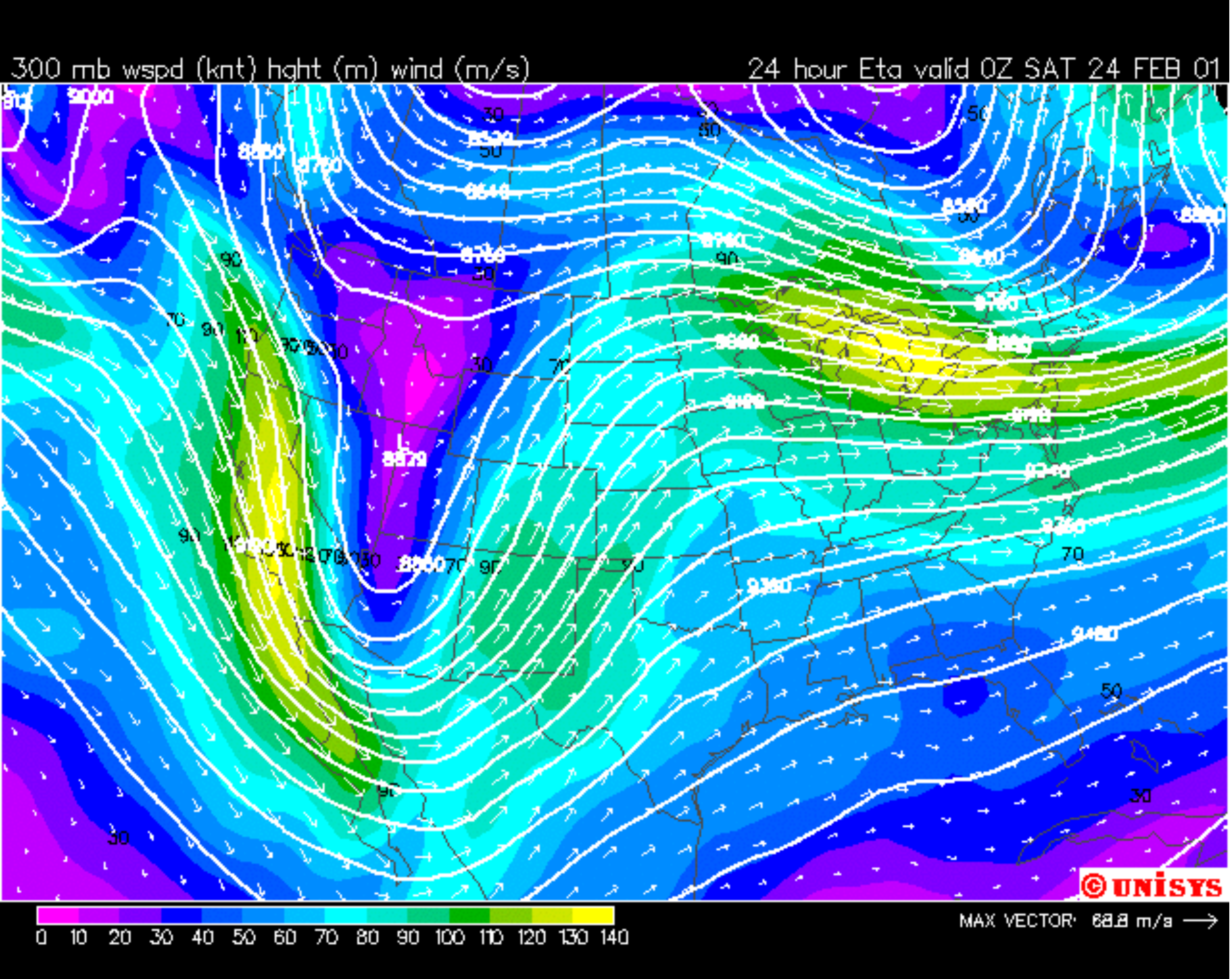
300 mb wspd (knt) hght (m) wind (m/s)
24 hour Eta valid 0Z SAT 24 FEB 01
0 10 20 30 40 50 60 70 80 90 100 110 120 130 140
MAX VECTOR 68.8 m/s
©UNISYS

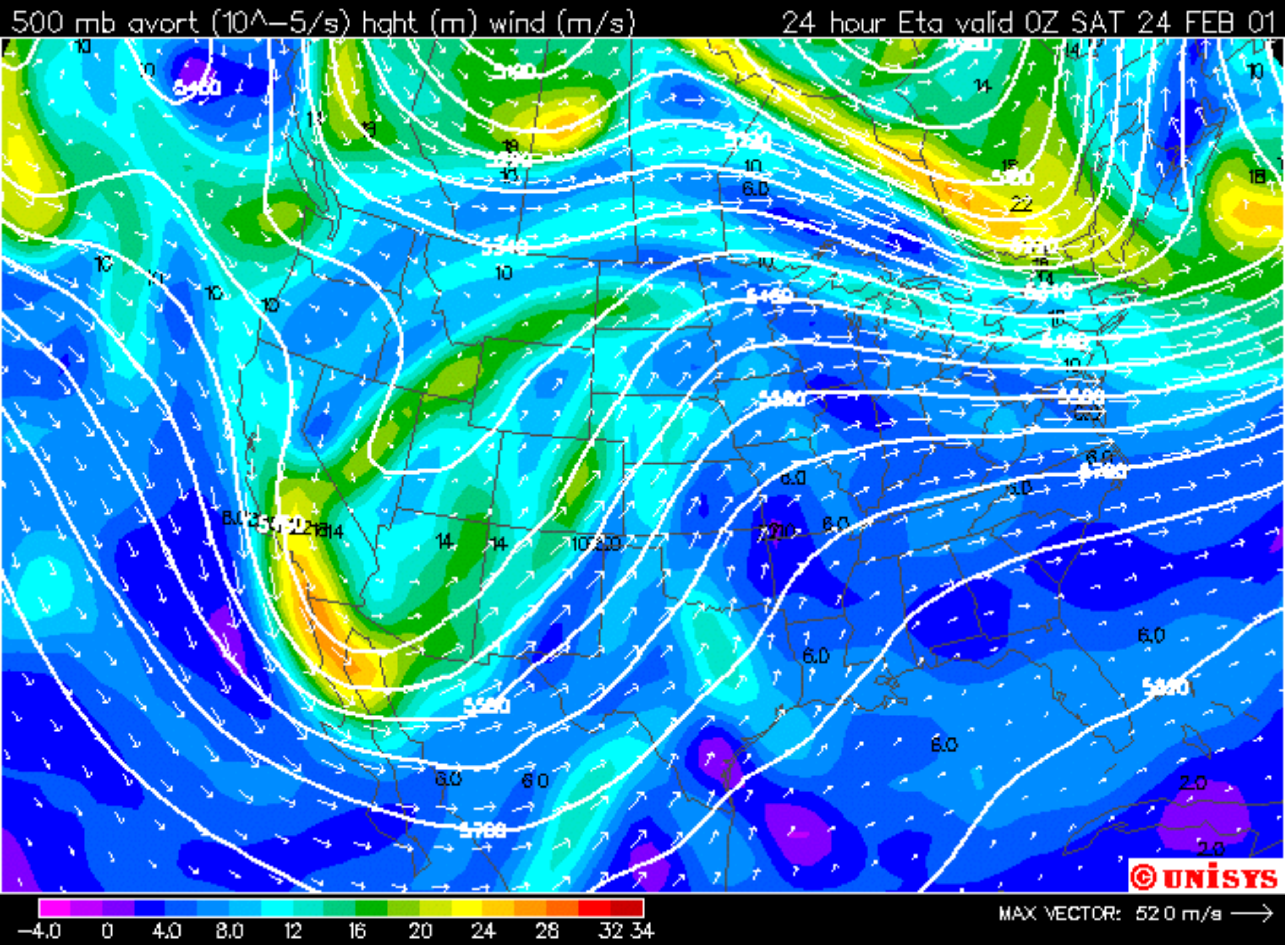
500 mb avort (10^-5/s) hght (m) wind (m/s)
24 hour Eta valid 0Z SAT 24 FEB 01
-4.0 0 4.0 8.0 12 16 20 24 28 32 34
MAX VECTOR: 52.0 m/s
© UNISYS

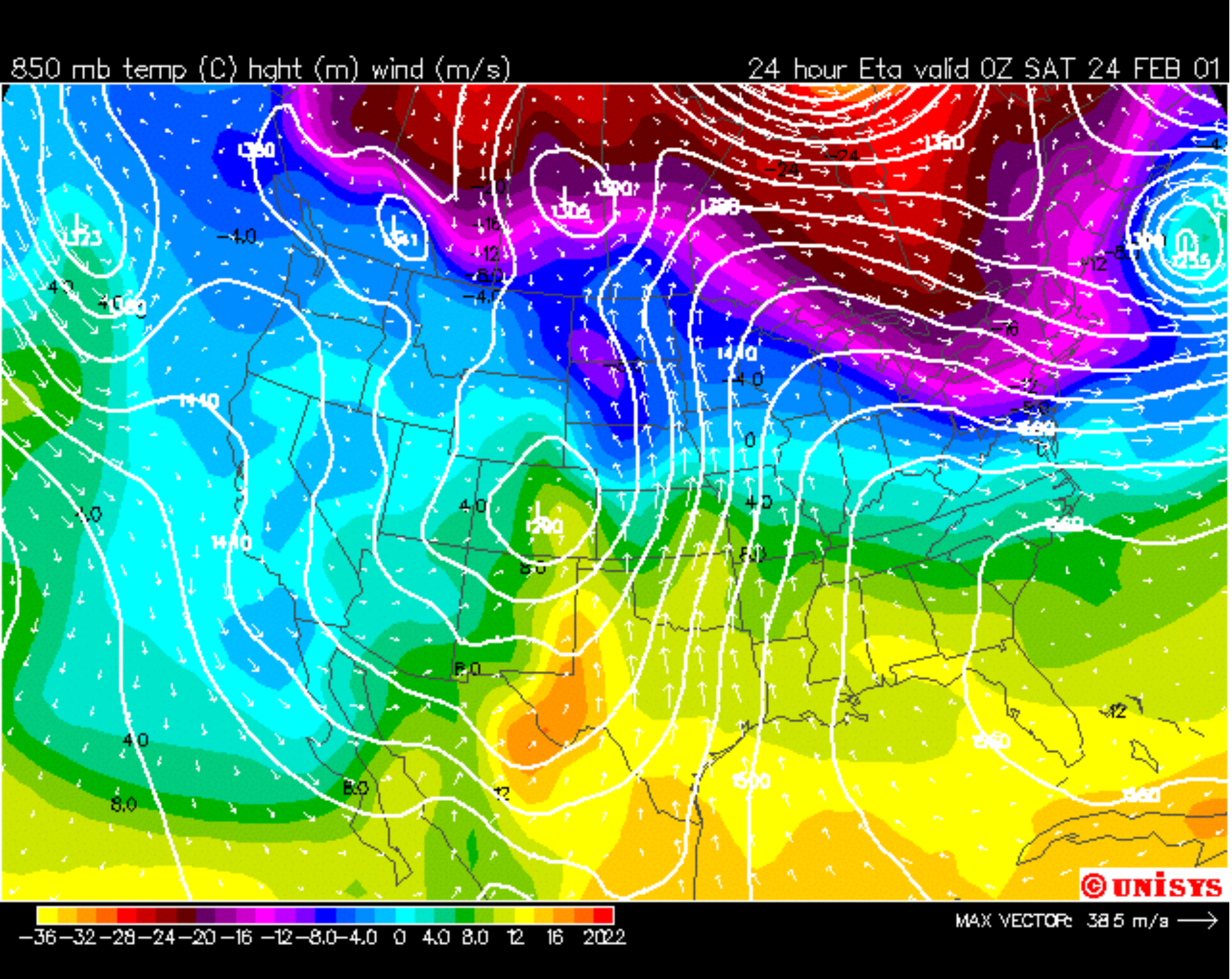
850 mb temp (C) hght (m) wind (m/s)
24 hour Eta valid 0Z SAT 24 FEB 01
−36 −32 −28 −24 −20 −16 −12 −8.0 −4.0 0 4.0 8.0 12 16 20 22
MAX VECTOR: 38.5 m/s
© UNISYS

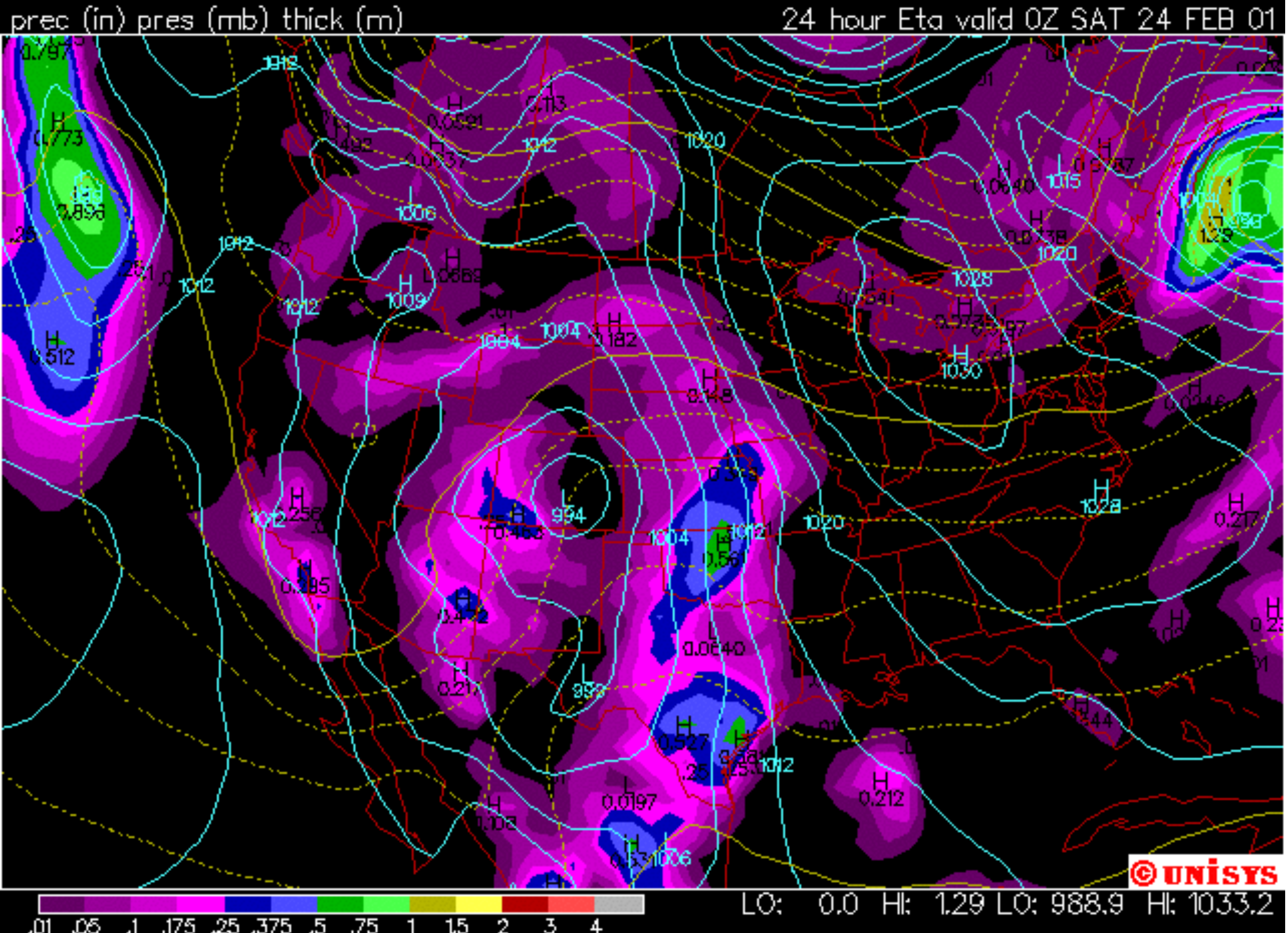
prec (in) pres (mb) thick (m)
24 hour Eta valid 0Z SAT 24 FEB 01
.01 .05 .1 .175 .25 .375 .5 .75 1 1.5 2 3 4
LO: 0.0 HI: 1.29 LO: 988.9 HI: 1033.2
© UNISYS

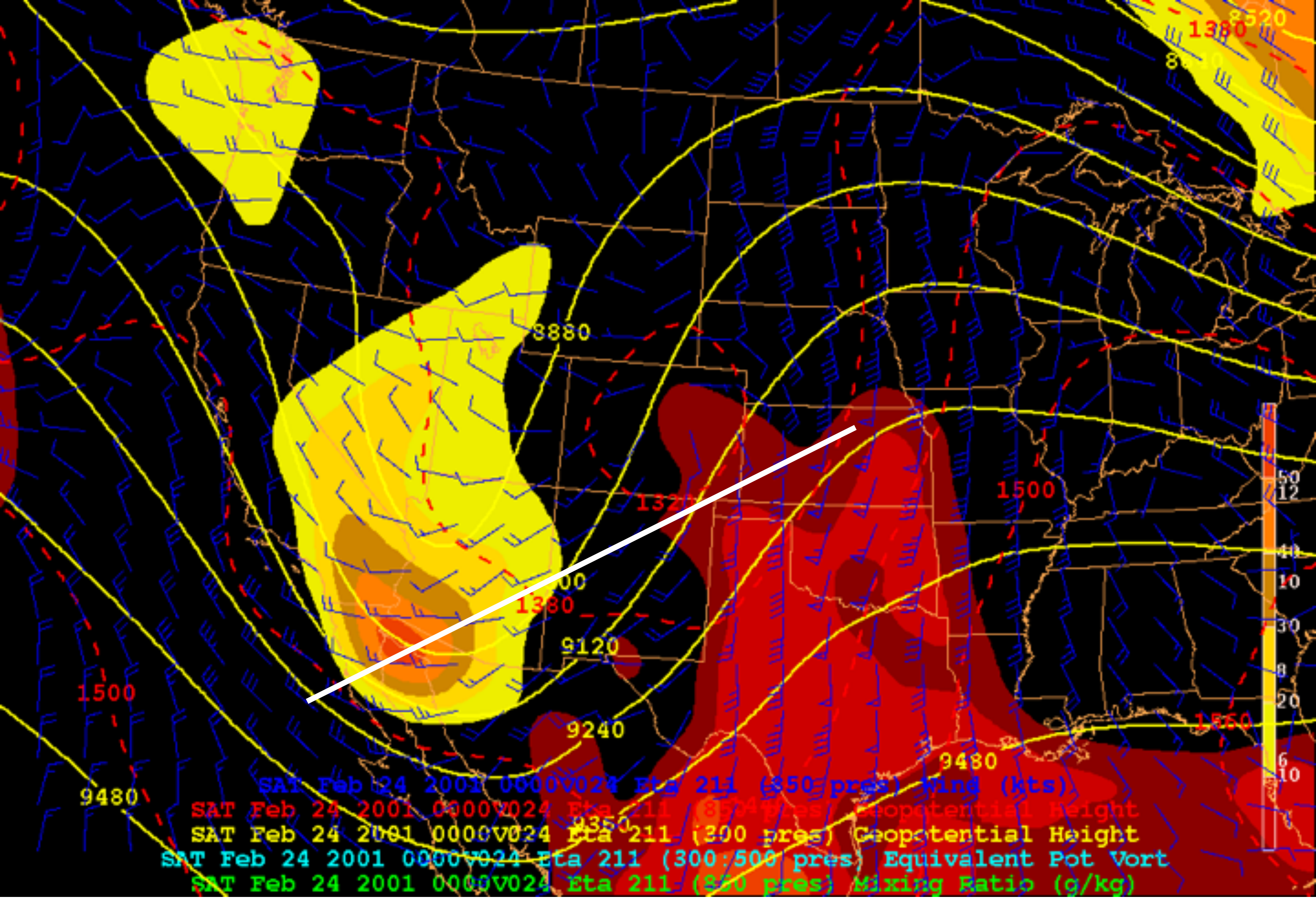

$$PV_e = \frac{\partial v_g}{\partial p}\frac{\partial \theta_e}{\partial x} - \frac{\partial u_g}{\partial p}\frac{\partial \theta_e}{\partial y} + (\zeta_g + f)\left(-\frac{\partial \theta_e}{\partial p}\right)$$ (see Martin, p. 226)

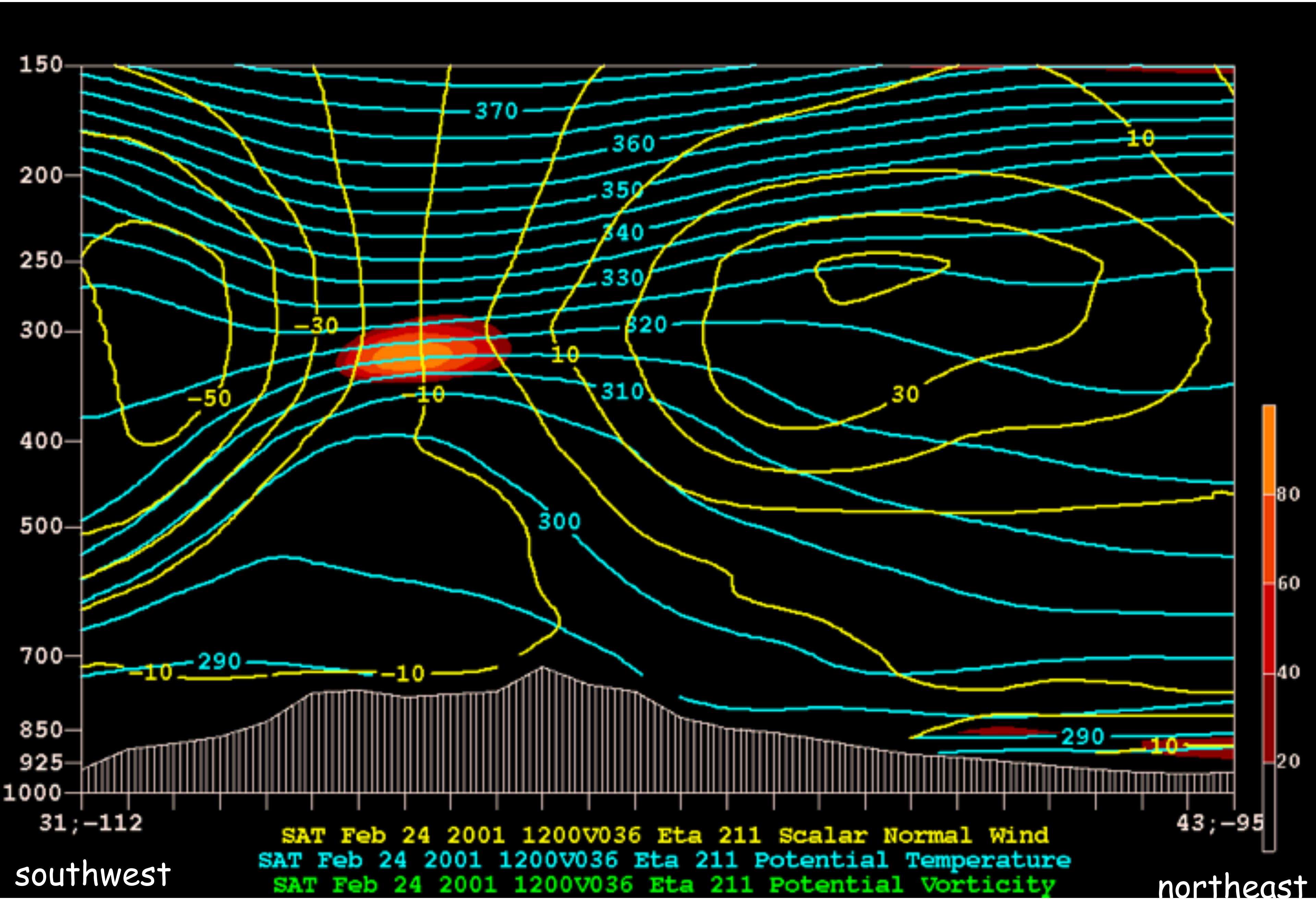

150
200
250
300
400
500
700
850
925
1000
370
360
350
340
330
320
310
300
290
290
10
10
30
-30
-50
-10
-10
-10
-10
10
20
40
60
80
31;-112
43;-95
SAT Feb 24 2001 1200V036 Eta 211 Scalar Normal Wind
SAT Feb 24 2001 1200V036 Eta 211 Potential Temperature
SAT Feb 24 2001 1200V036 Eta 211 Potential Vorticity
southwest
northeast

Low-level PV anomalies

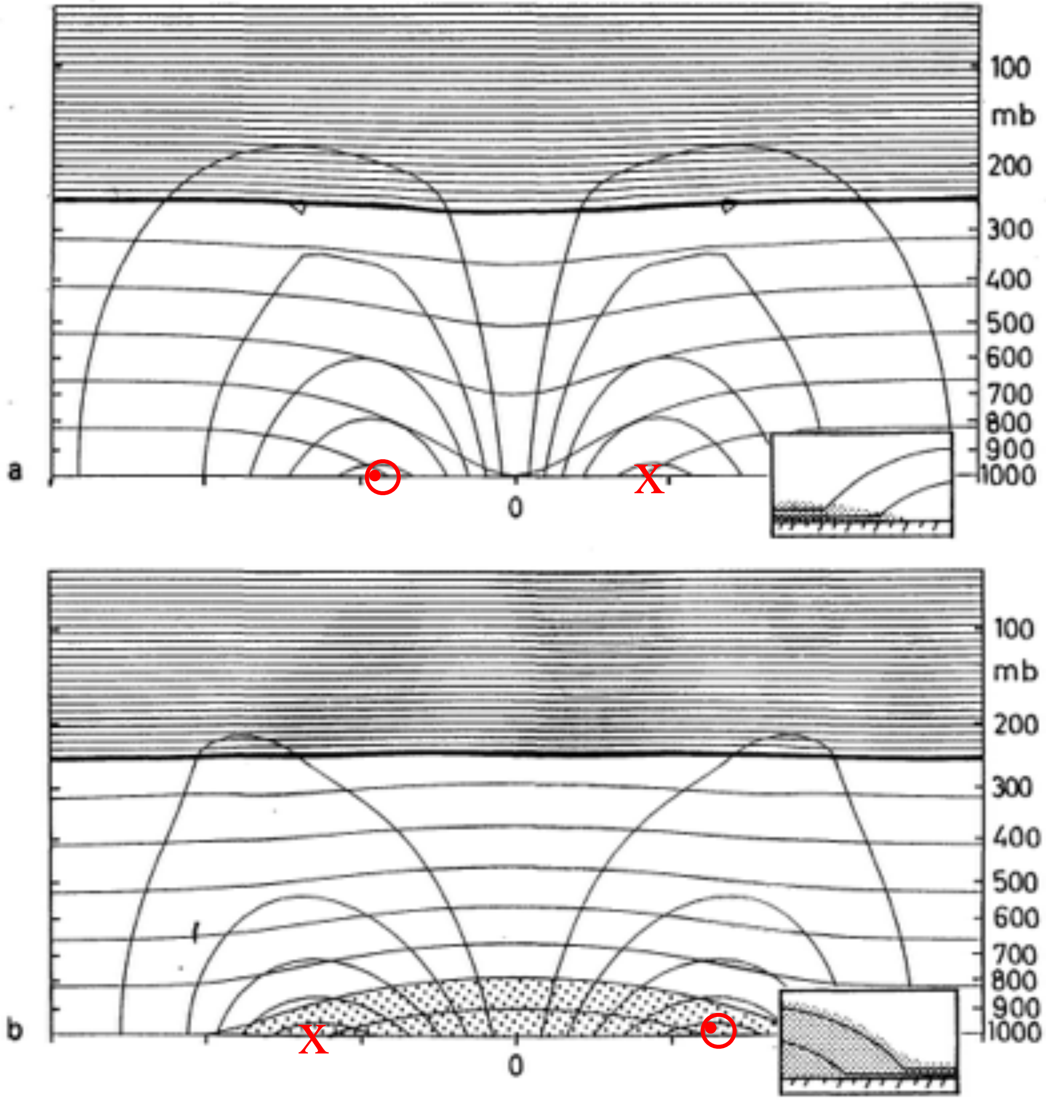

Figure 16.. Circularly symmetric flows induced by simple boundary temperature anomalies. The basic situation, and the method of solution, is as in Fig. 15 except that here there is no potential temperature variation along the tropopause, but the boundary potential temperature is taken to vary in the manner $\frac{1}{2}A\{\cos(\pi\bar{r}/r_0) + 1\}$ for $\bar{r} < r_0 = 1667$ km. The amplitude A was taken to be +10 K in (a) and −10 K in (b). The thick line again represents the tropopause, and the thin lines the isentropes every 5 K and the transverse velocity every 3 m s^{-1}. The zero isotach on the axis of symmetry is omitted. The warm anomaly induces a cyclonic circulation, and the cold anomaly an anticyclonic circulation. The surface pressure anomalies are −31 mb and +18 mb respectively, and the maximum (surface) winds are about 16 m s^{-1} and 17 m s^{-1} respectively. The relative vorticity extrema are at the surface and have values +0·8f and −0·5f respectively. The insets and stippling suggest the interpretation of the warm surface potential temperature anomaly as equivalent to a cyclonic IPV anomaly, and the cold surface potential temperature anomaly as part of an anticyclonic IPV anomaly (see text). For more details of the method of computation, see Thorpe (1985). Courtesy of A. J. Thorpe.

Low-level positive PV anomaly

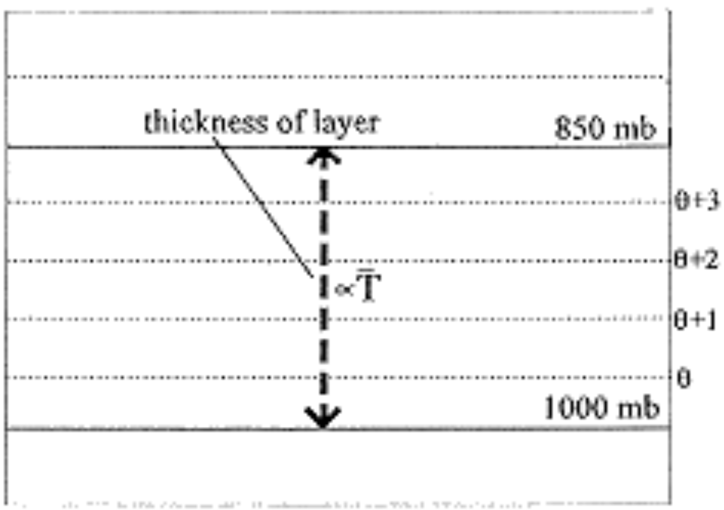

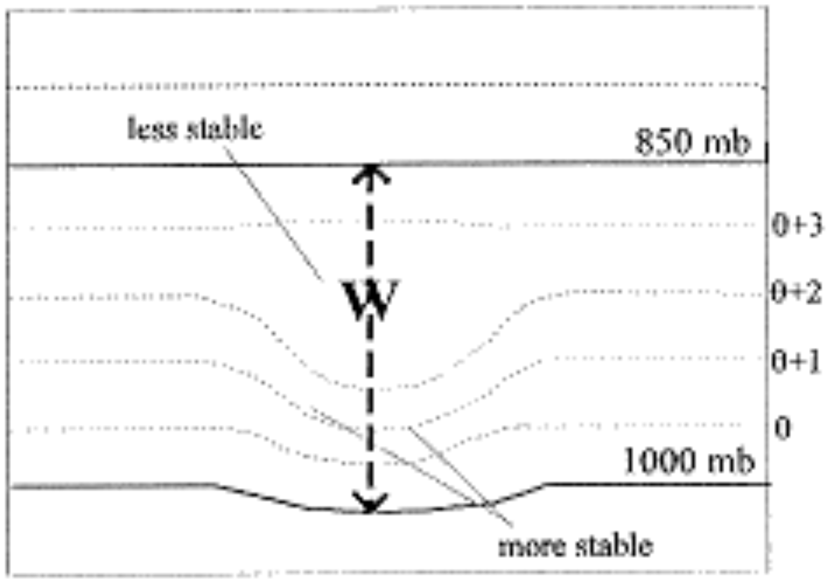

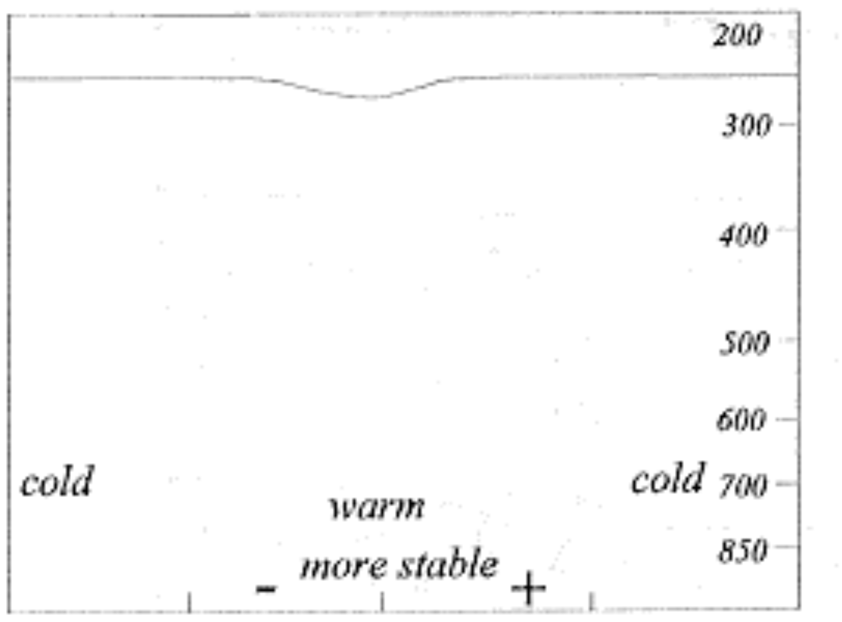

$$v_g(p_{850}) - v_g(p_{1000}) = K\left(\frac{\partial \theta}{\partial x}\right)$$

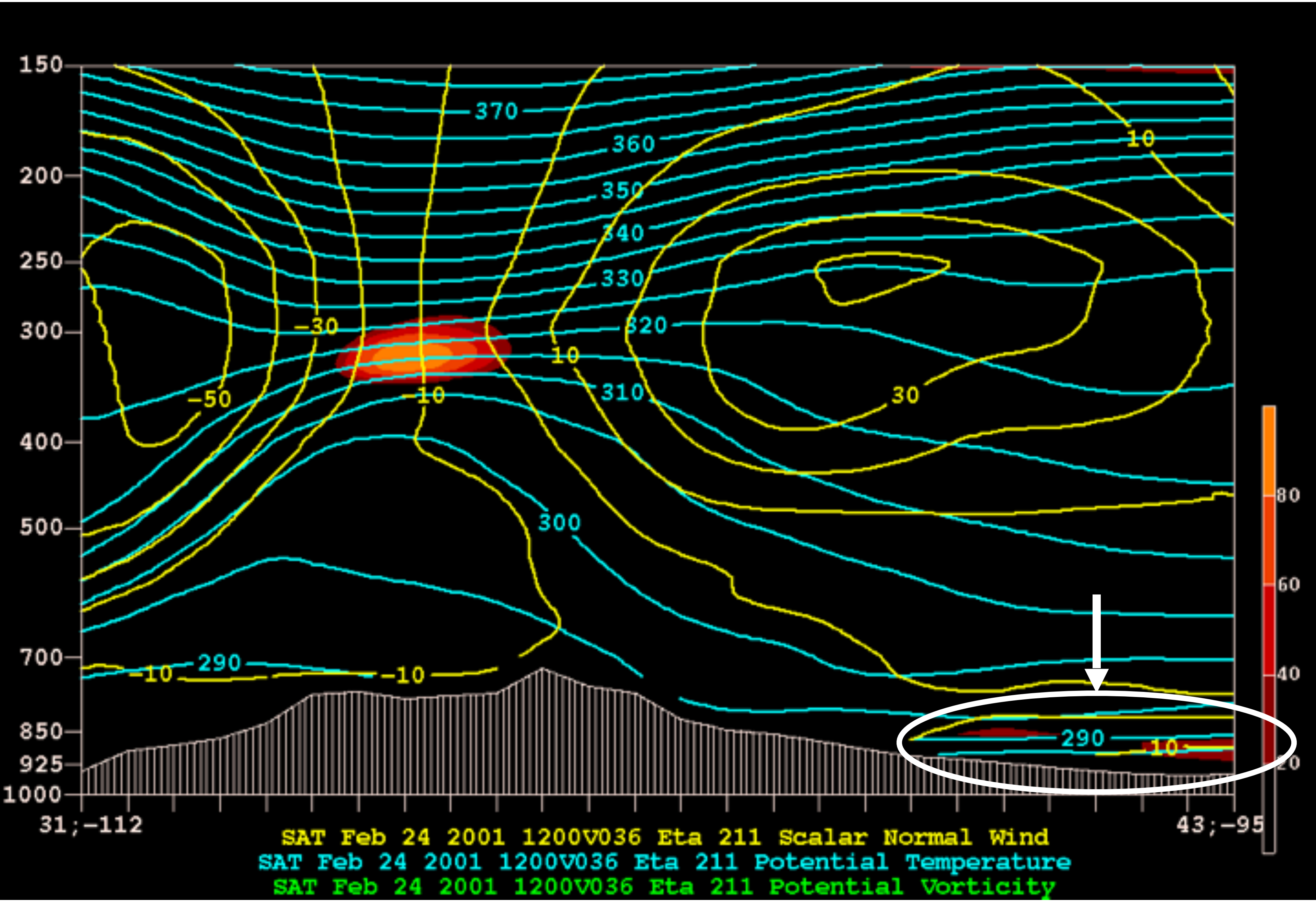
150
200
250
300
400
500
700
850
925
1000
370
360
350
340
330
320
310
300
290
-30
-50
-10
10
30
80
60
40
20
31;-112
43;-95
SAT Feb 24 2001 1200V036 Eta 211 Scalar Normal Wind
SAT Feb 24 2001 1200V036 Eta 211 Potential Temperature
SAT Feb 24 2001 1200V036 Eta 211 Potential Vorticity

Diagnosis of vertical motion

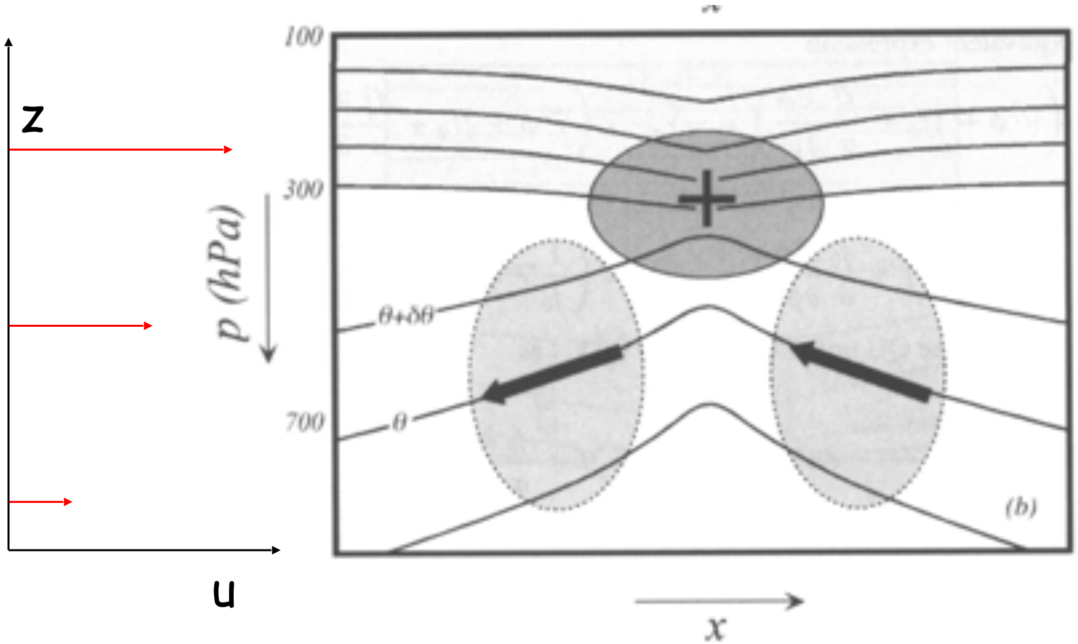

UL positive PV anomaly moves in from the west (left)

“storm”-relative adiabatic motion is shown

- in general, consider both UL and LL forcing
- assume a stationary pattern – locally temperature and vorticity remain unchanged
- uplift is due to a parcel’s adjustment to vorticity or temperature advection.

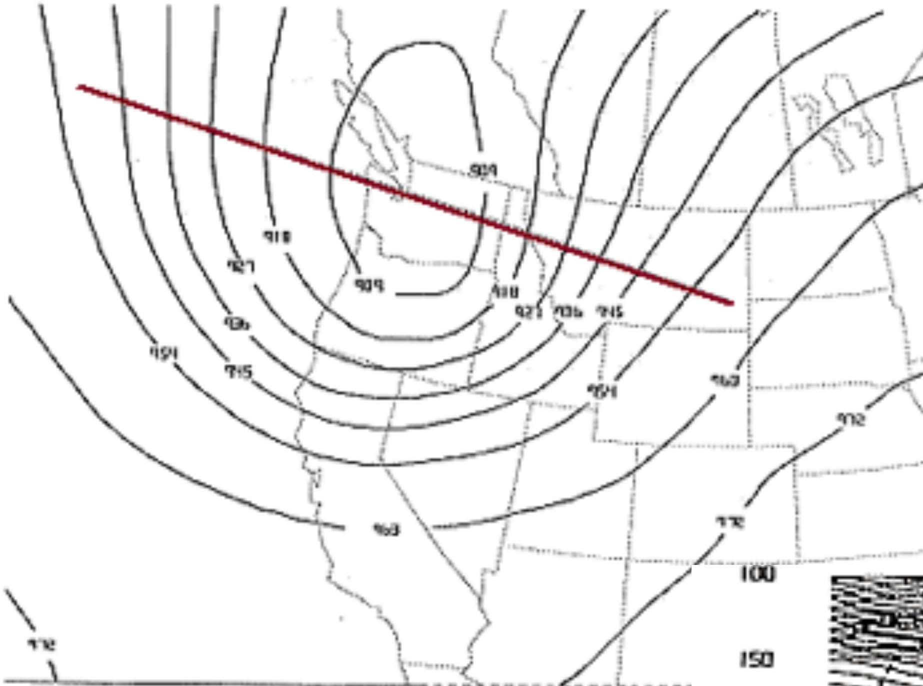

300 mb height

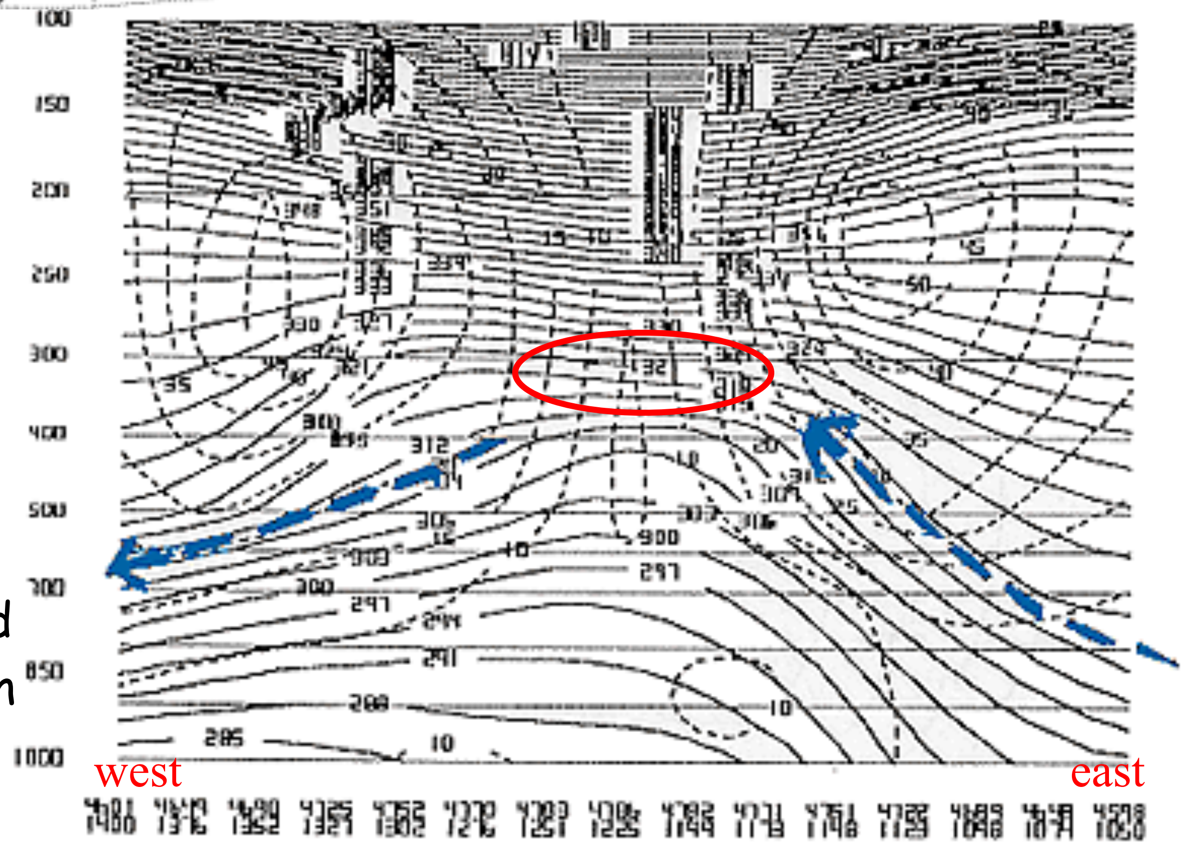

Cross section west-east

solid: θ

dashed: wind speed normal to x-section

	Vorticity conservation	Temperature conservation

Upper-level +PV'

Vorticity conservation

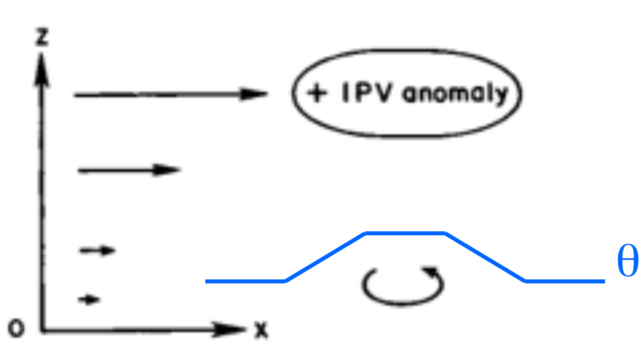

assume a IPV anomaly-relative frame of reference
the local PV (and abs vort) remain unchanged
then look at the QG vort eqn

$$\frac{\partial \zeta_g}{\partial t} = 0 = -\vec{v}_g \cdot \nabla_p (\zeta + f) + f\frac{\partial \omega}{\partial p}$$

$or\ CVA = f\delta \quad \delta = divergence$

consistency with QG thinking

$$\boxed{\frac{\partial AVA}{\partial z} < 0 \approx \frac{\partial CVA}{\partial z} > 0 \Rightarrow w > 0}$$

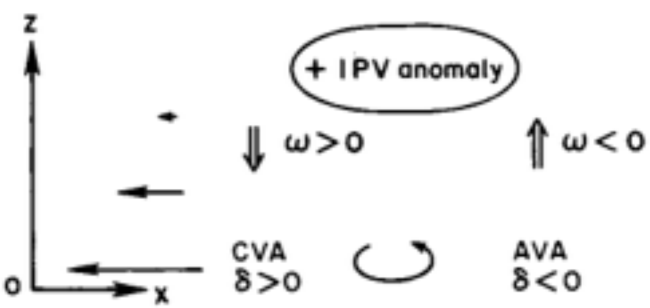

Temperature conservation

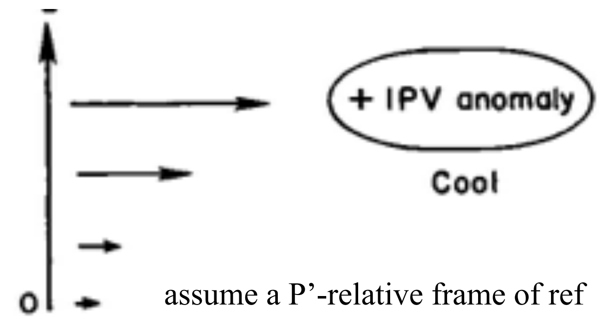

assume a P'-relative frame of ref
the P (and T) remain unchanged
then look at the QG 1st law of TD

$$\frac{\partial T}{\partial t} = 0 = -\vec{v}_g \cdot \nabla_p (T) + \frac{\sigma p \omega}{R}$$

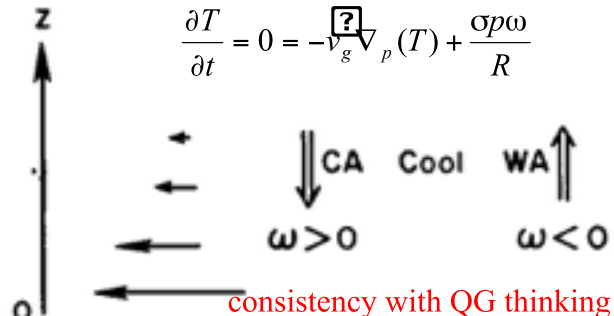

consistency with QG thinking

$$\boxed{WAA \Rightarrow w > 0}$$

Low-level +PV'

Vorticity conservation

consistency with QG thinking

$$\boxed{\frac{\partial AVA}{\partial z} > 0 \Rightarrow w < 0}$$

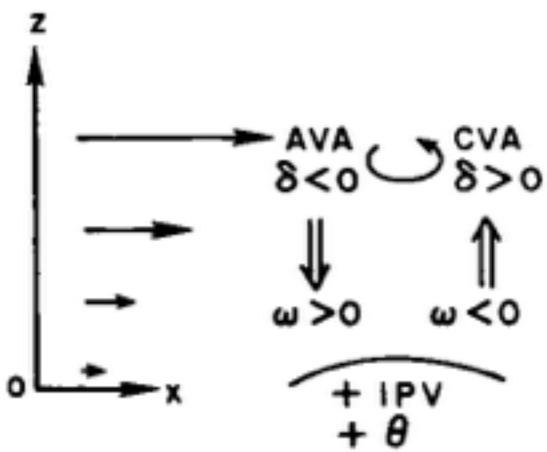

Temperature conservation

consistency with QG thinking

$$\boxed{WAA \Rightarrow w > 0}$$

Motion of upper-level trofs & ridges

find the anomaly propagation direction

see Fig. 9.8 in Martin (2006)

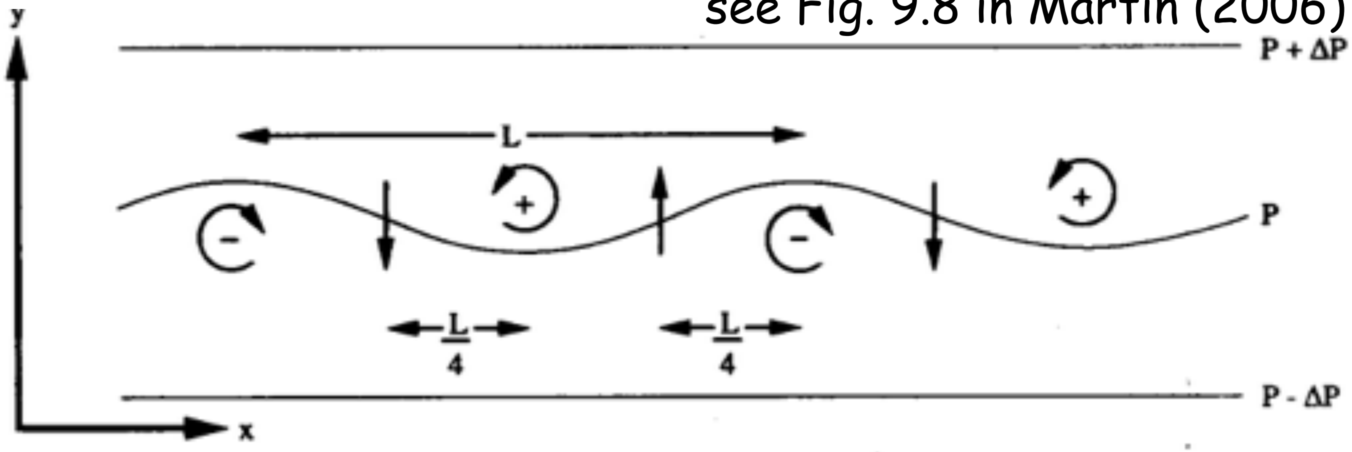

Motion of low-level PV anomalies

see Fig. 9.9 in Martin (2006)

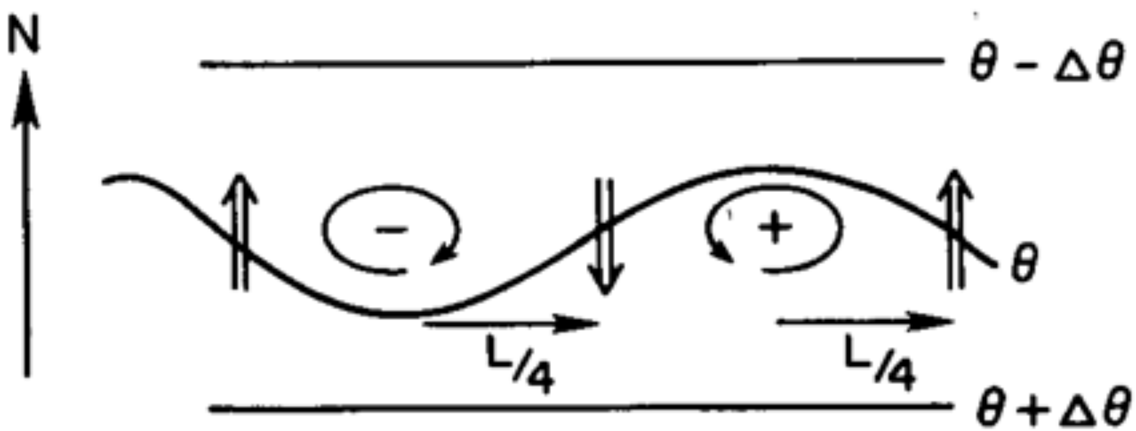

Lateral (or vertical) Rossby wave propagation

time 1

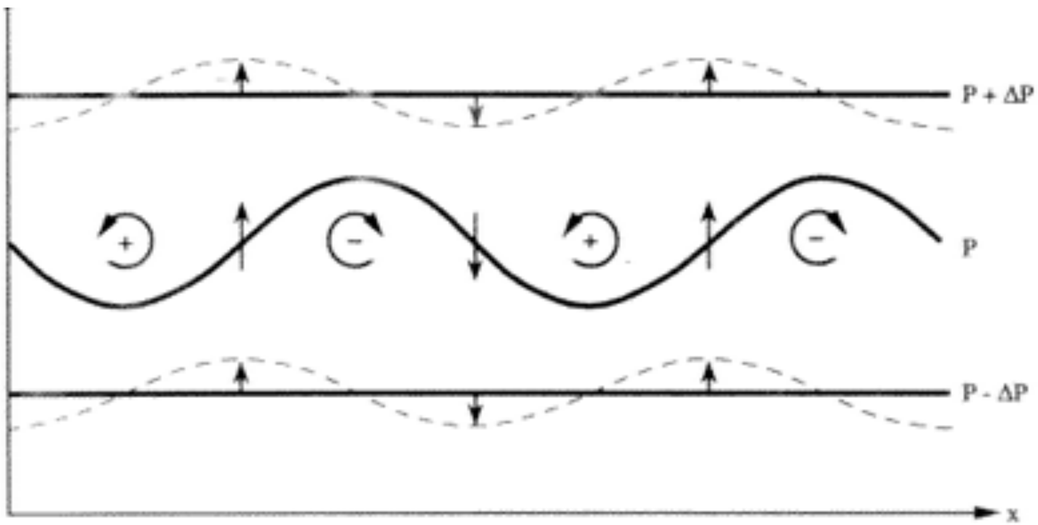

time 2

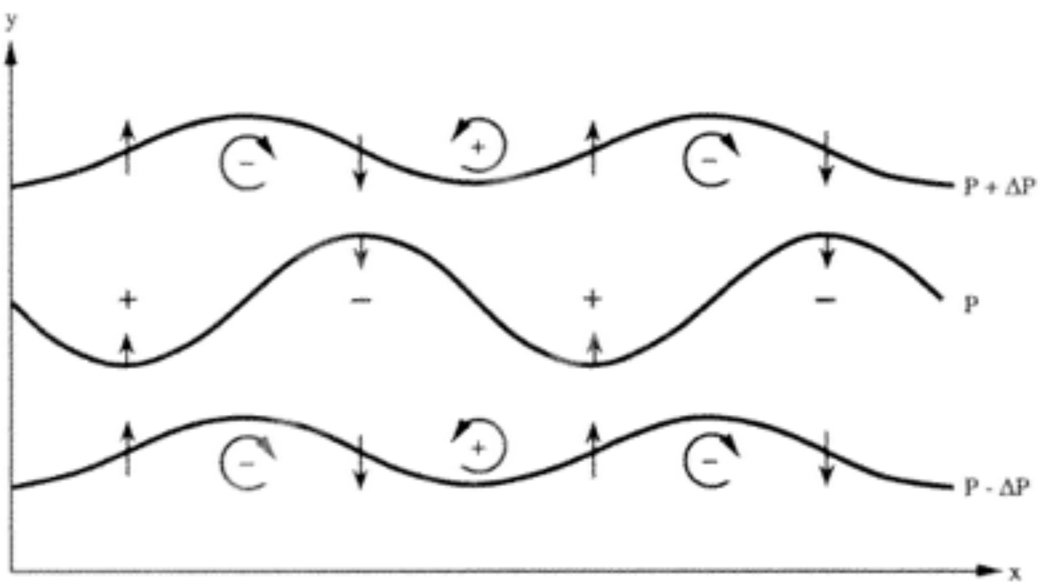

energy is dispersed laterally

- wave energy created to the side
- local wave energy decreases

Motion of low-level PV anomalies near a mountain range

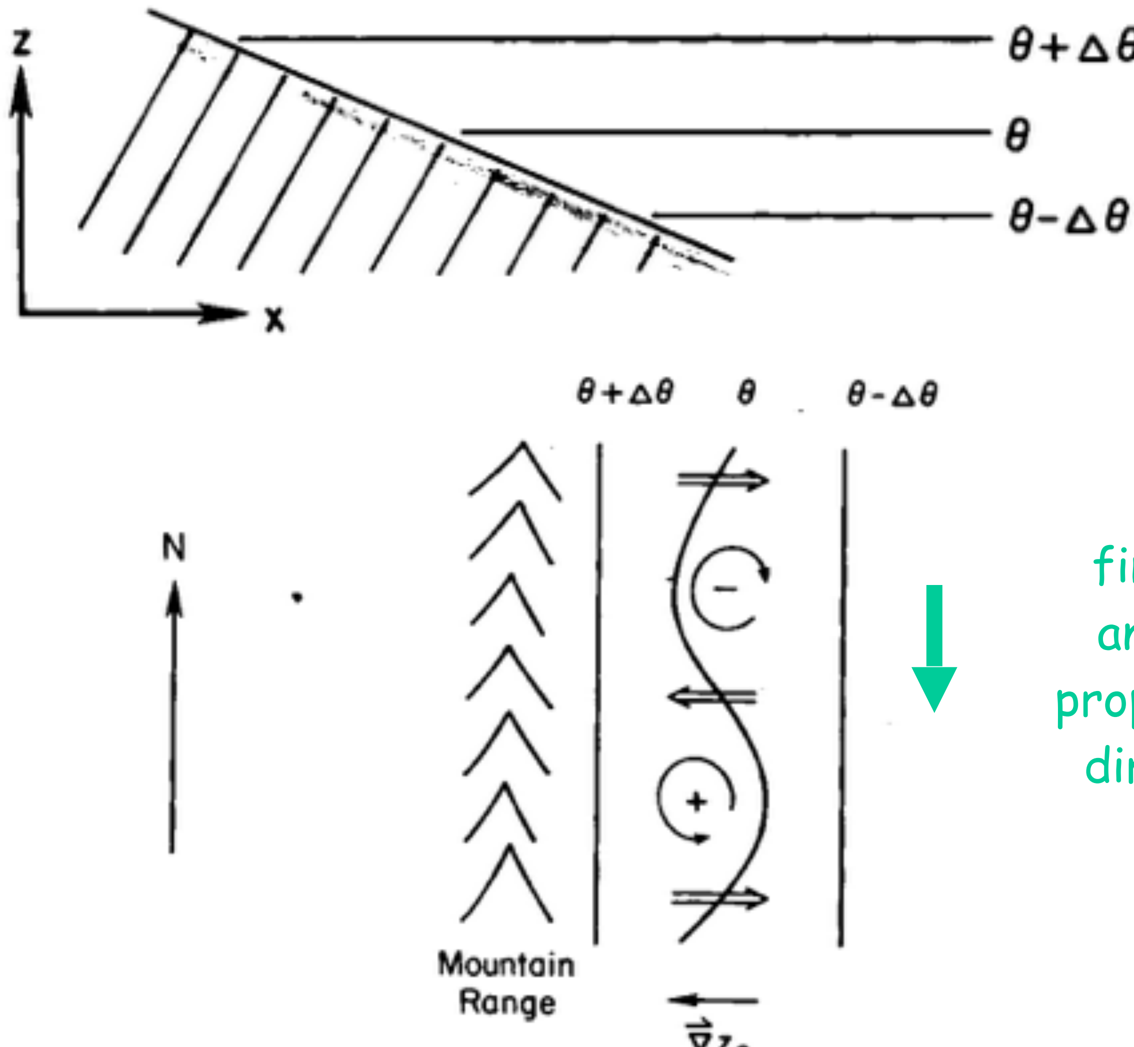

find the anomaly propagation direction

Chapter 9.3: baroclinic instability in terms of IPV thinking

UL-LL PV' interaction

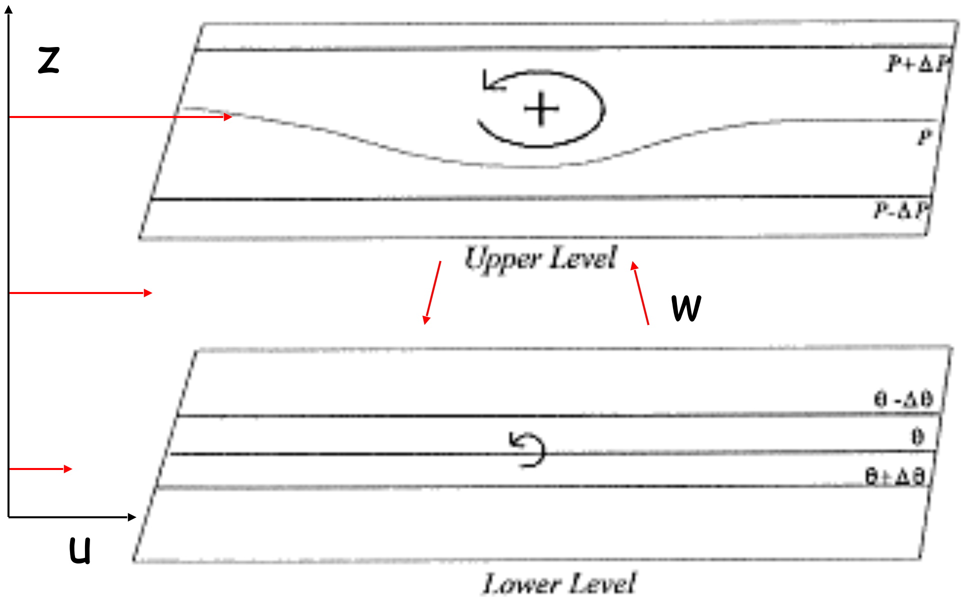

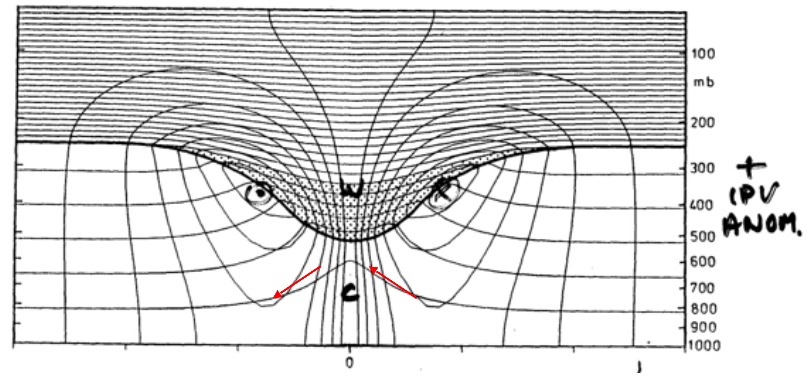

step 1: UL positive PV anomaly induces circulation in LL baroclinic region

UL-LL PV' interaction: baroclinic instability

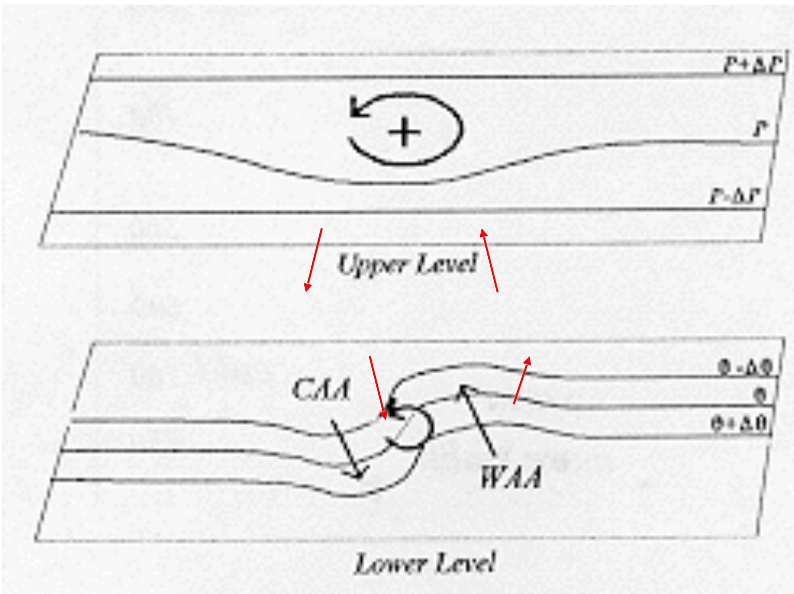

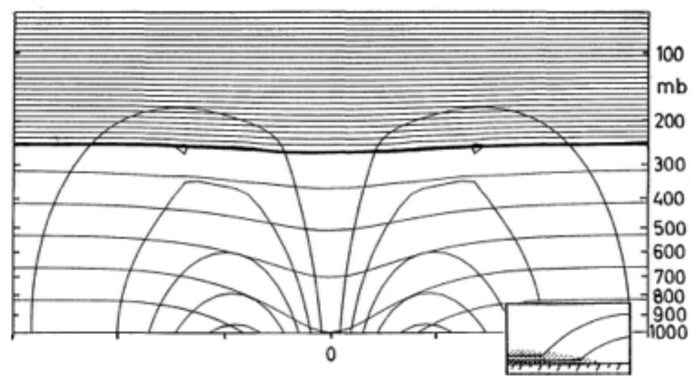

step 2: this circulation creates a LL pos PV anomaly, due to WAA

UL-LL PV' interaction: baroclinic instability

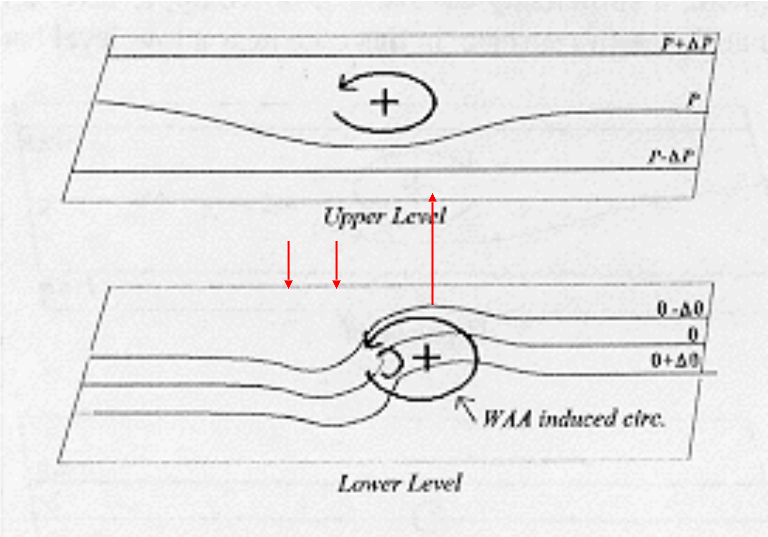

step 3: LL pos PV anomaly strengthens, and influence is felt aloft

UL-LL PV' interaction: baroclinic instability

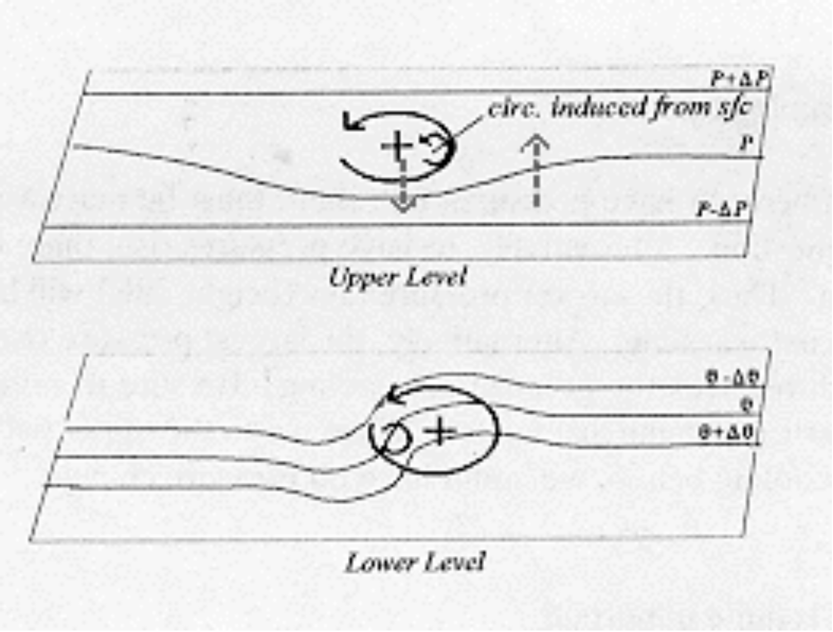

step 4: LL pos PV anomaly induces circulation aloft, which intensifies UL pos PV anomaly. This two-way interaction is baroclinic instability in terms of PV.

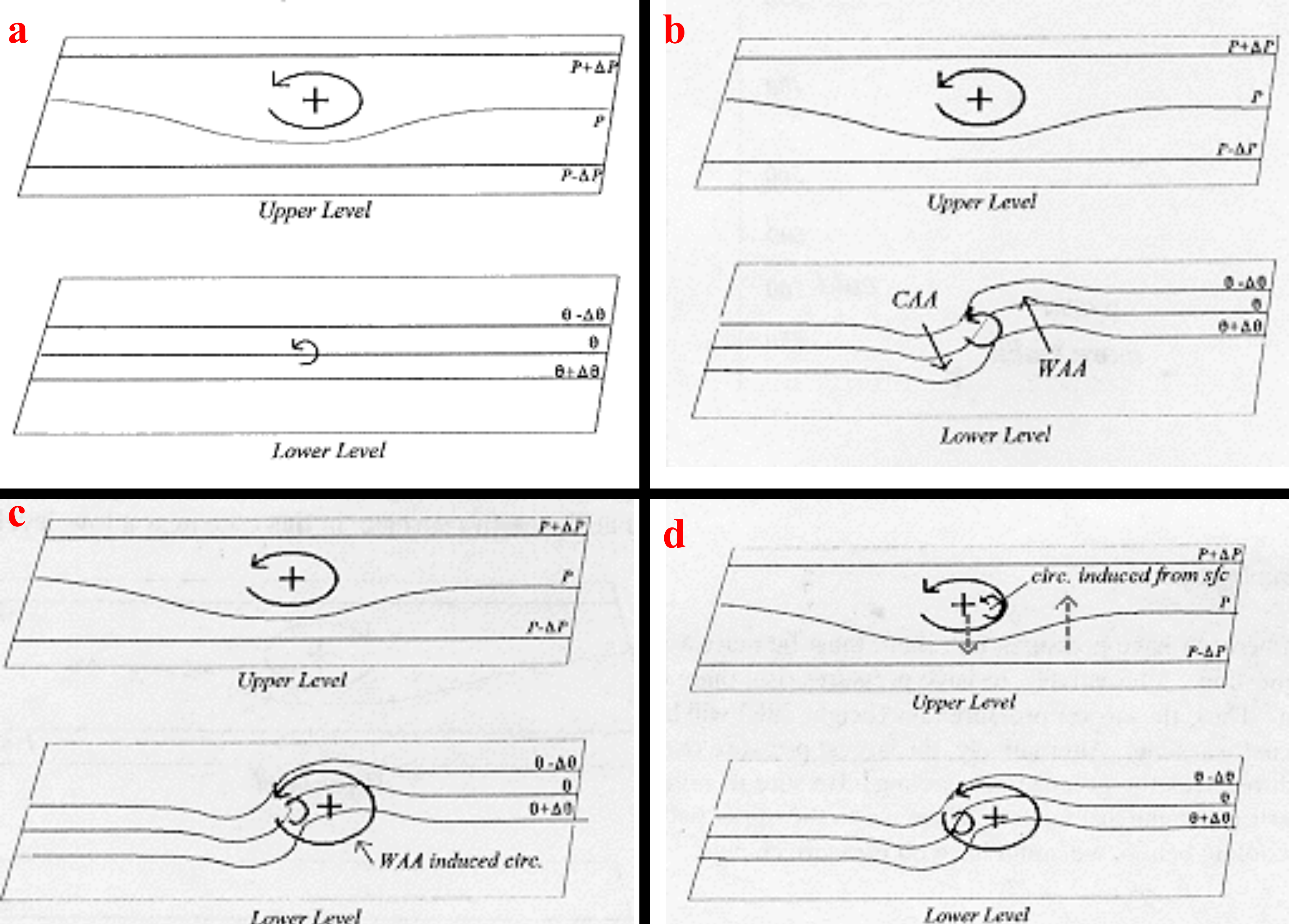

Baroclinic instability & lifecycle

UL-LL PV' interaction: baroclinic instability

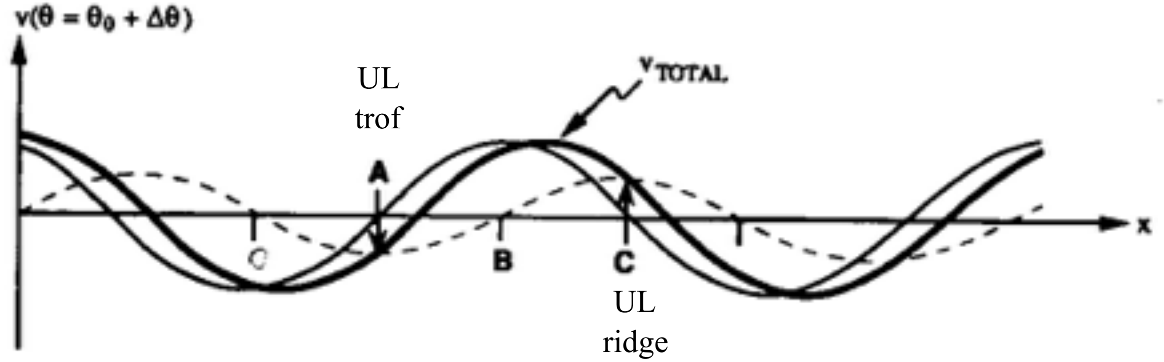

➔Westward tilt with height is baroclinically unstable
➔ Surface and UL anomalies may "lock" on to each othe

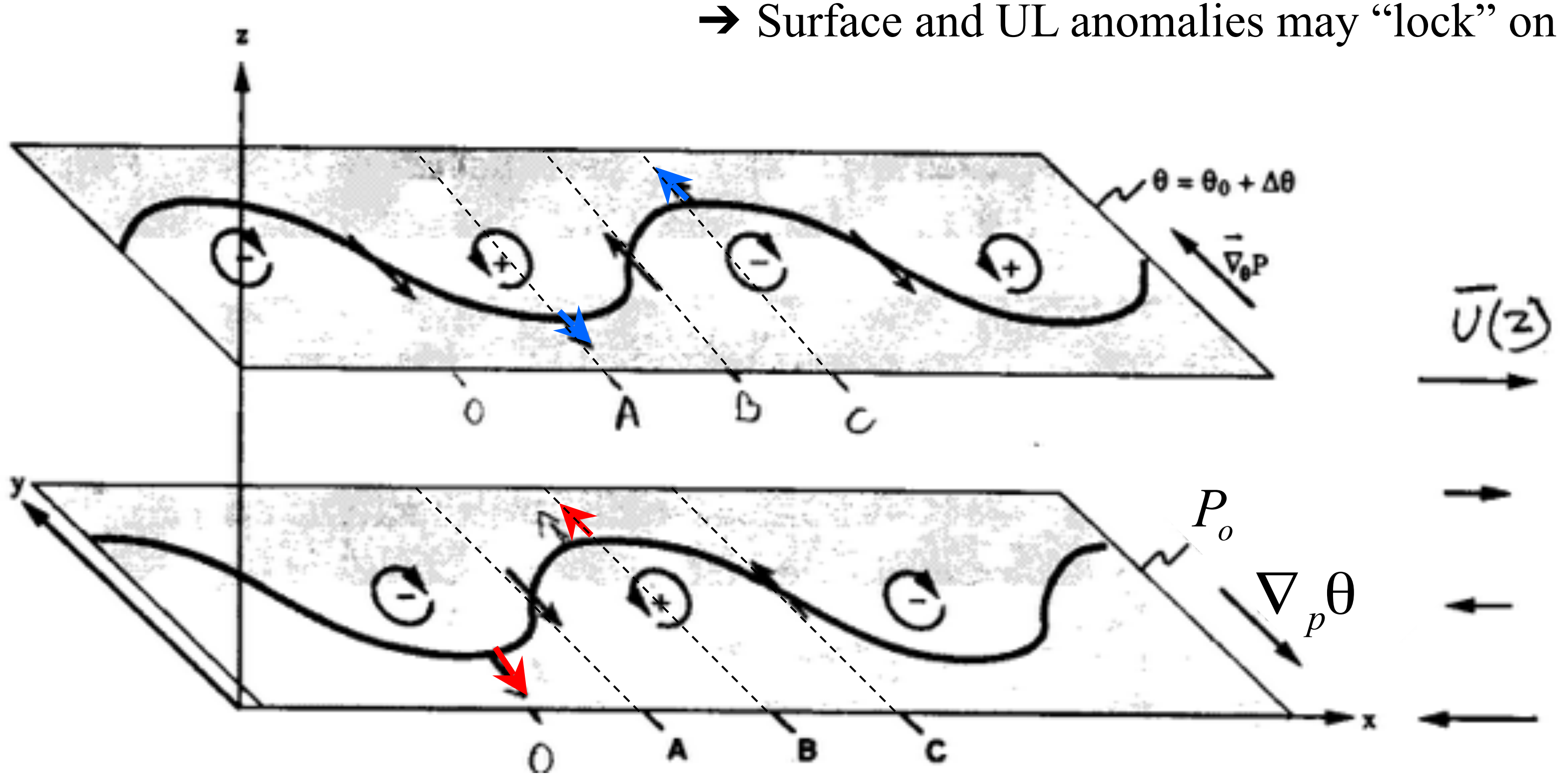

red: UL PV anomaly affecting low-levels blue: LL PV anomaly affecting upper-le

Baroclinic wave evolution (non-linear effects)

If a number of baroclinic developments occur close together, with surface and UL systems well locked, then a low-index flow (u small) regime develops, as if the P' was blocked by 'walls' to N & S. Remember that baroclinic energy tends to spread meriodionally.

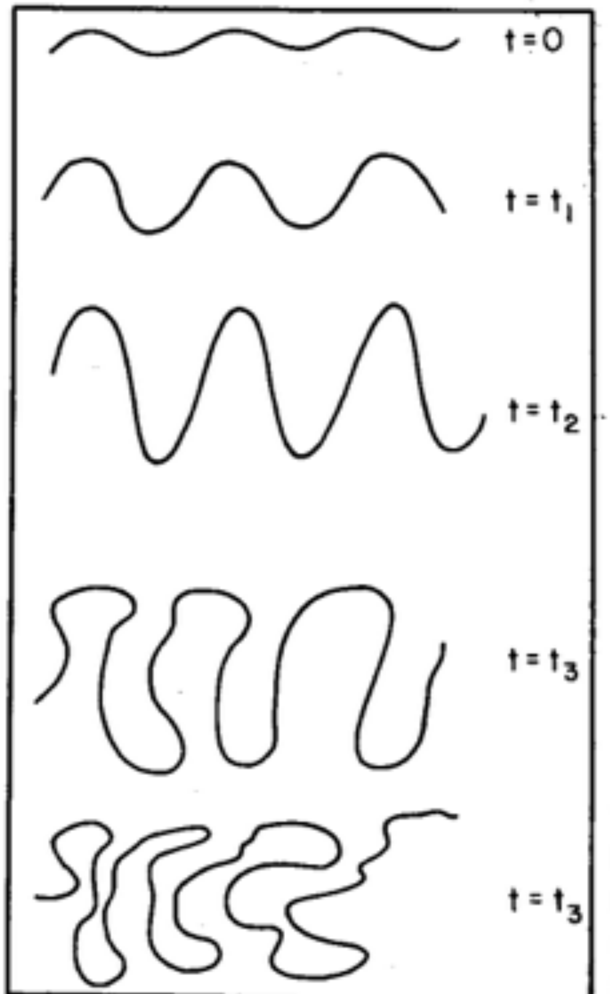

If the mean flow U varies with latitude, the PV anomalies become tilted
(here we are south of the main jet, or du/dy>0 → tilt >0)

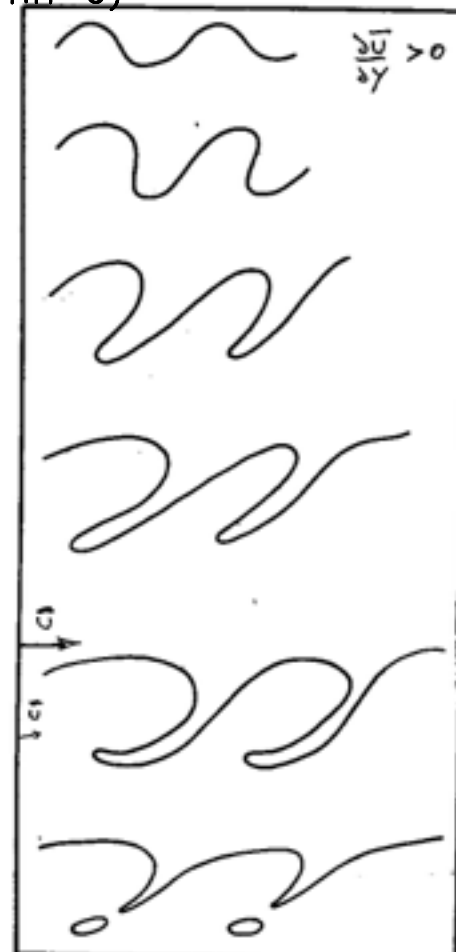

Baroclinic instability – an IPV perspective

- An upper level PV anomaly approaches a low-level baroclinic band.
- The circulation associated with the upper level PV anomaly is felt throughout the troposphere so that a low-level circulation begins along the low-level baroclinic band (induction)
- The low-level circulation produces and enhances regions of warm and cold advection in the lower levels.
- A surface low pressure area forms in the warm pool, in a region with a history of low-level warm air advection
  - Warm air advection produces a + PV anomaly and the largest surface pressure falls .
  - Hydrostatically, the resulting low pressure center is more a result of low-level tropospheric warming versus upper-level stratospheric warming.
- The circulation associated with this low-level +PV anomaly is felt through the entire troposphere. The upper portion of this effect helps to amplify the upper level +PV anomaly and to slow its progress.
- This strengthening upper PV anomaly, in turn, strengthens the surface anomaly and so on (mutual amplification).
- As the upper level PV anomaly strengthens, the upper level stratospheric warm air advection begins to dominate the lower level warm advection region in terms of net column warming. Thus, the surface low begins to fall back into the cold tropospheric air underneath the warm column.
- Eventually the surface low falls directly beneath the upper level warm pool. The system slowly fills and the process is complete.

Meridional PV' interaction: barotropic instability

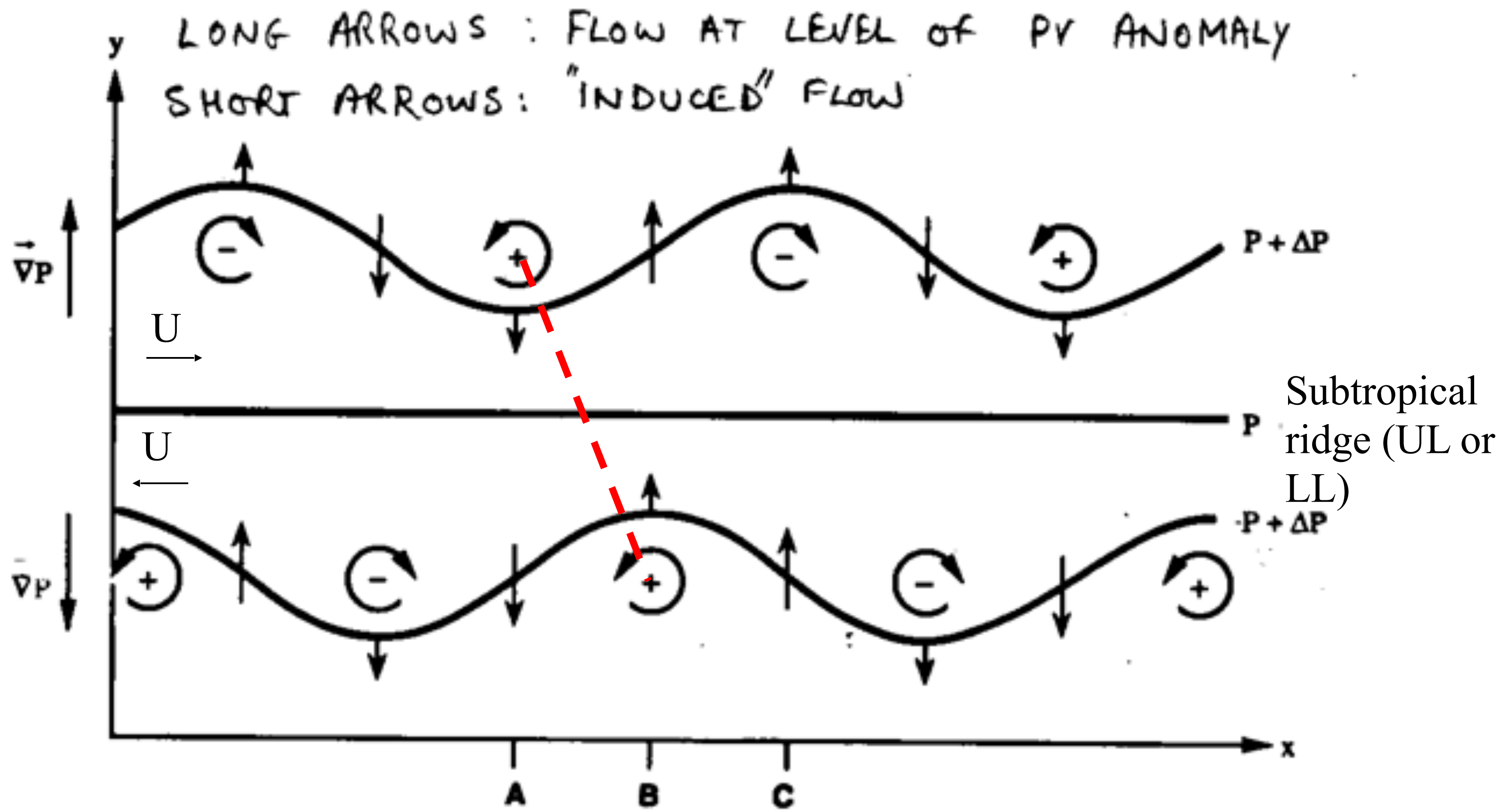

Both normal and inverted trofs move in opposite direction to the mean flow. They may become locked and amplify each other (barotropic instability on equatorward side) if the trof tilts westward with latitude (negative tilt) across the subtropical ridge.

Chapter 9.4: Generation of low-level PV by diabatic (latent) heating

How are PV anomalies **generated**?

$$\frac{\tilde{D}P}{Dt} = \frac{\partial P}{\partial t} + \vec{v} \bullet \nabla_\theta P = \frac{P}{\sigma}\frac{\partial(\sigma\dot{\theta})}{\partial\theta} + \frac{g}{\sigma}\vec{k} \bullet \nabla_\theta \times \left(\vec{F}_r - \dot{\theta}\frac{\partial\vec{v}}{\partial\theta}\right) \text{(Holton 4.36)}$$

vertical gradient of diabatic heating

$$\sigma = -\frac{\partial p}{\partial\theta}$$

curl of friction force

equivalent of 'tilting' term, but driven by horizontal gradients in diabatic heating

- UL PV anomalies are due primarily to differential advection (separation from a PV reservoir)
- LL PV anomalies can be **created** by:
  - Differential diabatic heating
    - tropical cyclones, marine extratropical cyclones …
  - Friction
    - this includes orography → linkage with lee cyclogenesis

diabatic heating

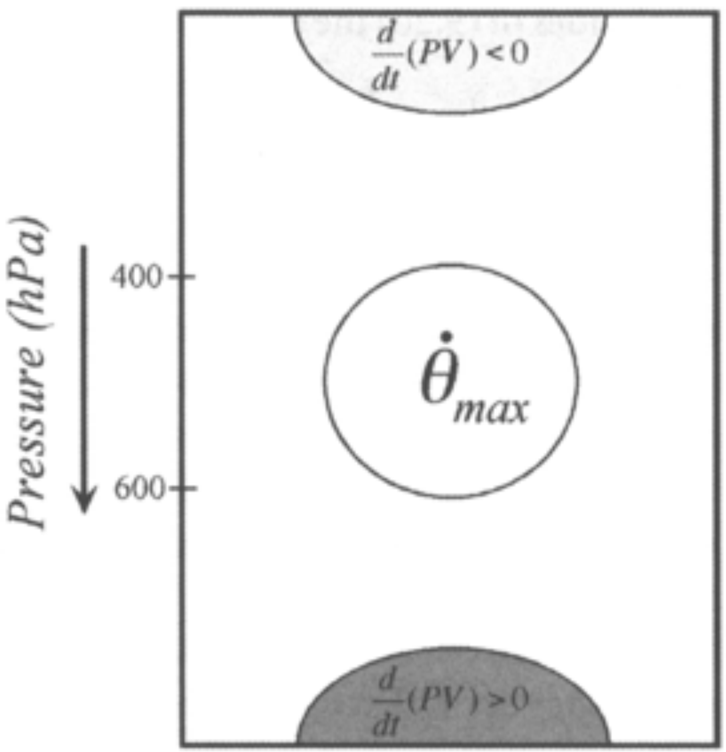

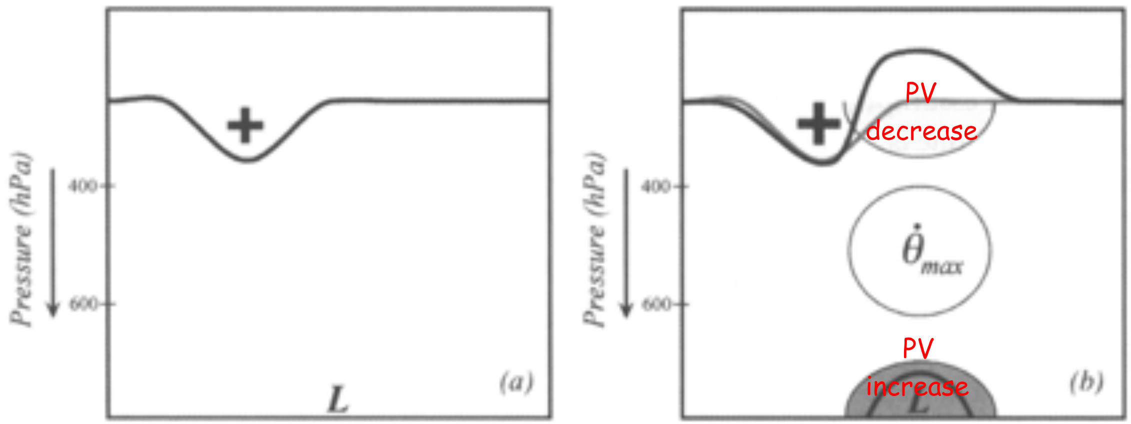

Figure 9.12 (a) Relationship between an upper tropospheric positive PV anomaly (+ sign) and a surface low-pressure center ('L'). (b) Ascent downstream of the PV anomaly produces latent heat release manifest as a $\dot{\theta}_{max}$. PV erosion aloft deforms the bold PV contour to the east of the original anomaly, making that anomaly even more anomalous (larger + sign). PV production in the lower troposphere intensifies the surface cyclone with high values of PV developing near the center indicated by the bold black line surrounding the 'L'

vertical gradient of diabatic heating

$$\frac{\tilde{D}P}{Dt} \cong \frac{P}{\sigma}\frac{\partial(\sigma\dot{\theta})}{\partial\theta} \cong P\frac{\partial\dot{\theta}}{\partial z}$$

diabatic heating

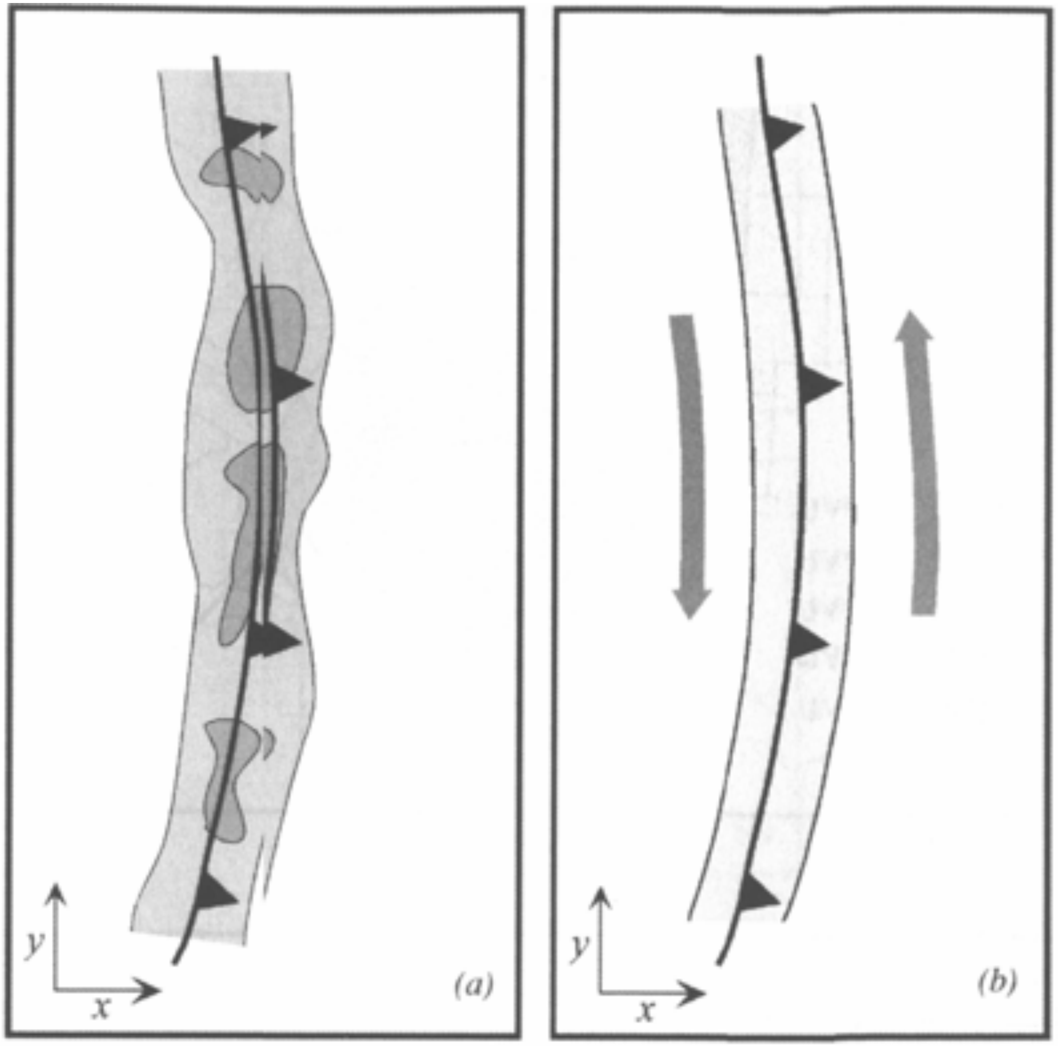

Figure 9.14 (a) Schematic ‹ cold frontal precipitation distribution with shading representing rad echoes in the precipitation along the front. (b) Gray shading indicates the thin, lower tropospher positive PV anomaly created vvia diabatic heating associated with the cold frontal precipitation. Bo arrows represent the low-level ‹ cyclonic flow associated with the diabatically generated PV

Rapid cyclogenesis and LL diabatic PV generation

Stoelinga 1996, MWR

A Potential Vorticity–Based Study of the Role of Diabatic Heating and Friction in a Numerically Simulated Baroclinic Cyclone

MARK T. STOELINGA*

*National Center for Atmospheric Research,** Boulder, Colorado*

(Manuscript received 16 May 1995, in final form 21 September 1995)

ABSTRACT

A particularly intense case of western Atlantic baroclinic cyclogenesis was investigated in this study. Specifically, the roles of latent heat of condensation and surface friction were examined from the potential vorticity or "PV thinking" perspective. The methodology used for this study involves three key components: 1) a full-physics mesoscale model, which provides a continuous and dynamically consistent dataset and provides full user control over physical processes; 2) a partitioned PV integration, which temporally integrates the accumulation of PV due to various physical processes in the model's Eulerian framework: and 3) the piecewise inversion method of Davis and Emanuel, which calculates the balanced wind and mass field associated with particular PV anomalies. Potential vorticity features obtained through the partitioned integration technique were inverted to yield their direct contributions to the total circulation. In addition, sensitivity studies were carried out to determine the overall impact of various nonconservative processes on the cyclone development.

Results of the PV integration showed that latent heating created a significant positive anomaly above the surface warm and bent-back fronts at the level of maximum heating. Inversion of this feature showed that it explained approximately 70% of the total balanced nondivergent circulation at low levels during the mature stage of the storm. The circulation associated with latent-heating-generated PV also enhanced the coupling between the surface and upper-level waves, both by hastening the eastward propagation of the surface wave and by slowing the eastward propagation of the upper-level wave. Comparison of the control experiment with a sensitivity test, in which latent heating was withheld, showed that latent heating also enhanced upper-level divergence, which expanded the downstream ridge and kept an upper-level small-scale PV anomaly coupled to the low-level disturbance. However, cyclogenesis still occurred in the absence of latent heating, due to a second, larger-scale upper PV anomaly that approached from the northwest. Surface friction caused the formation of mainly positive PV at low levels, primarily in the easterly flow of the warm frontal zone, where the dominant mechanism was frictional formation of southward-oriented horizontal vorticity in the presence of a strong southward temperature gradient. Inversion of this PV yielded a small cyclonic circulation centered on the surface low. However, a frictionless simulation produced a slightly stronger cyclone, due to indirect enhancement of the upper-level PV anomaly and the generation of low-level PV by thermal diffusion in the narrow warm sector of the storm.

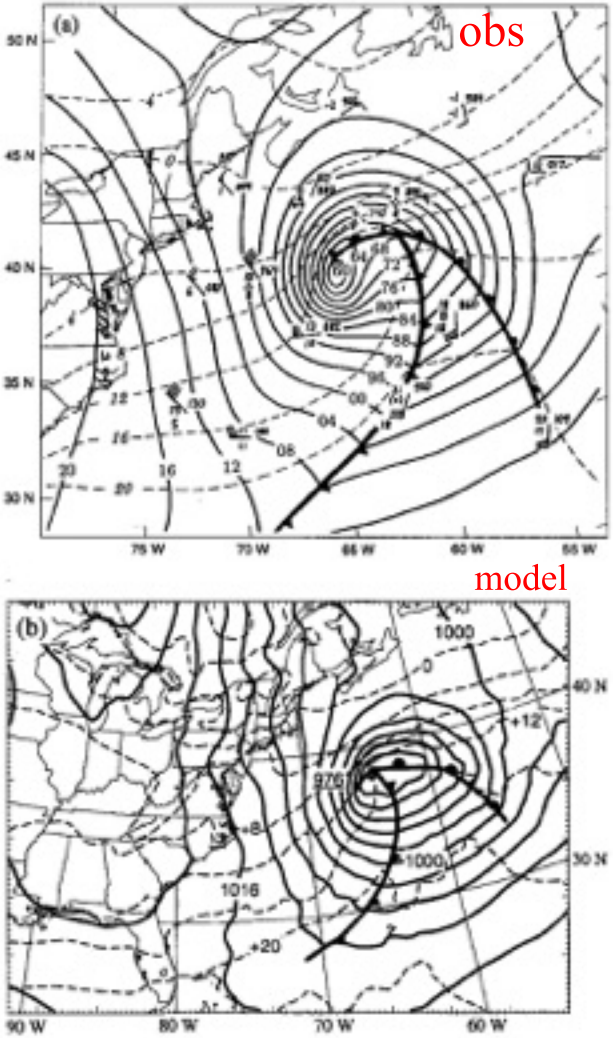

FIG. 1. Sea level pressure (mb, solid), temperature (°C, dashed), and surface frontal analyses at 0000 UTC 24 February 1987 based on (a) observations and (b) the corresponding 36-h model forecast. Station models in (a) depict wind (full barb—5 m s^{-1}), sea level pressure (mb) at upper right, temperature (°C) at upper left, dewpoint (°C) at lower left, and current weather symbol at left. Cloud cover and sea surface temperature are omitted, and no distinction is made between ship and buoy observations.

5-day mean

P and θ pattern

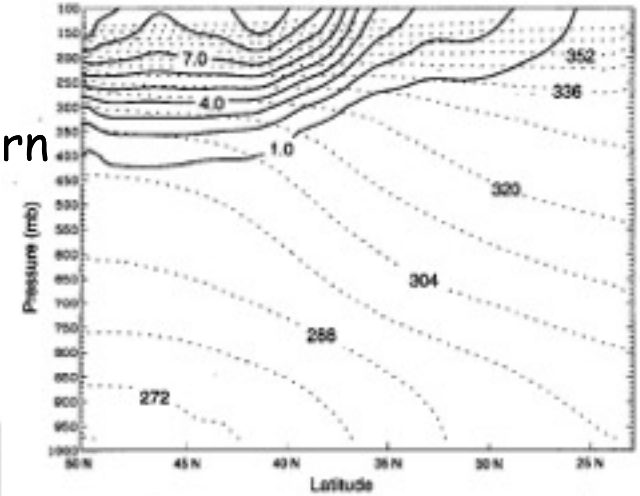

FIG. 4. North–south cross section (near 71°W) of 5-day mean fields (centered at 0000 UTC 24 February) derived from NMC analyses, including potential temperature (K, dashed) and PV (PVU, solid). Note: 1 PV unit (or PVU) = 10^{-6} K m^2 kg^{-1} s^{-1}.

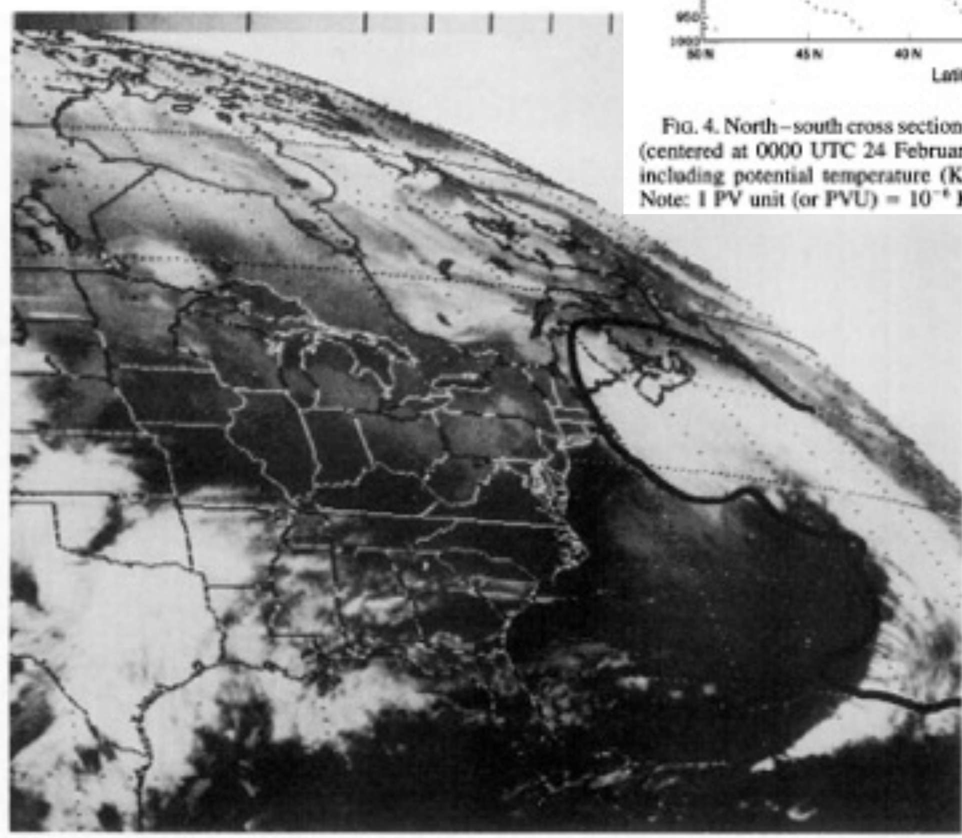

FIG. 3. GOES infrared satellite image valid at 0000 UTC 24 February. Heavy contour denotes −30°C isotherm of brightness temperature estimated from model output at corresponding forecast time (36 h). Arrow indicates location of −30°C on the gray scale.

Stoelinga 1996

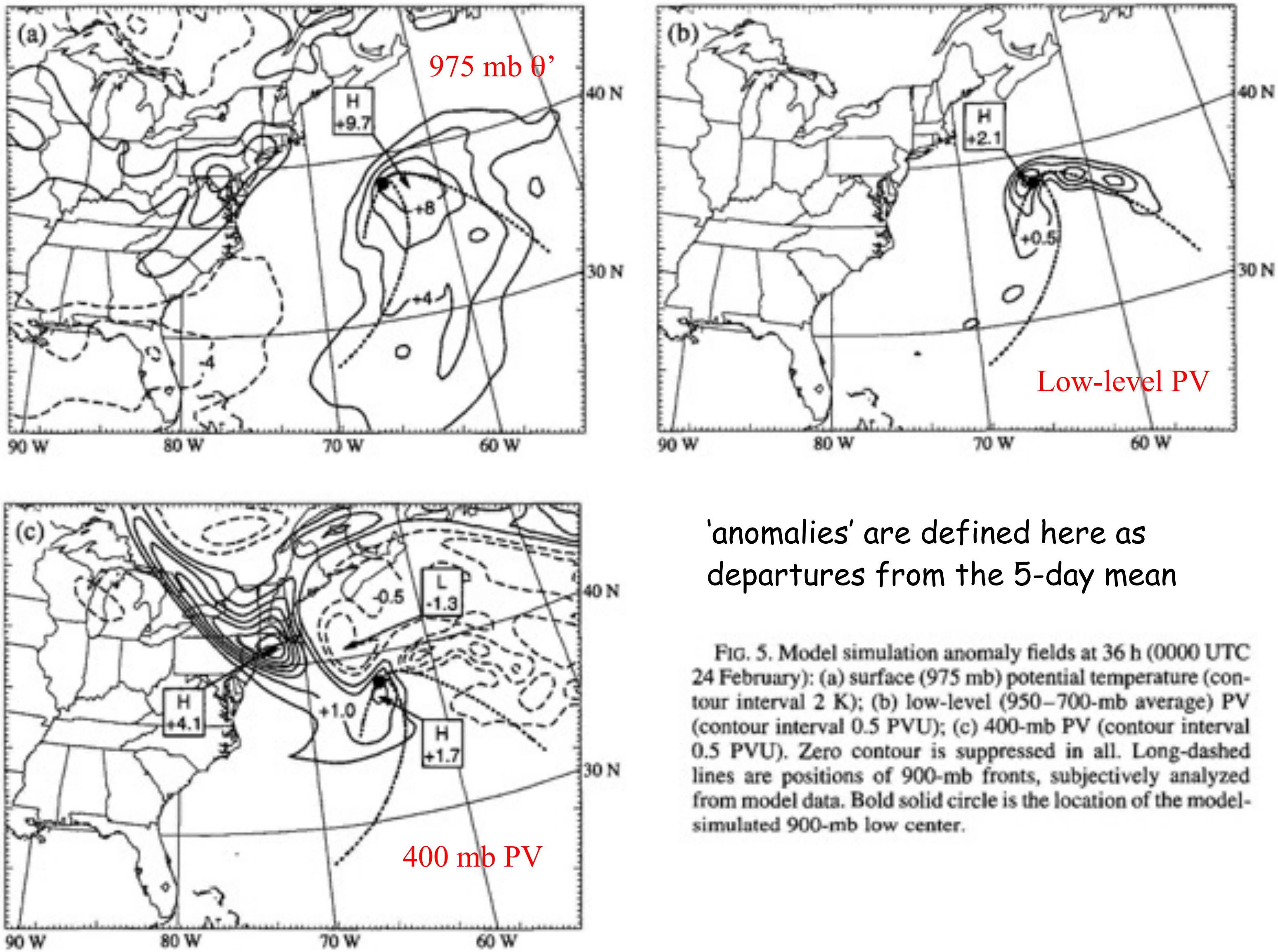

'anomalies' are defined here as departures from the 5-day mean

FIG. 5. Model simulation anomaly fields at 36 h (0000 UTC 24 February): (a) surface (975 mb) potential temperature (contour interval 2 K); (b) low-level (950–700-mb average) PV (contour interval 0.5 PVU); (c) 400-mb PV (contour interval 0.5 PVU). Zero contour is suppressed in all. Long-dashed lines are positions of 900-mb fronts, subjectively analyzed from model data. Bold solid circle is the location of the model-simulated 900-mb low center.

Stoelinga 1996

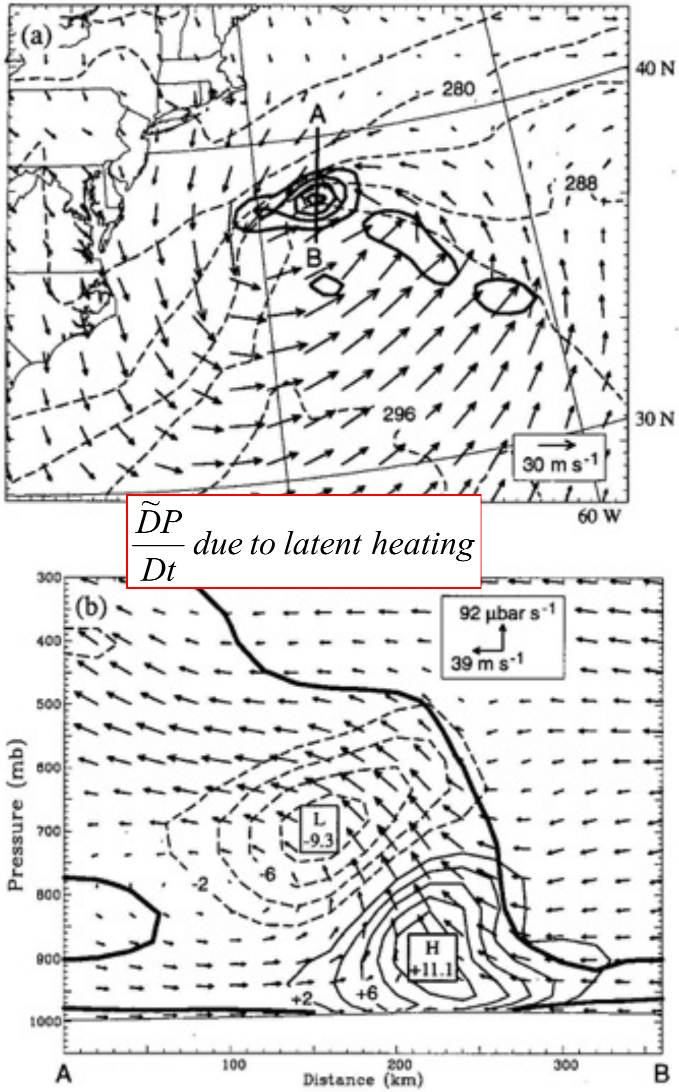

$\frac{\widetilde{D}P}{Dt}$ due to latent heating

FIG. 8. Low-level (0.7 km above sea level) generation of PV by explicit latent heating at 30 h (1800 UTC 23 February): (a) Lagrangian PV tendency due to explicit latent heating (G_{lh} in text, solid lines, contour interval 2×10^{-2} PVU s^{-1}, zero contour suppressed), wind vectors (scale shown at lower right), and potential temperature (dashed lines, contour interval 4 K); (b) cross section [along line *AB* shown in (a)] of Lagrangian PV tendency due to explicit latent heating (thin lines, contour interval 2×10^{-2} PVU s^{-1}, zero contour suppressed), vectors showing ground-relative circulation in the plane of the cross section (scale shown at upper right), and relative humidity (single solid contour of 95%).

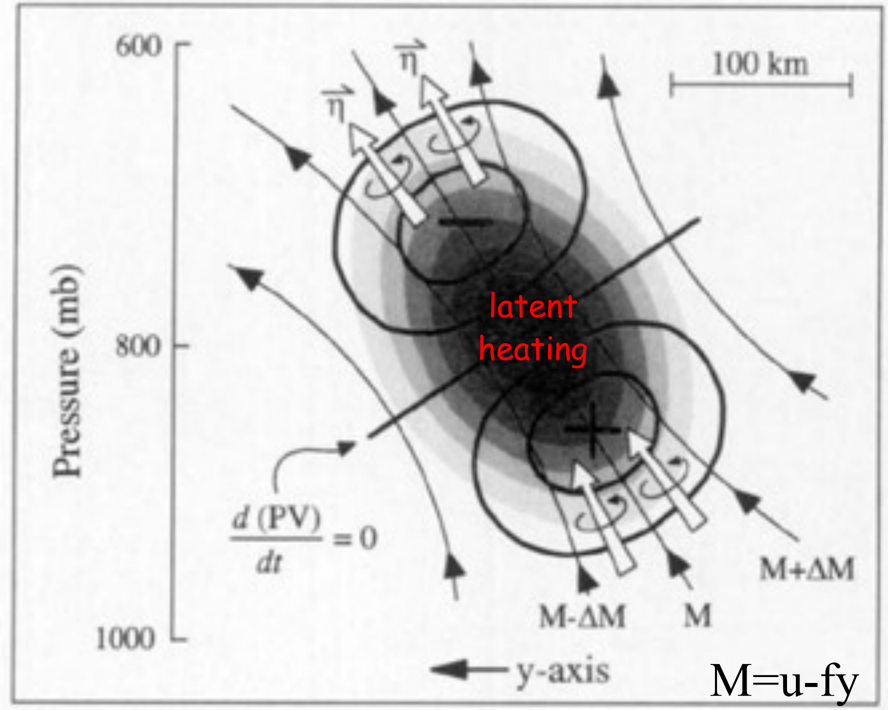

FIG. 9. Generation of PV by latent heating in an idealized 2D frontal zone. Thin solid lines are contours of absolute momentum. Arrowheads on thin solid lines indicate that they are also streamlines. White arrows are absolute vorticity vectors. Heavy solid lines are contours of PV generation due to latent heating, with maxima of generation and depletion indicated by "+" and "−" symbols, respectively. Intensity of gray shading is proportional to upward vertical velocity, latent heating, and PV.

$$\frac{\widetilde{D}P}{Dt} \cong \frac{P}{\sigma}\frac{\partial(\sigma\dot{\theta})}{\partial\theta} \cong P\frac{\partial\dot{\theta}}{\partial z}$$

Stoelinga 1996

Chapter 9.5: additional applications
(a) piecewise PV inversion

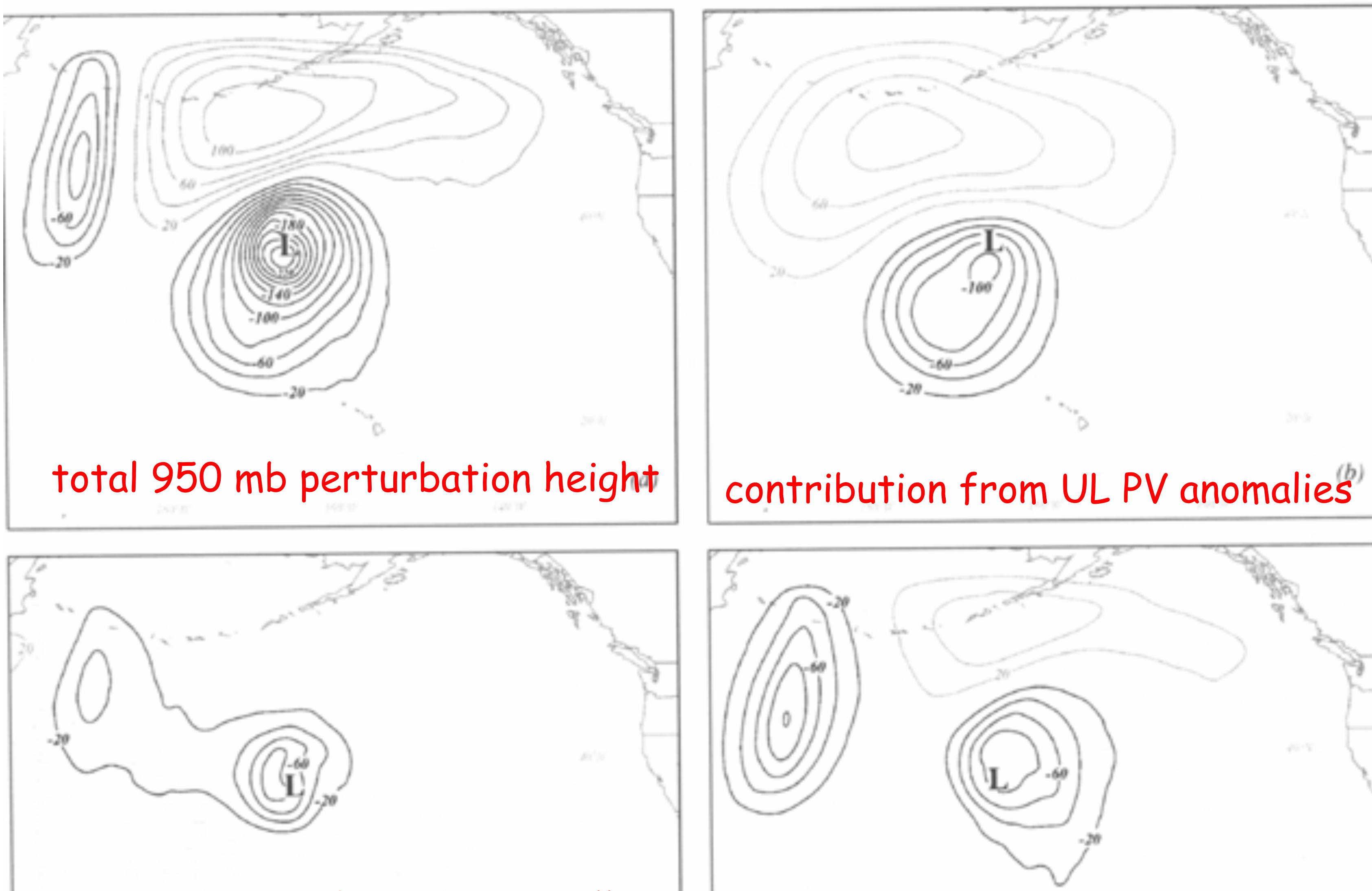

total 950 mb perturbation height

contribution from UL PV anomalies

contribution from diabatically generated PV anomalies

contribution from LL PV anomalies

(b) IPV perspective of the occlusion process

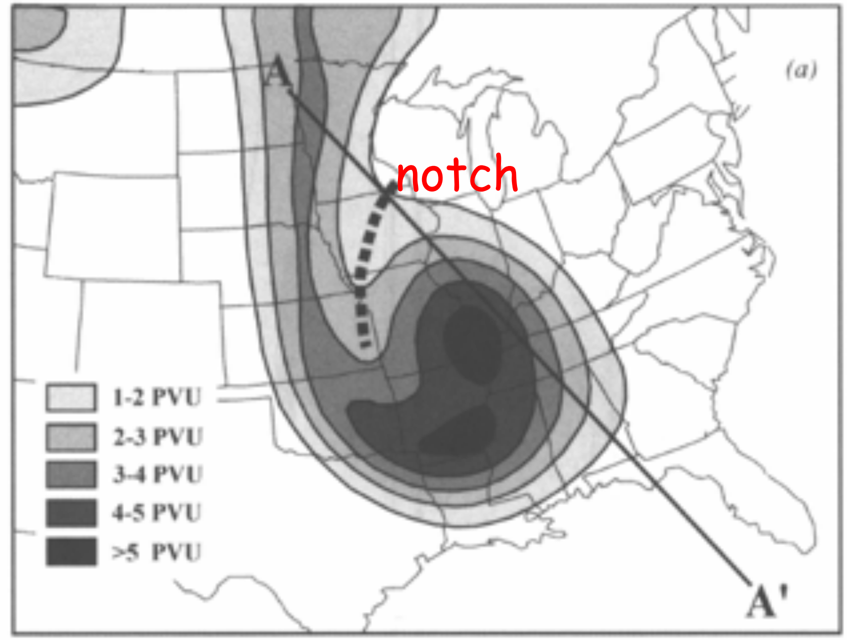

- "treble-clef" PV structure aloft
- "notch" is due to advection of LL low-PV air into upper levels (warm conveyor belt, trowal)
- tropopause fold possible

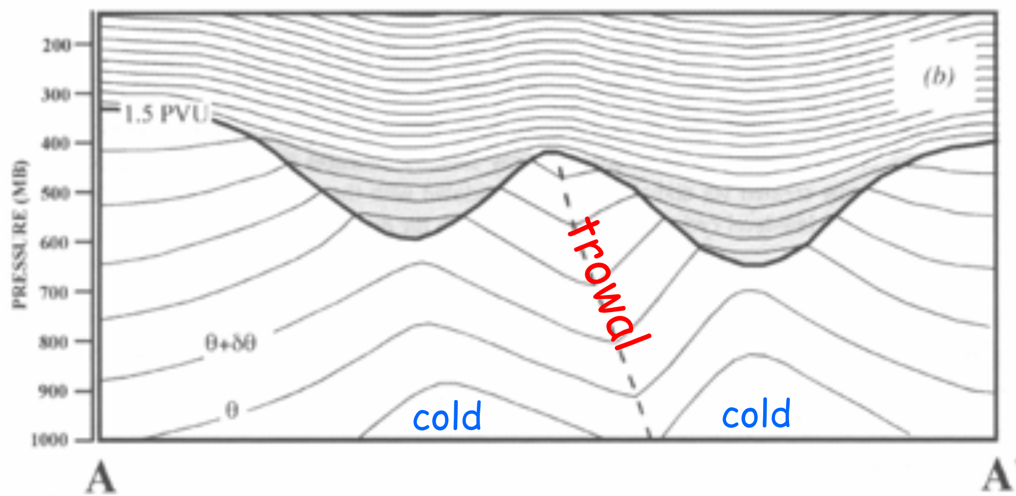

Figure 9.15 (a) Schematic of treble-clef-shaped upper tropospheric PV structure described in the text. Solid lines are isopleths of PV on an isobaric surface contoured and shaded in PVU (1 PVU = 10^{-6} m^2 K kg^{-1}s^{-1}). The thick dashed line identifies the PV 'notch' described in the text. (b) Schematic cross-section of potential temperature (θ) in the vicinity of a treble-clef-shaped upper tropospheric PV signature. The dashed axis denotes the sloping axis of warm air in the troposphere characteristic of an occluded cyclone

(b) IPV perspective of the occlusion process

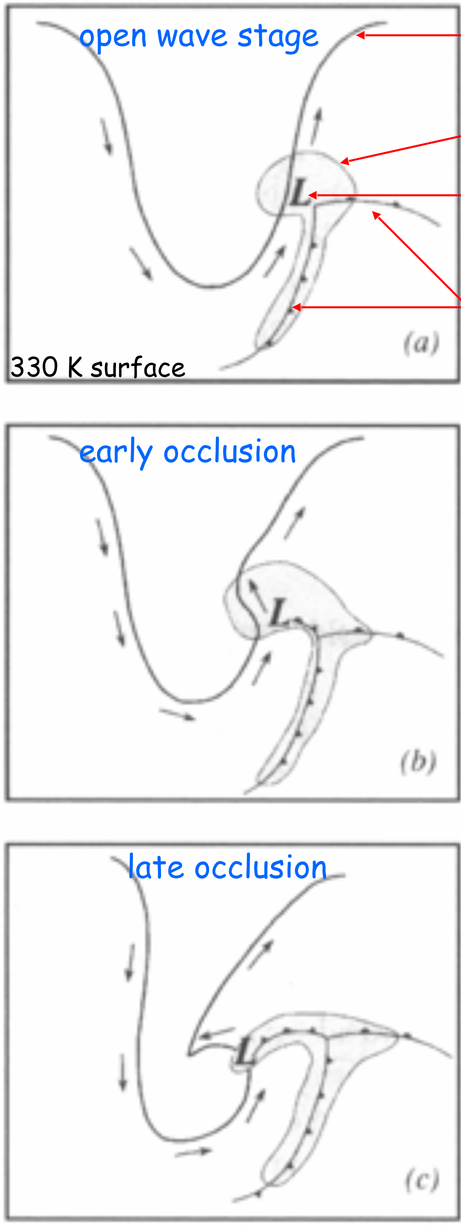

note PV decay in the notch in (c) by both diabatic heating and advection

Figure 9.16 Schematic illustrating the synergy between diabatic erosion of PV and negative advection of PV at the tropopause during occlusion. Gray shading represents the erosion of tropopause PV by diabatic heating associated with the cyclone, the surface position of which is marked by the 'L'. Traditional surface frontal symbols indicate surface frontal locations. The thick soild line represents the PV = 2 PVU isopleth at the tropopause. Arrows represent the tropopause-level flow associated with the upper tropospheric PV feature. (a) The open wave stage. Heating is concentrated along the cold front and in the vicinity of the developing surface cyclone. (b) Commencement of occlusion. Persistent diabatic erosion in the northwest quadrant of the cyclone deforms the upper tropospheric PV contour northwest of the surface cyclone. Tropopause-level flow is also deformed in that vicinity. (c) Fully occluded stage. Cyclone is far removed from the peak of the surface warm sector. Heating is no longer proximate to the 'notch' in the upper tropospheric PV. Tropopause-level flow controls intensification of the notch through negative PV advection in the upper troposphere

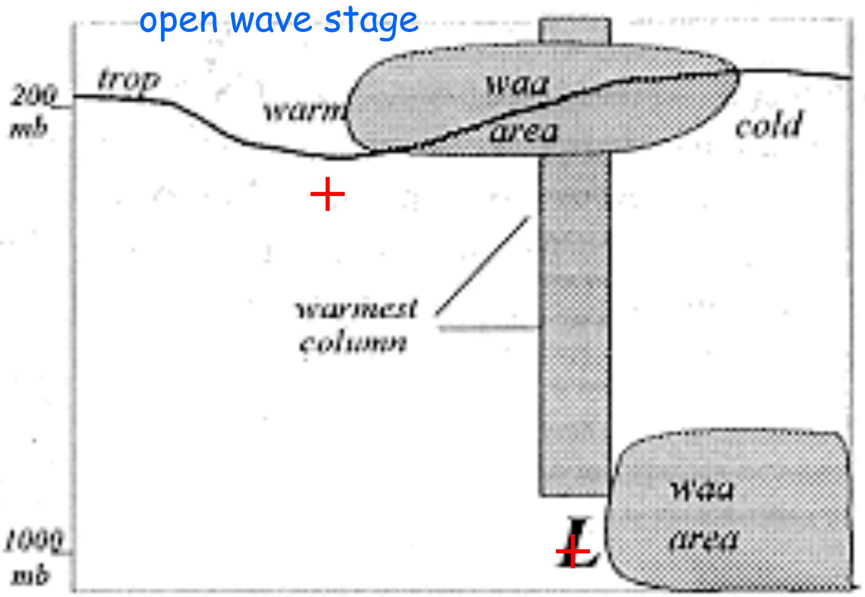

(b) IPV perspective of the occlusion process

strong + PV anomaly aloft produces deep tropopause depression & warm air

interpret the surface pressure changes as due to temperature changes aloft (each level is weighted equally, since dln p ~dz)

$$\frac{\partial z(p_b)}{\partial t} = \frac{R}{g}\int_{p_b}^{p_t} \frac{\partial T_v}{\partial t}\, d(\ln p)$$ (from hydrostatic balance)

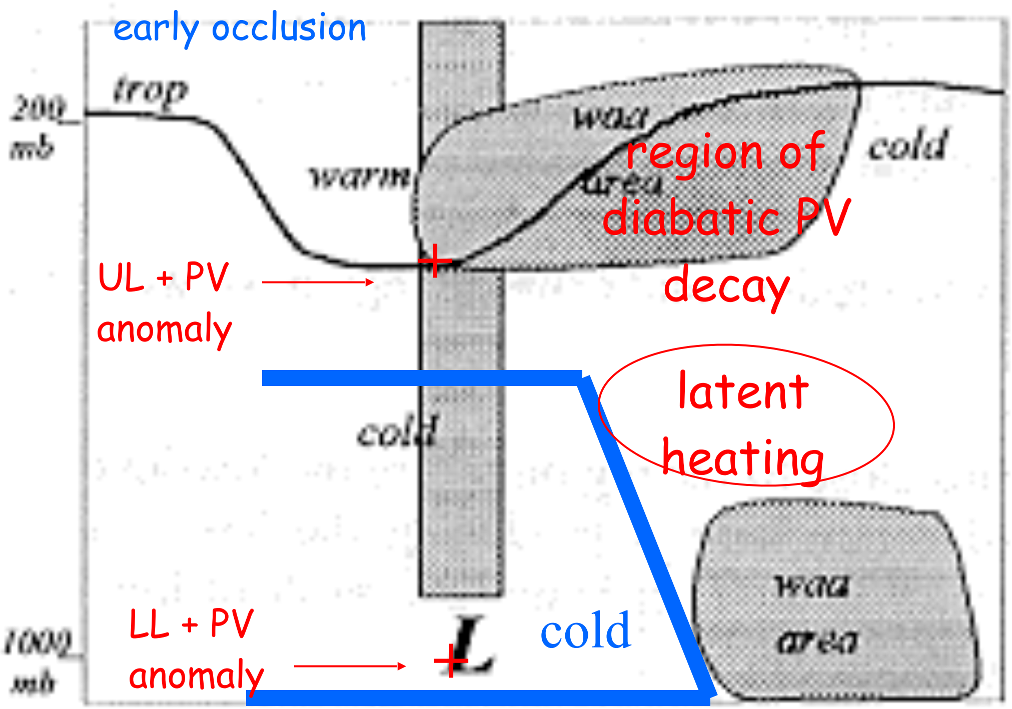

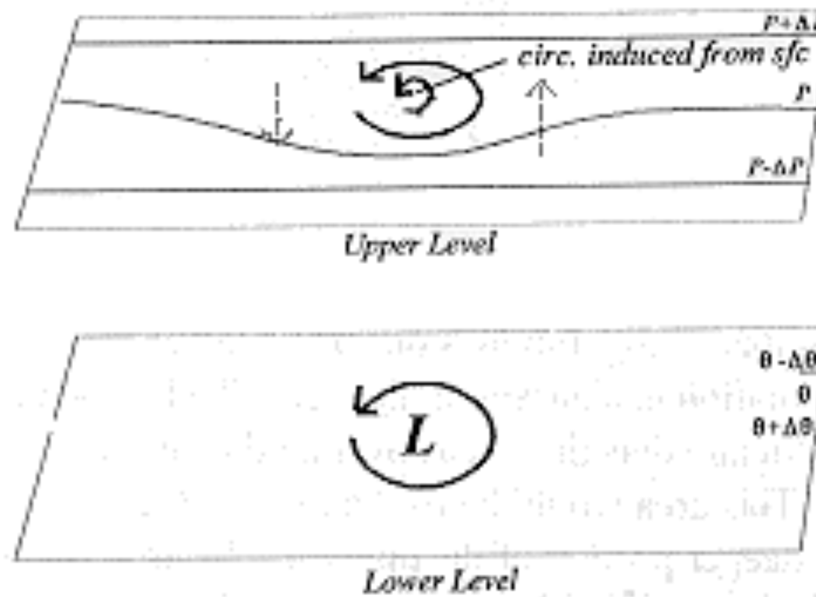

(Hirschberg and Fritsch 1991)

(c) PV superposition & attenuation

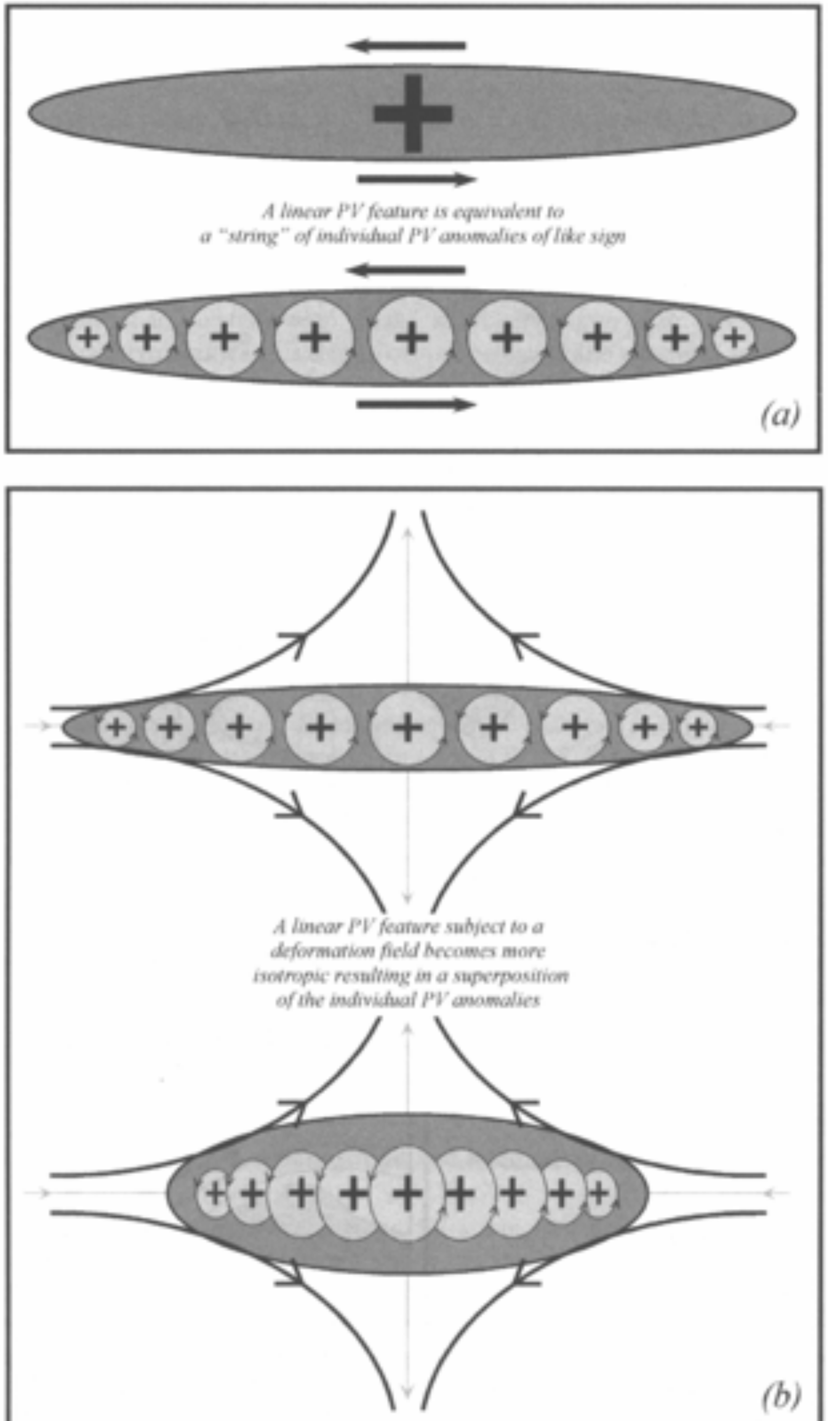

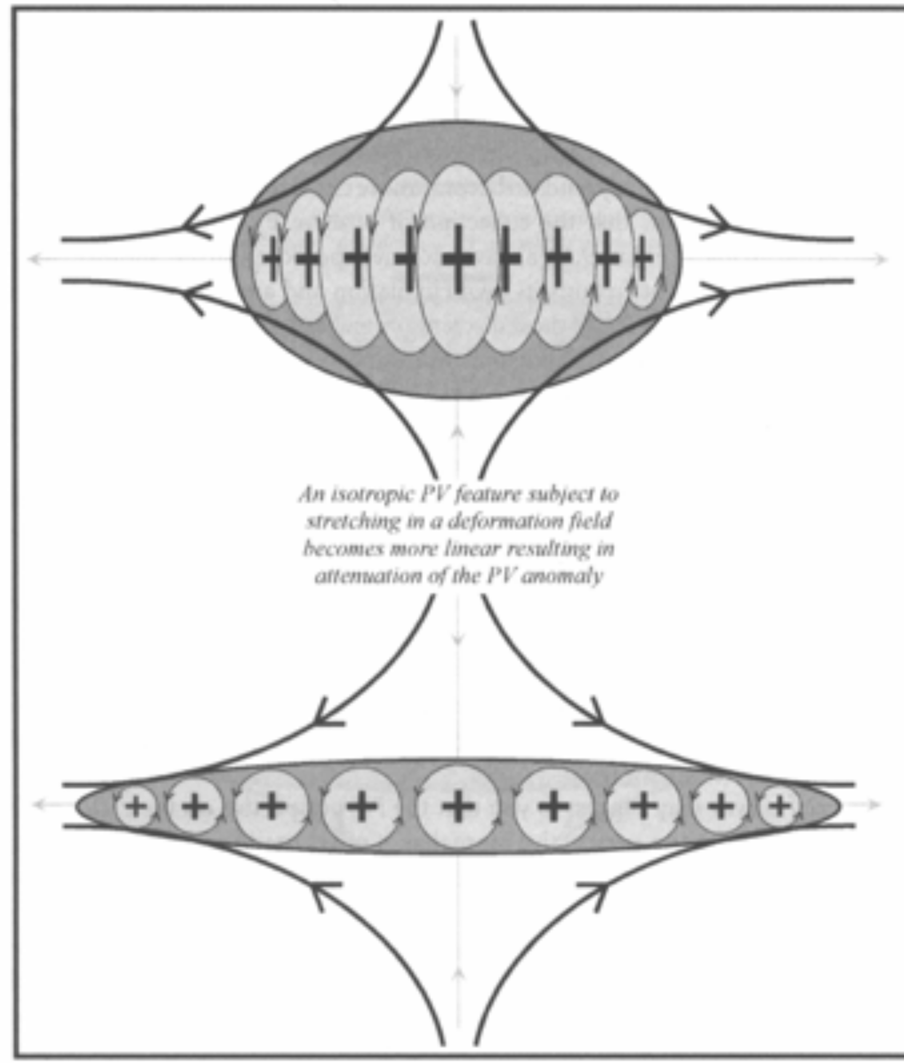

Figure 9.20 Schematic illustrating PV attenuation. A positive PV anomaly subjected to a deformation field can be stretched into a thin line of individual PV anomalies thus reducing the potency of the circulation associated with the anomaly. Such a process is known as PV attenuation

IPV perspective of lee cyclogenesis

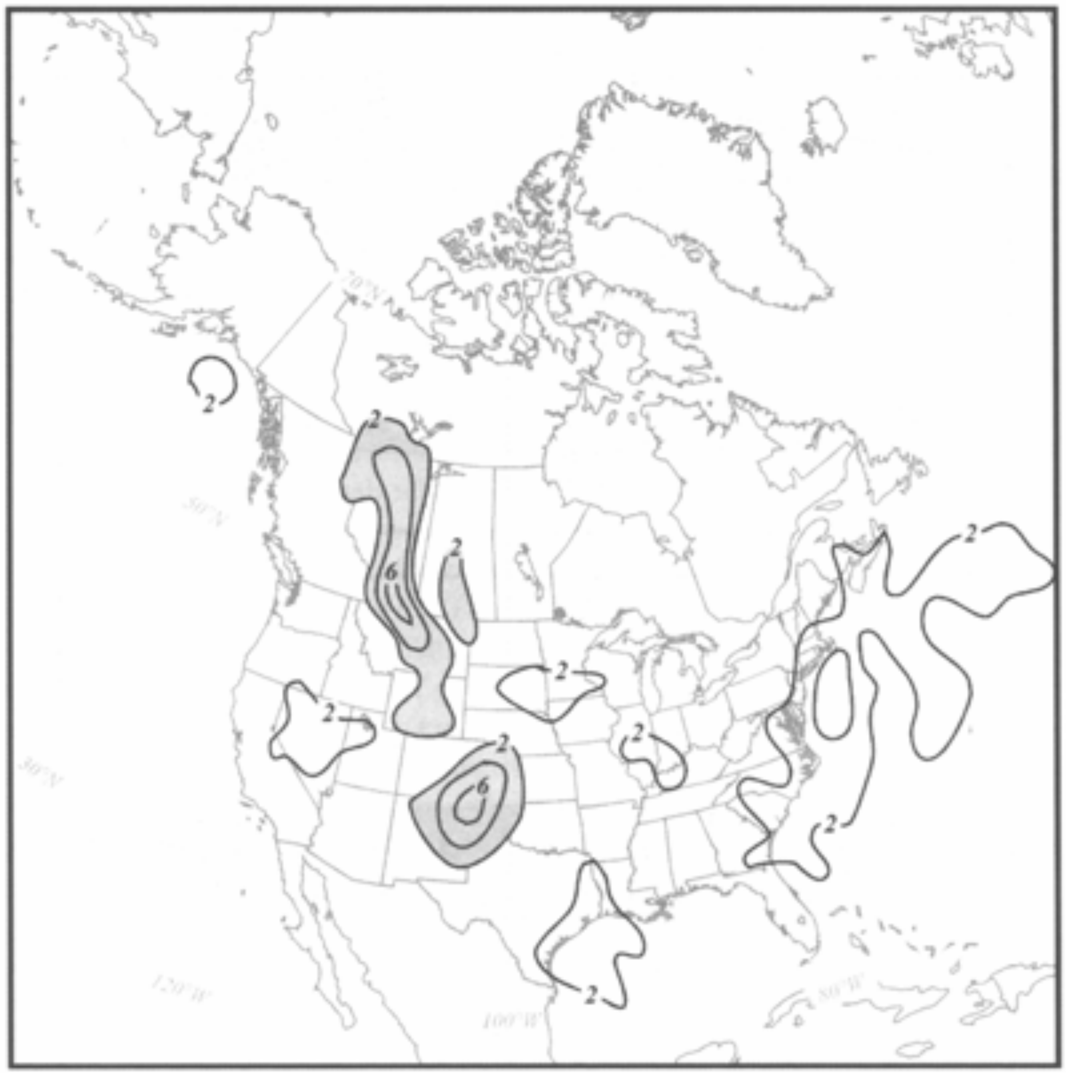

Figure 9.17 Areal distributions of cyclogenesis frequencies for the month of January from 1950 to 1977. Gray shaded regions represent lee cyclogenesis areas east of the Rocky Mountains. Adapted from Zishka and Smith (1980)

lee cyclogenesis and PV generation

first some background about lee cyclogenesis

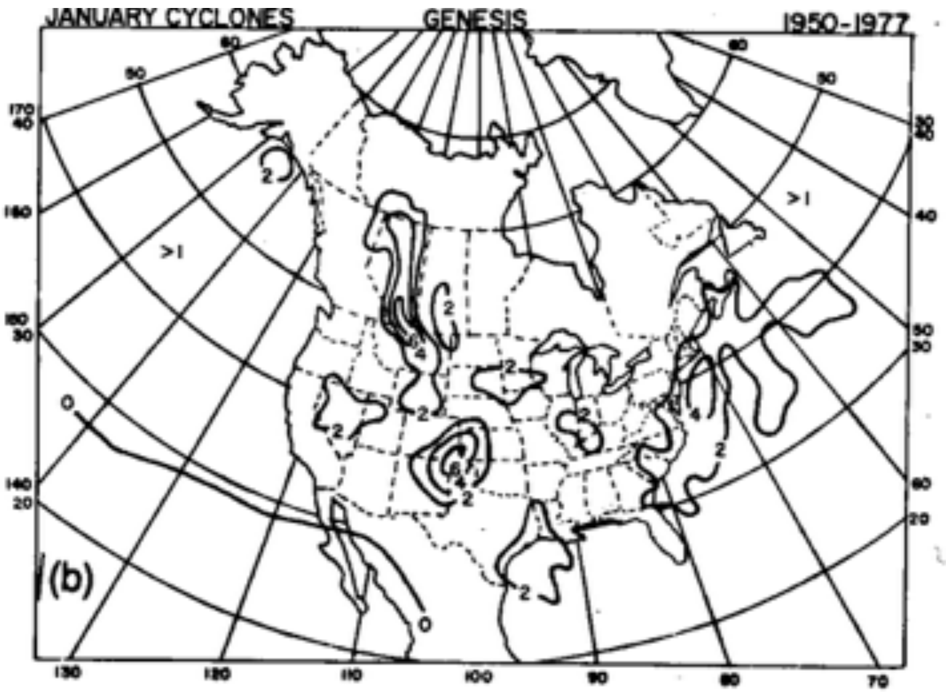

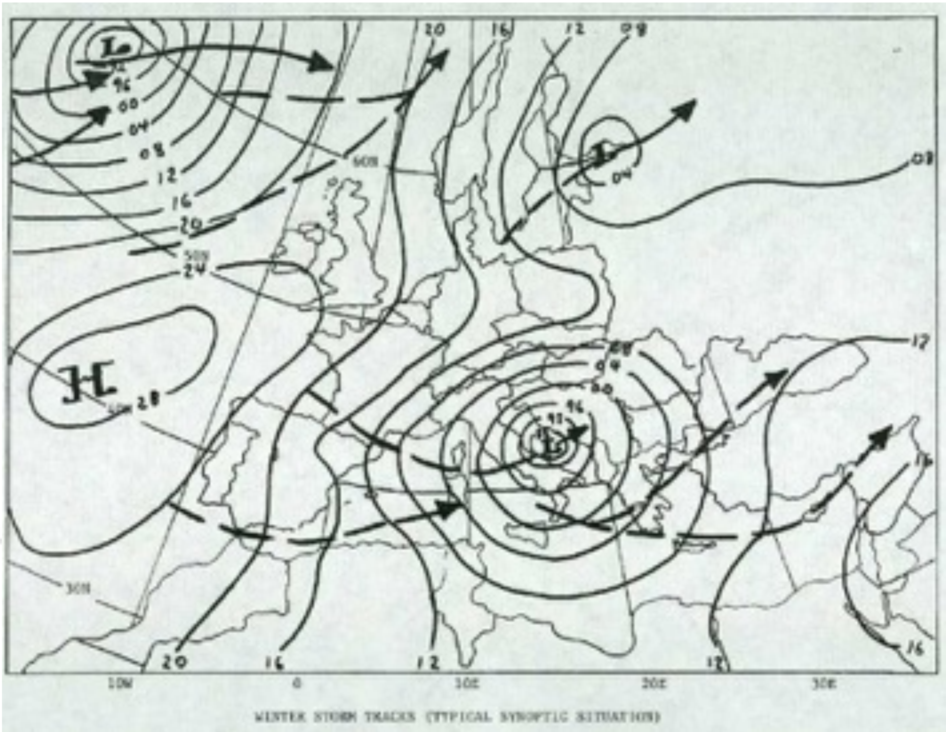

Rocky Mtn lee cyclogenesis climatology

(source: Sanders et al 1985)

Alpine lee cyclogenesis

Dashed lines: prevailing tracks of surface lows in winter

Theory: PV conservation and lee troughing

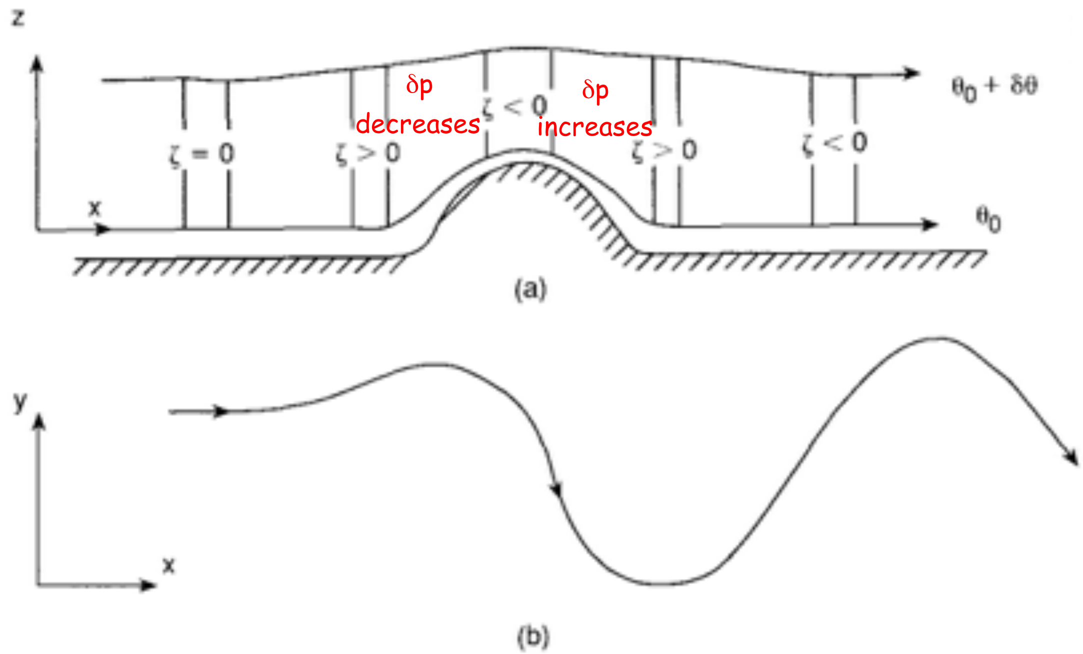

Fig. 4.9 Schematic view of westerly flow over a topographic barrier: (a) the depth of a fluid column as a function of x and (b) the trajectory of a parcel in the x, y plane.

Conserve

$$P = g(\zeta_\theta + f)\left(-\frac{\delta\theta}{\delta p}\right)$$

$$P \approx \frac{\zeta_\theta + f}{\delta p}$$

assumption: PV is uniformly distributed over the depth of the troposphere

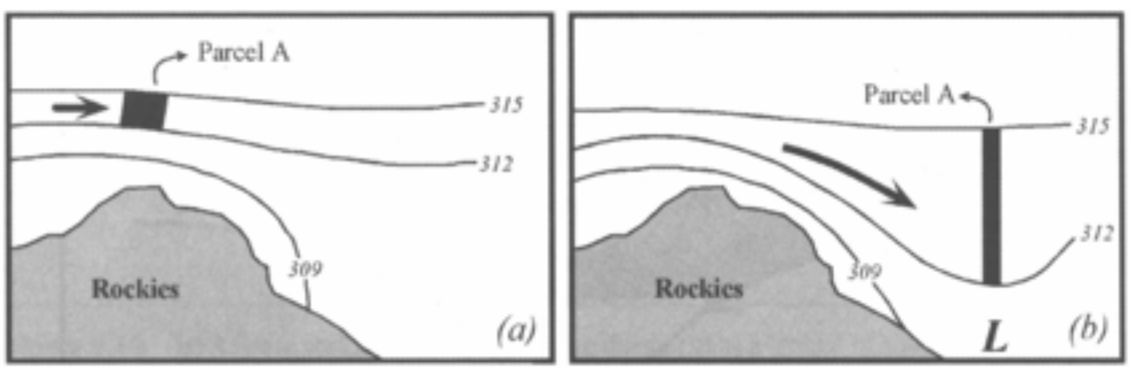

Figure 9.18 (a) Westerly flow (bold arrow) impinging on the Rocky Mountains. Parcel A is confined between the 312 K and 315 K isentropes. (b) As the flow pushes Parcel A over the ridge of the Rockies, the 312 K isentrope is forced toward the surface and the parcel is stretched in the vertical. A surface low-pressure center ('L') develops in response to the conservation of PV

lee troughing can be explained by subsidence

Assume adiabatic heating, no horizontal advection
→ warming is due to subsidence alone

$\partial T / \partial t = (T/\theta)\ \partial\theta/\partial p\ \omega$
$\sim (T/\theta)\ \partial\theta/\partial z\ w$
$\sim (1) * 3.5 K/km * dz/dt$ (assume typical values)

à δT (in K) ~ 3.5*subsidence depth (in km)

à this warming over the depth of the subsidence layer causes cyclogenesis:

$$\frac{\partial z(p_b)}{\partial t} = \frac{R}{g} \int_{pb}^{pl} \frac{\partial T_v}{\partial t} d(\ln p)$$

QG explanation
(Alpine cyclogenesis!)

from Bluestein (1993)

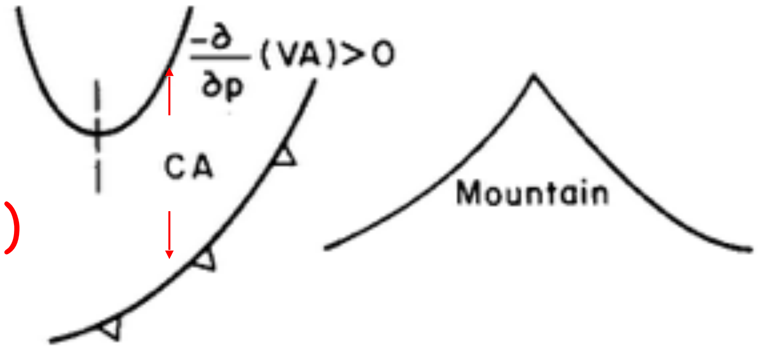

$\omega \approx \omega_V + \omega_T \sim 0$ (mature system over western Europe)

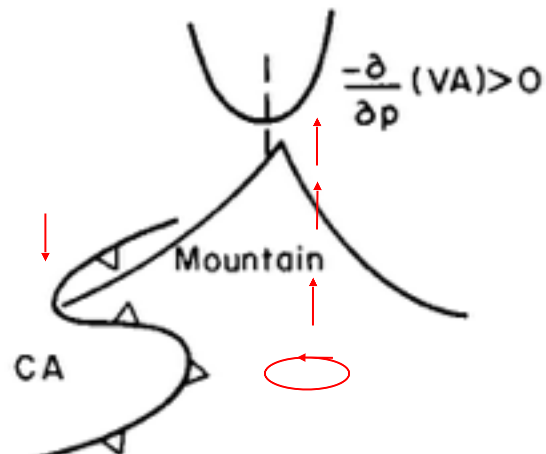

$\omega \approx \omega_V + \omega_T \sim \omega_V < 0$

Figure 1.135 Effects of blocking by the Alps on surface cyclogenesis. (top) Vorticity advection becoming more cyclonic with height $[(-\partial(VA)/\partial p)>0]$ associated with rising motion ($\omega_V<0$); cold advection (CA) associated with sinking motion ($\omega_T>0$). (bottom) Low-level cold air blocked by the mountains, and forced to flow around the sides. Vorticity advection becoming more cyclonic with height unopposed by cold advection; rising motion and low-level convergence induce surface cyclogenesis.

Further QG explanation
(Alpine cyclogenesis!)

The upward motion in the lee of the mountains is QG-forced because the jet is supergeostrophic. This updraft cools the cold side of the jet, and the secondary circulation will also decelerate it.

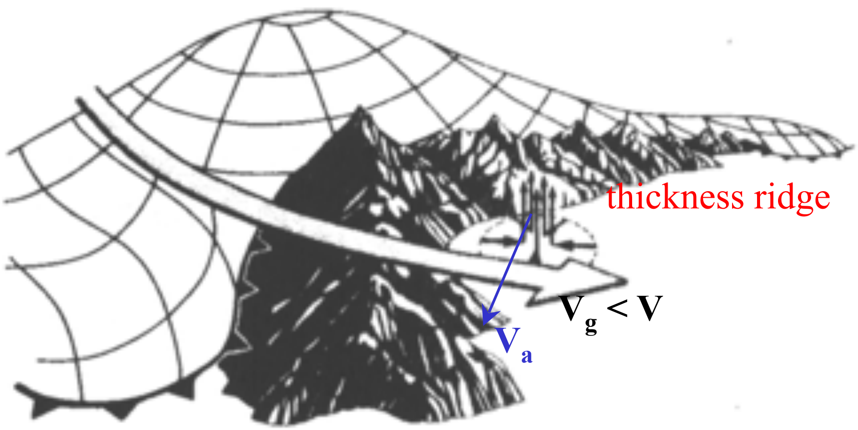

FIG. 2. A schematic rendition of the geostrophic adjustment process initiated when a jet streak propagates across a mesoscale mountain range while its "dome" of cold air remains blocked upstream.

Mattocks and Bleck, MWR 1986

Alpine lee cyclogenesis and LL PV generation: a modelling study

Aebisher and Schar 1998

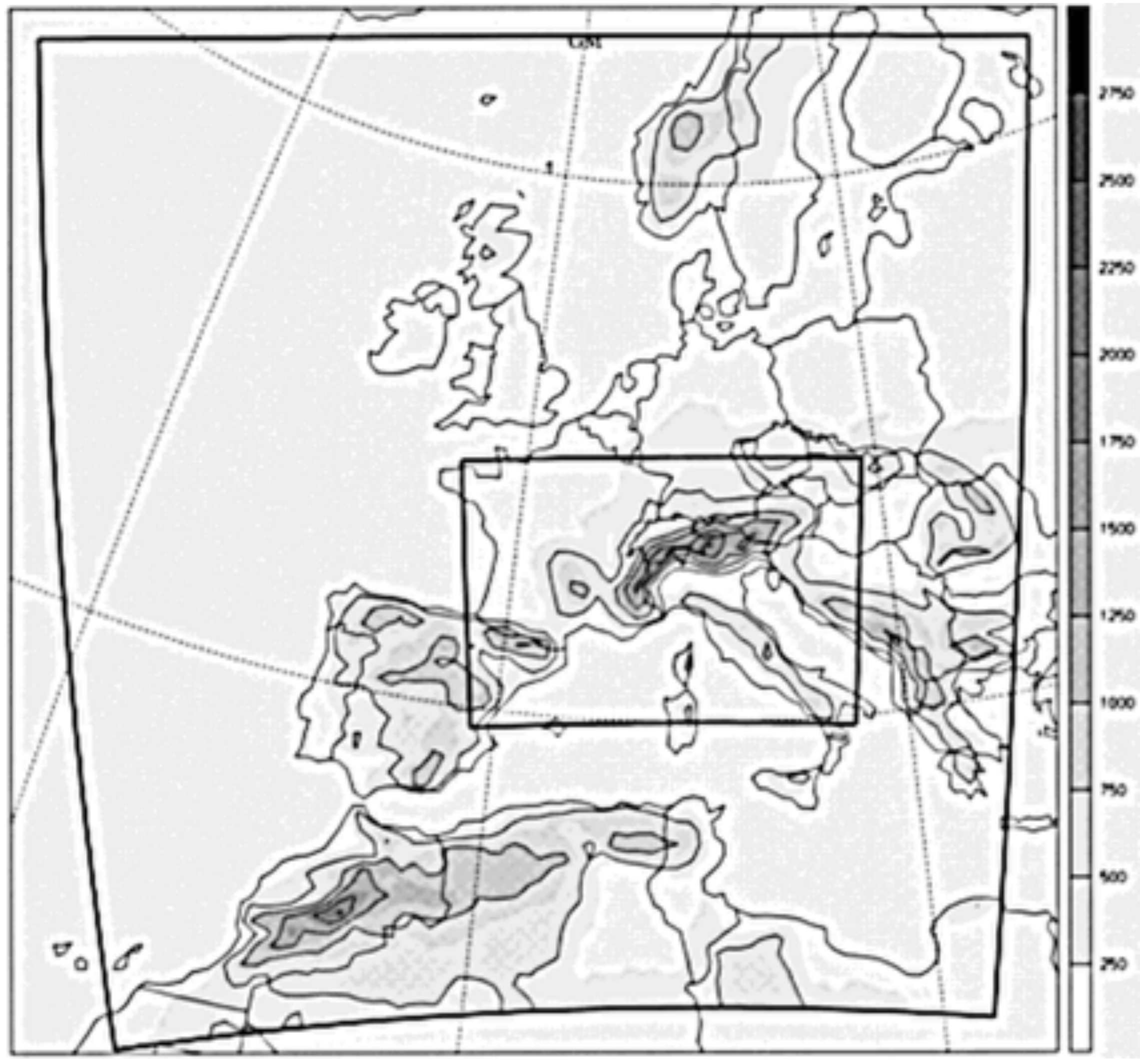

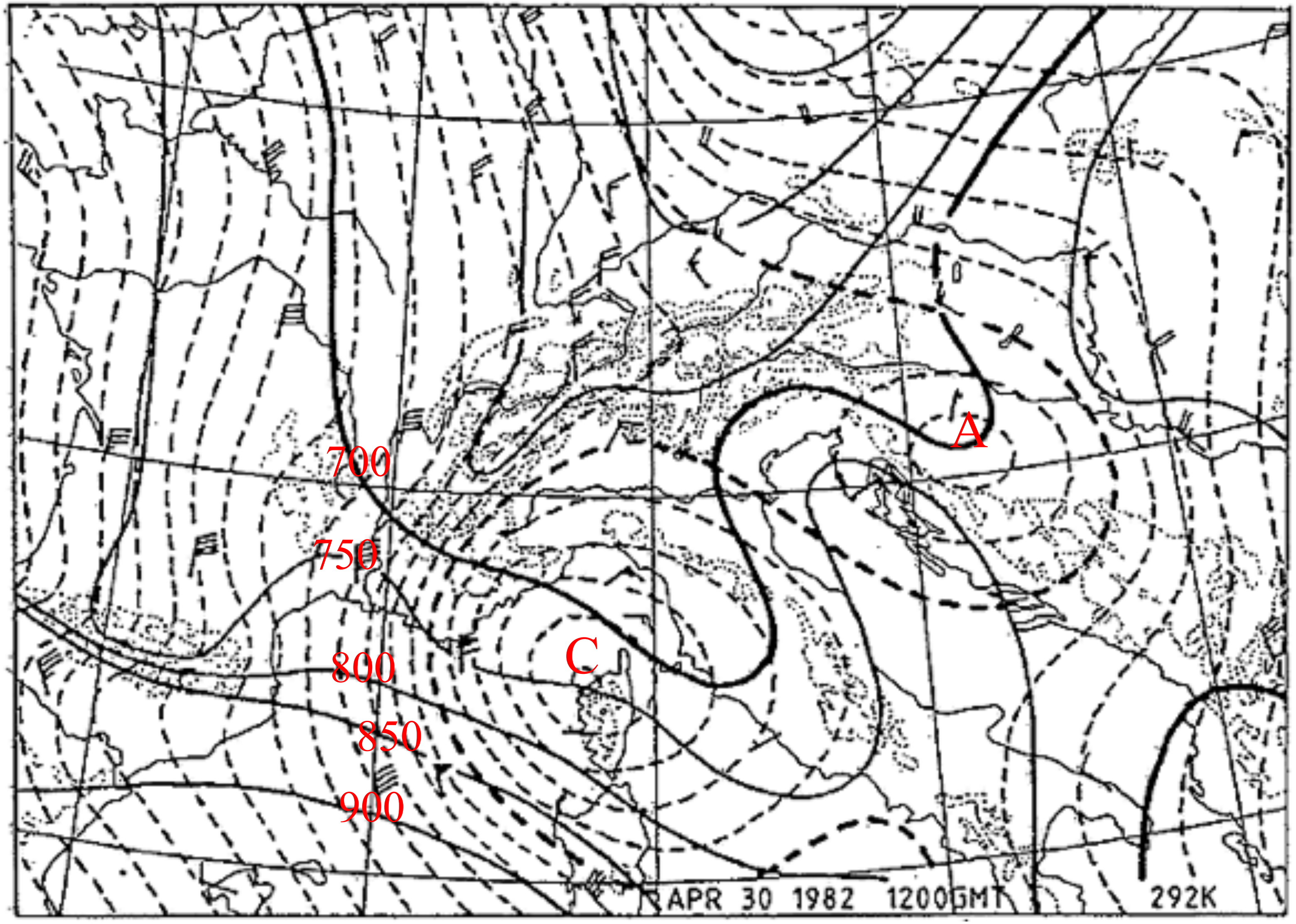

Solid: pressure height (bold=700 mb); dash: montgomery streamfunction

Note the counter-rotating vortices on the SW and E side of Alps. Fr=U/(HN) <1

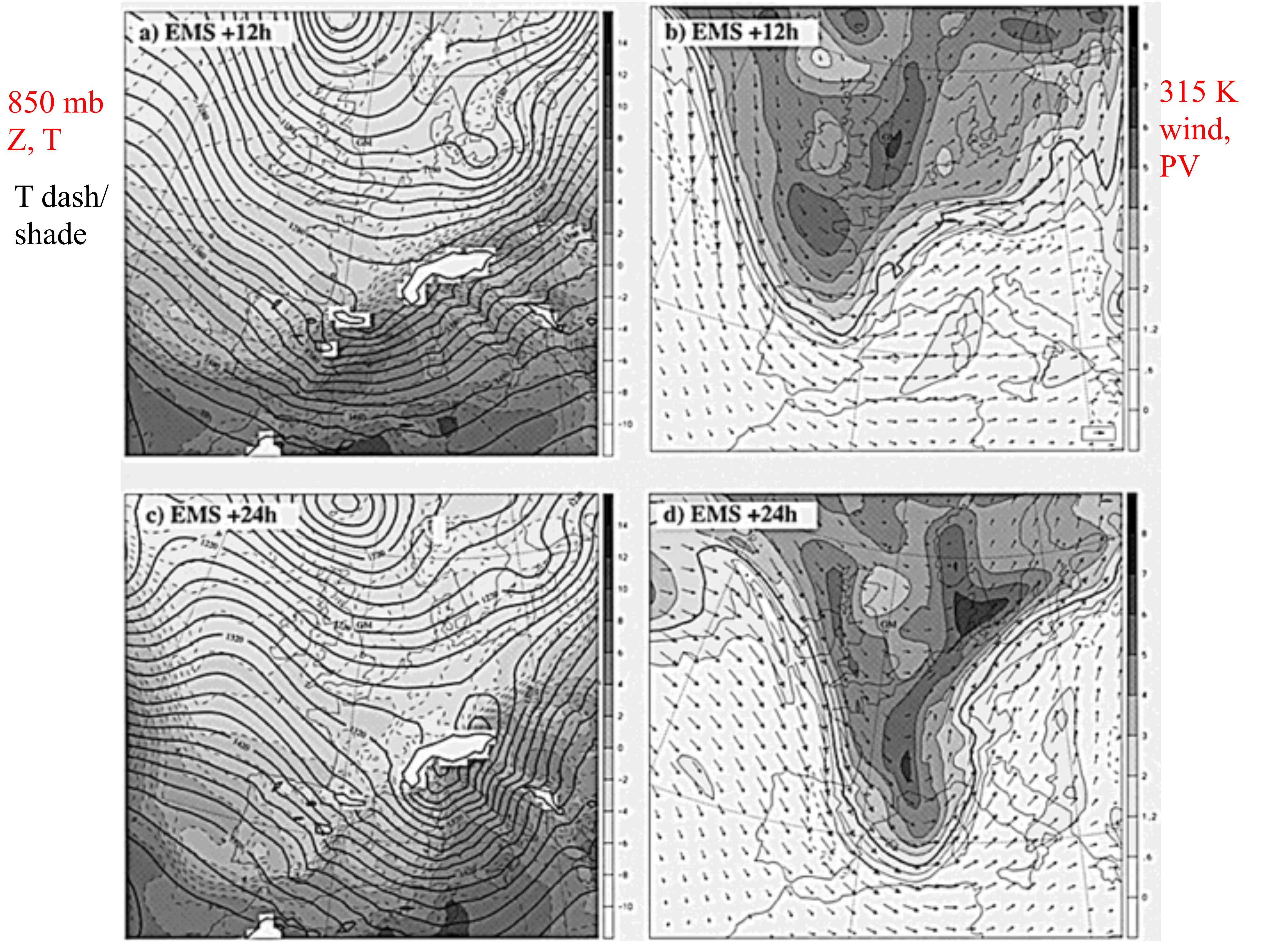

850 mb
Z, T
T dash/
shade
a) EMS +12h
b) EMS +12h
315 K
wind,
PV
c) EMS +24h
d) EMS +24h

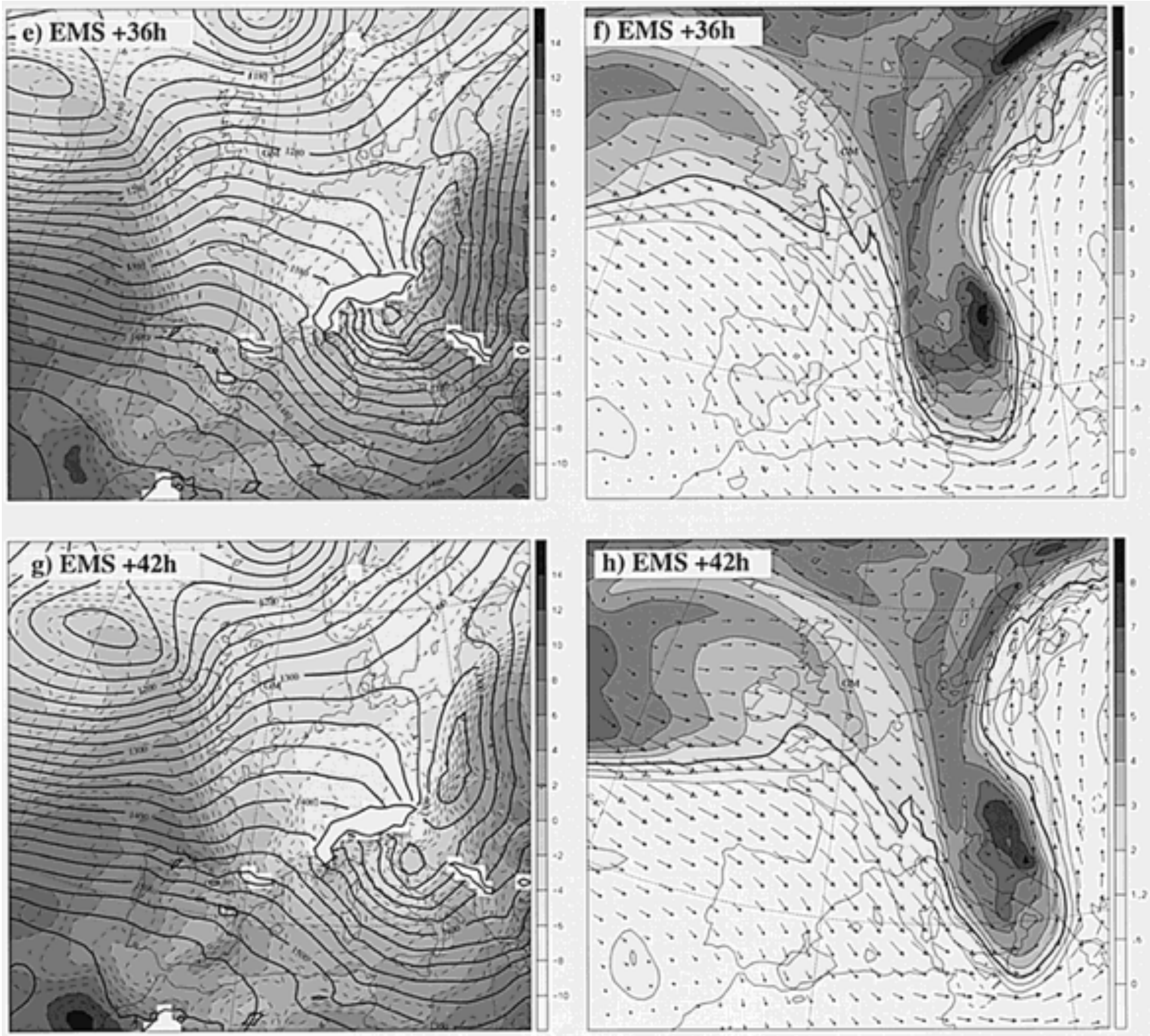

e) EMS +36h
f) EMS +36h
g) EMS +42h
h) EMS +42h
14
12
10
8
6
4
2
0
-2
-4
-6
-8
-10
8
7
6
5
4
3
2
1.2
.6
0

Surface analysis

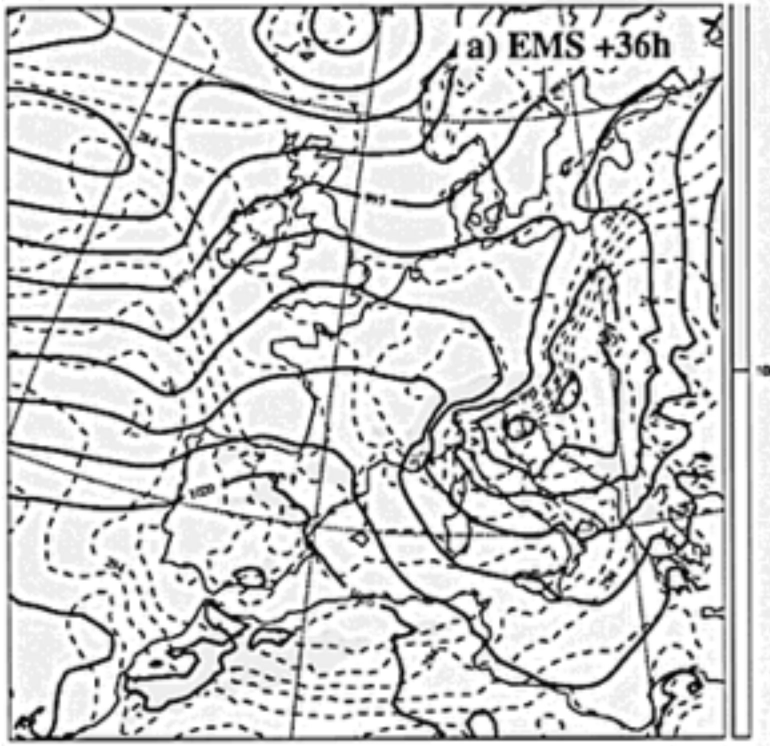

model

obs

24 hr rainfall

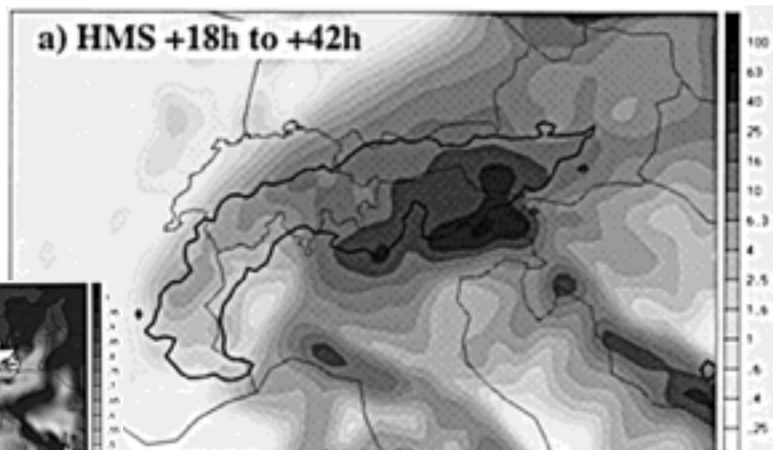

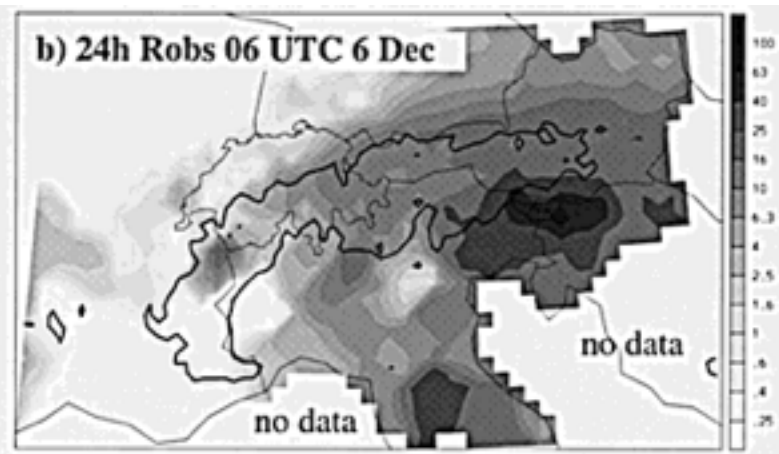

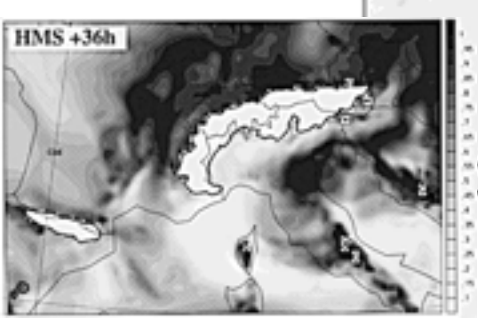

← 850 mb relative humidity

Hi-res model run produces LL +PV 'streamers' in lee of Alps

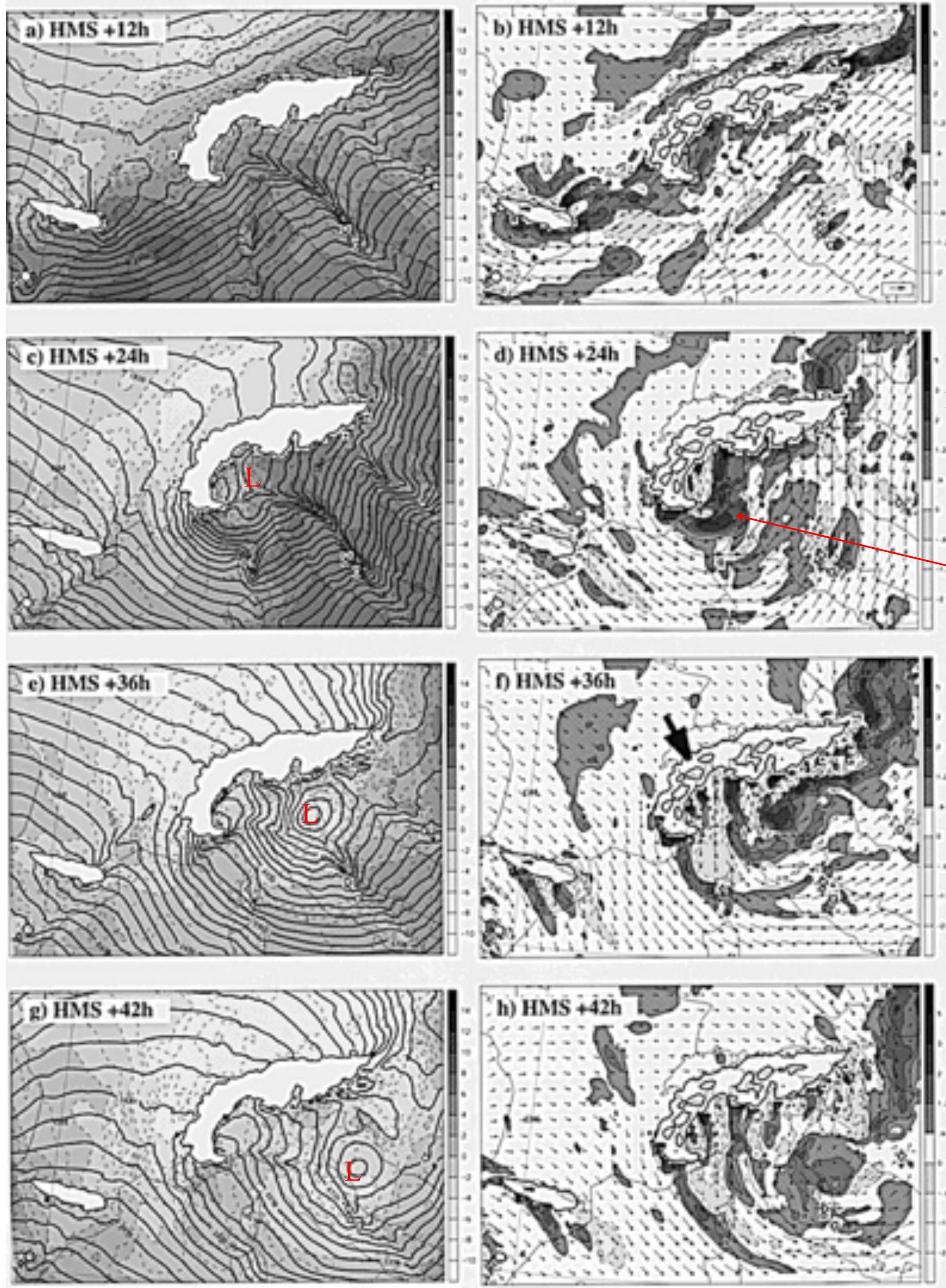

Note the shear vorticity, suggesting that the PV is generated by friction along orography

300 mb

Some PV is not generated but advected down from UL in downslope wind storm (note slope of isentropes)

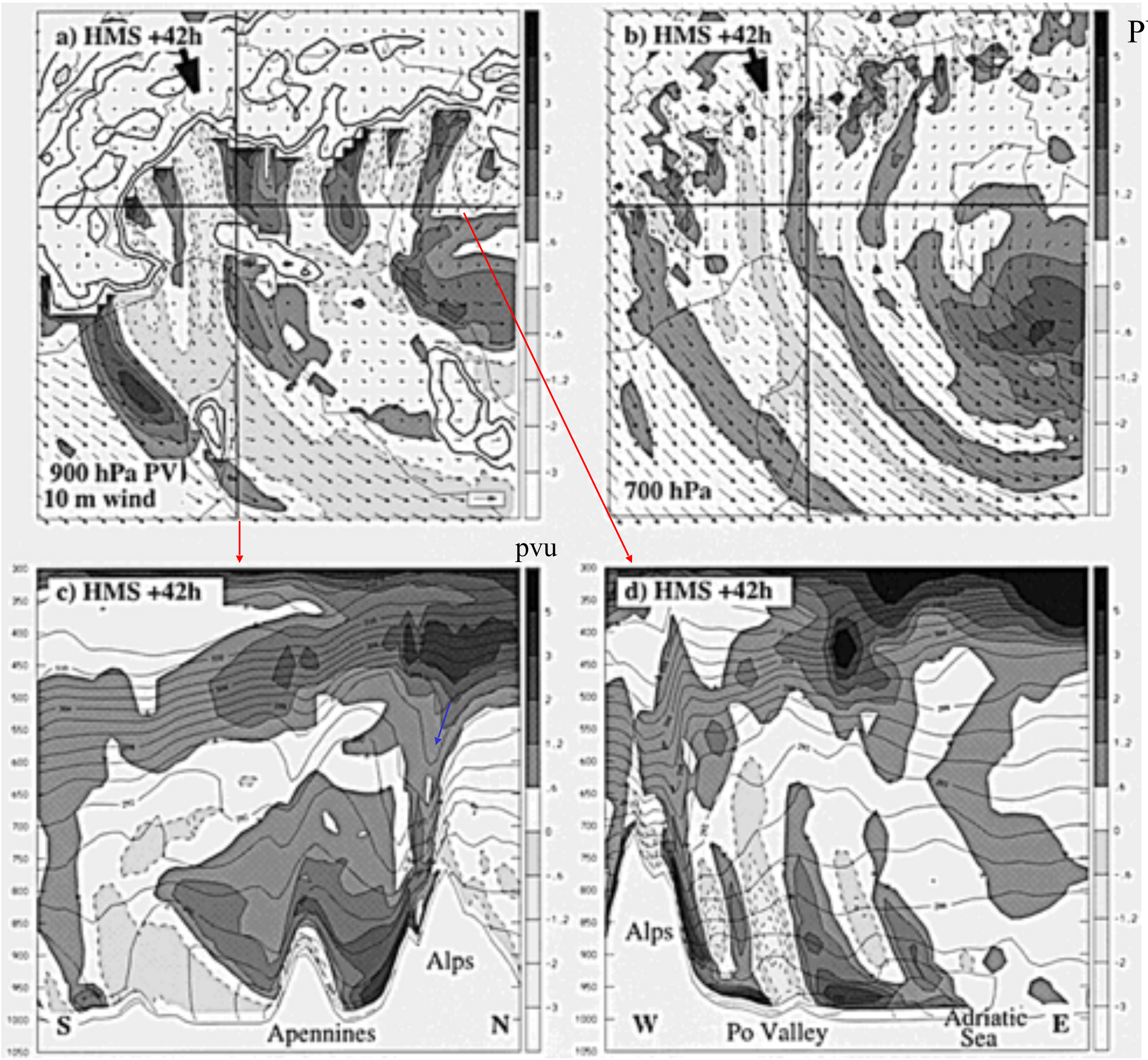

Next: use model to isolate the effects of latent heating, friction, and terrain comp

Dry simulation still produces PV streamers, but not the PV max near the heavy rain (lee cyclon

850 mb
Z, T

T dash/
shade

850 mb
wind,
PV

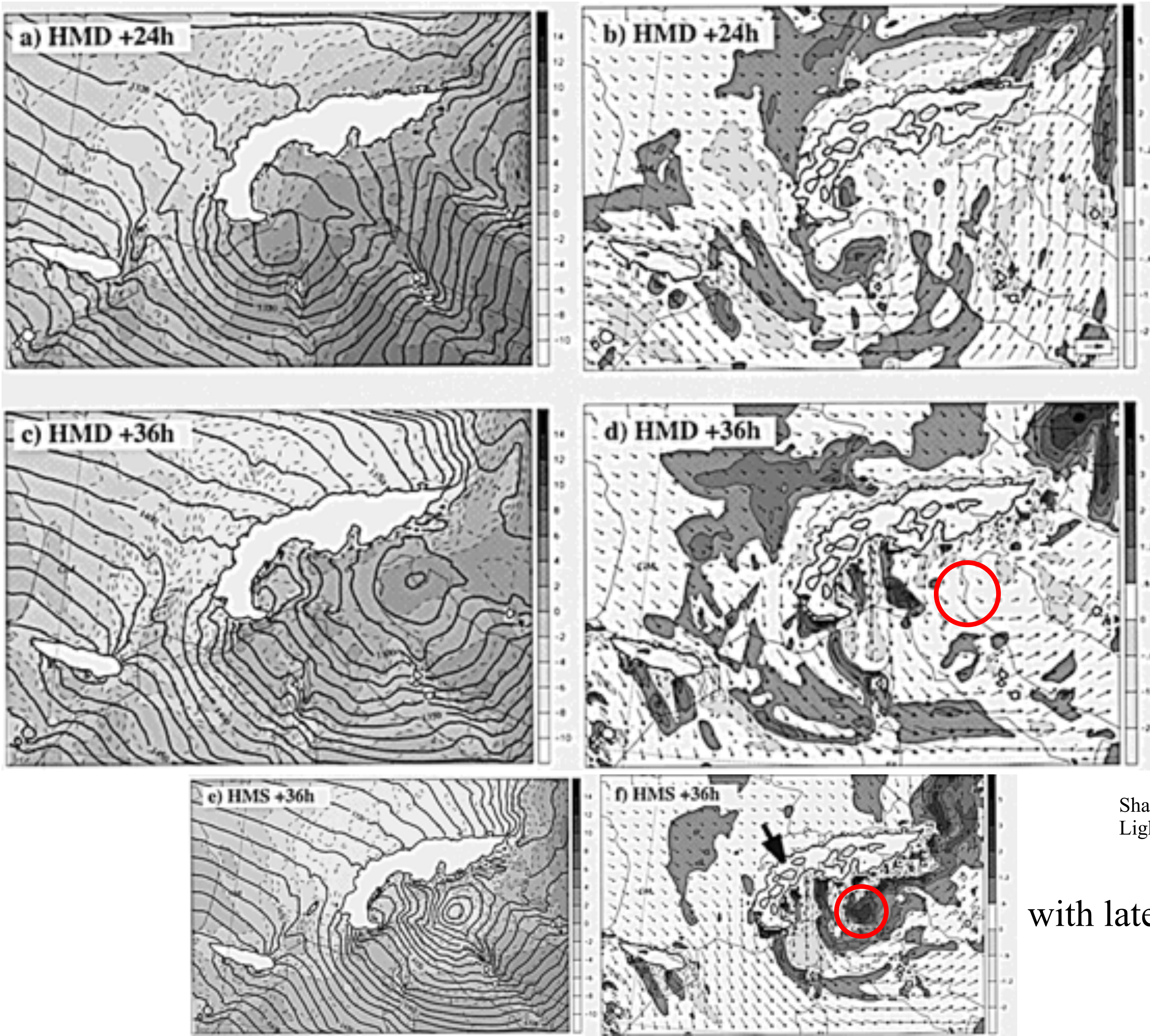

dry run:
weaker lee cyclo
less PV

Shaded: >0.6 pvu
Light-shaded: PV<0

with latent heating

Reduced friction (half the roughness length)

850 mb
Z, T

T dash/
shade

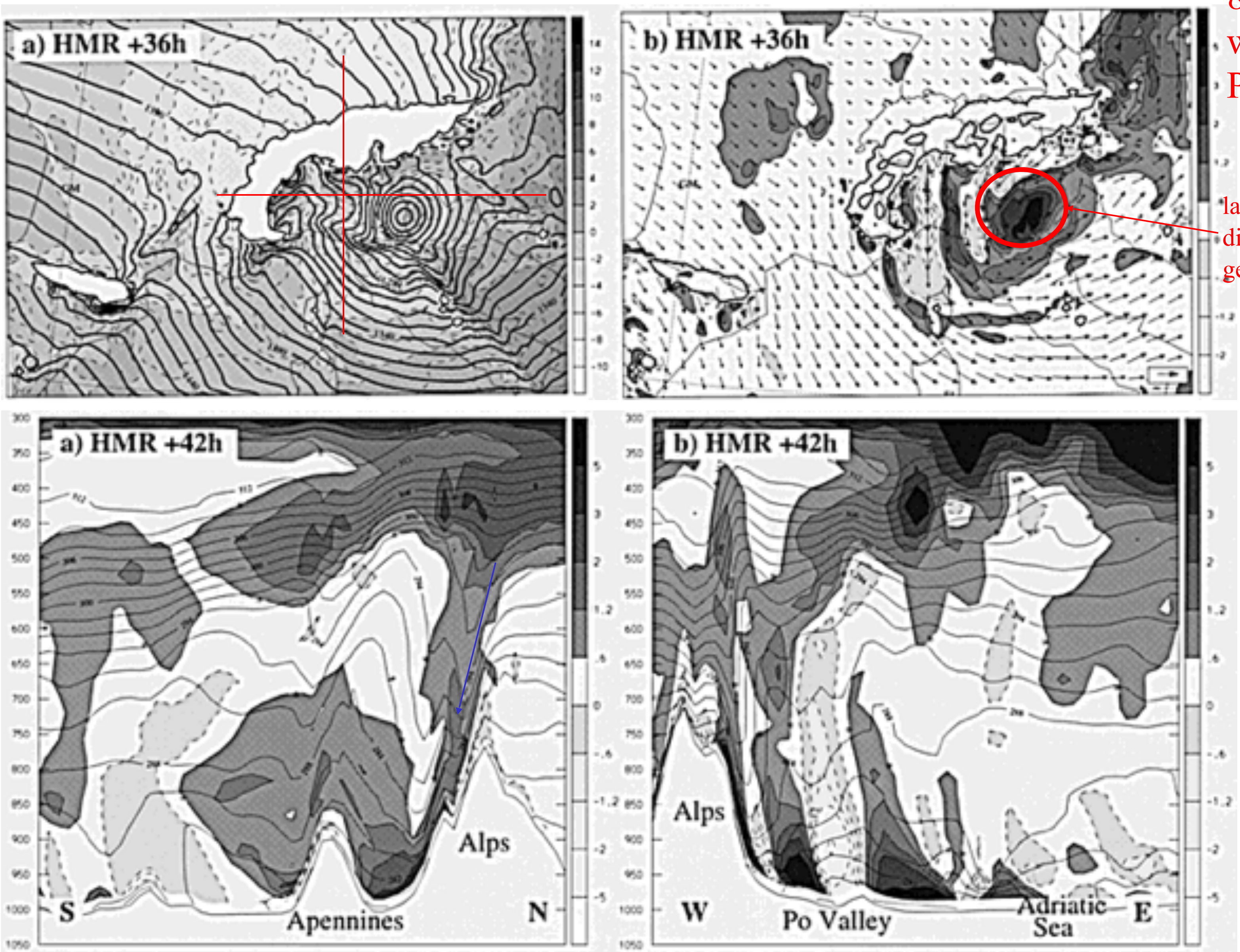

850 mb
wind,
PV

largely
diabatically
generated PV

Lee-side PV streamers are proportionally fed more by downward transport than by friction-generated shear

850 mb
Z, T

T dash/
shade

Simplified topography

One main friction-generated
PV streamer

plus

a largely diabatically-generated
PV core

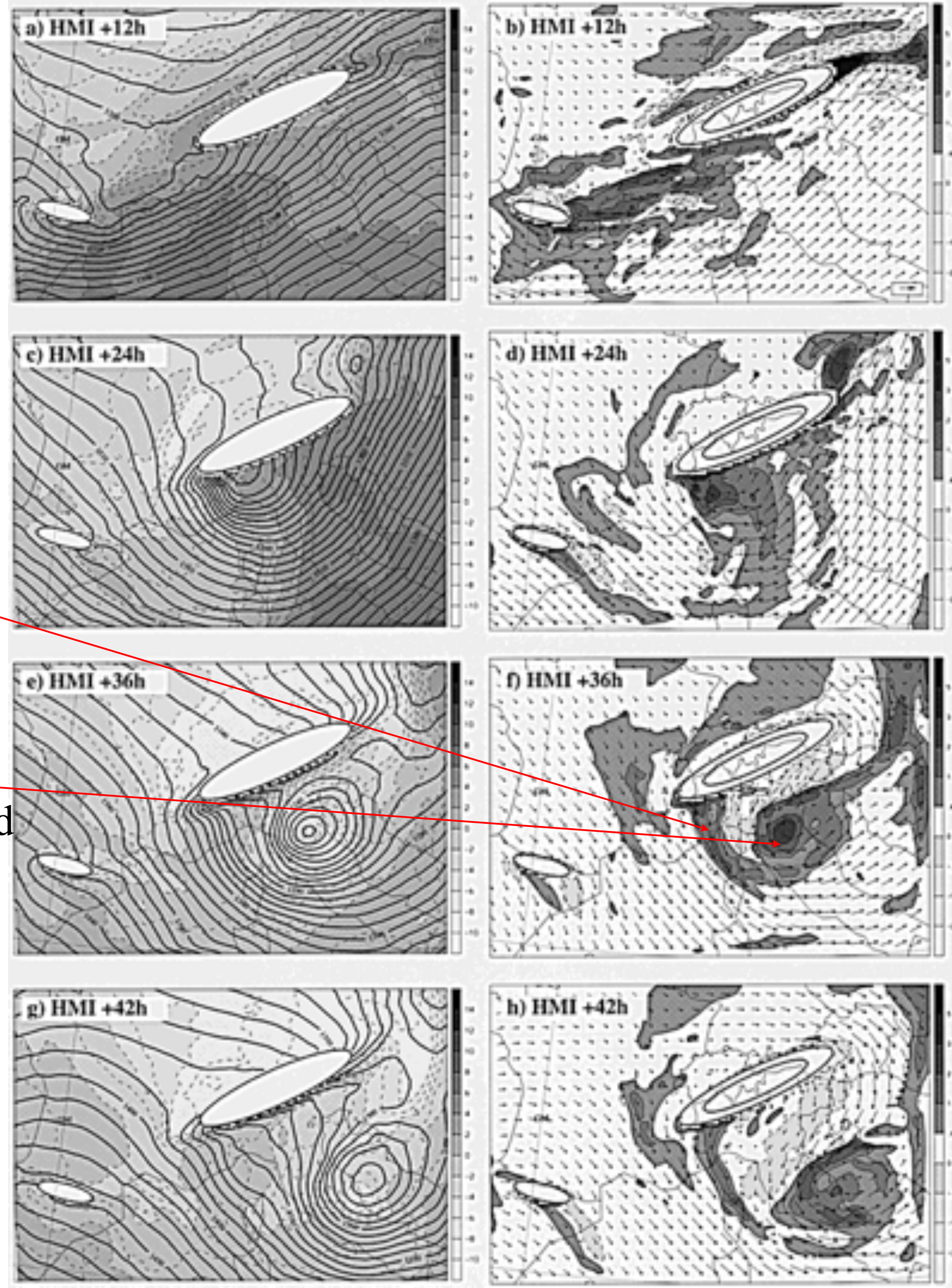

850 mb
wind,
PV

PV and wind, 850 mb, showing PV banners in other circumstances

Prefrontal southerly flow
(PV genesis by the Pyrenees??)

Föhn

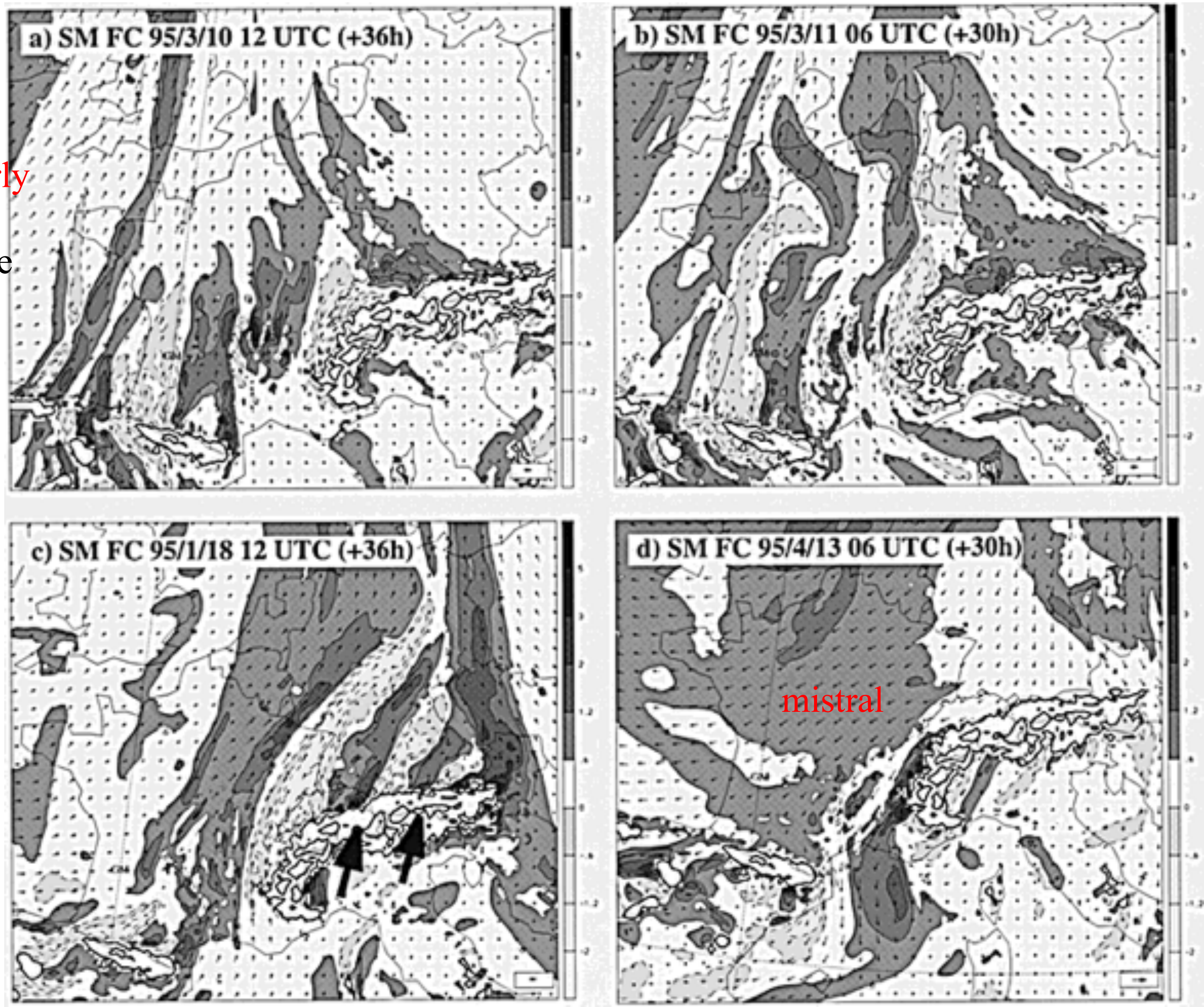

Low-level PV generation mechanisms
(Aebisher and Schar 1998)

- diabatic processes (low- to mid-level latent heat release)
- downward transfer of high PV
  - downslope windstorms
  - deep tropopause folds
- orography
  - PV streamers (or banners) tend to form when 850 mb wind crosses steep terrain
  - Banner pairs (+/-) are associated with topographic edges/gaps
  - Banners are due to flow splitting ($Fr=U/NH < 1$)
  - The ability for a model to capture this PV generation is very resolution-dependent
  - The smaller banners tend to dissipate faster than the bigger ones ($L < L_R$, the Rossby Radius of deformation) $L_R = \frac{NH}{\zeta + f}$

- alpine lee cyclogenesis
  - The first stage is mainly due to the main banner shedding off SW tip of the Alps. This anomaly is due to flow splitting. Some high PV may be advected from aloft.
  - These banners combine to become large (and thus long-lived) enough to generate 'balanced flow'.
  - This balanced vortex is large enough to interact with UL PV anomaly and to start baroclinic cyclogenesis. Thus latent heating further enhances PV in the lee cyclone.
  - Banners likely to form also in lee of the Front Range, and the main PV banner may explain location/strength of Colorado low (in its pre-baroclinic stage).